University of Texas at El Paso
DigitalCommons@UTEP

Open Access Theses & Dissertations

2018-01-01

Attributes Of The Fisher Valley Megaflap And Comparison To The Gypsum Valley Megaflap, Paradox Basin, Utah And Colorado: Implications For Controls On Megaflap Formation

Kate Grisi
University of Texas at El Paso, kategrisi@gmail.com

Follow this and additional works at: https://digitalcommons.utep.edu/open_etd

Part of the Geology Commons, and the Sedimentology Commons

Recommended Citation
Grisi, Kate, "Attributes Of The Fisher Valley Megaflap And Comparison To The Gypsum Valley Megaflap, Paradox Basin, Utah And Colorado: Implications For Controls On Megaflap Formation" (2018). *Open Access Theses & Dissertations*. 1444.
https://digitalcommons.utep.edu/open_etd/1444

This is brought to you for free and open access by DigitalCommons@UTEP. It has been accepted for inclusion in Open Access Theses & Dissertations by an authorized administrator of DigitalCommons@UTEP. For more information, please contact lweber@utep.edu.

ATTRIBUTES OF THE FISHER VALLEY MEGAFLAP AND COMPARISON TO THE GYPSUM VALLEY MEGAFLAP, PARADOX BASIN, UTAH AND COLORADO: IMPLICATIONS FOR CONTROLS ON MEGAFLAP FORMATION

KATE C. GRISI

Master's Program in Geological Sciences

APPROVED:

Katherine A. Giles, Ph.D., Chair

Richard P. Langford, Ph.D.

Gary L. Gianniny, Ph.D.

Charles Ambler, Ph.D.
Dean of the Graduate School

Copyright ©

By

Kate Grisi

2018

ATTRIBUTES OF THE FISHER VALLEY MEGAFLAP AND COMPARISON TO THE GYPSUM VALLEY MEGAFLAP, PARADOX BASIN, UTAH AND COLORADO: IMPLICATIONS FOR CONTROLS ON MEGAFLAP FORMATION

by

KATE C. GRISI, B.S.

THESIS

Presented to the Faculty of the Graduate School of

The University of Texas at El Paso

in Partial Fulfillment

of the Requirements

for the Degree of

MASTER OF SCIENCE

Department of Geological Sciences

THE UNIVERSITY OF TEXAS AT EL PASO

August 2018

ACKNOWLEDGEMENTS

I would like to thank my advisor, Dr. Katherine Giles, for her guidance throughout this project and her inspiring passion for science. I would also like to thank the other members of my committee, Dr. Richard Langford and Dr. Gary Gianniny, for their insights and assistance. This project would not have been possible without my many field assistants: Lupe Alvarez, Matt Costa, Jenna Faith, Emily Graves, M. Tarik Iraz, David Lankford-Bravo, Ezequiel Moreno, and Alondra Soltero. I would also like to thank Nila Matsler, for her invaluable administrative support and personal guidance. Additionally, this project was made possible with funding from the Institute of Tectonic Studies, the Geological Society of America, the American Association of Petroleum Geologists, and the University of Texas at El Paso.

ABSTRACT

Megaflaps are panels of steeply dipping to overturned strata that extend kilometers up the side of a salt diapir or equivalent weld. They often form important components of salt-diapir related hydrocarbon systems, though little is known about their geologic characteristics or how they form. In this study, I collected structural, stratigraphic, and sedimentologic data of the Fisher Valley megaflap and compared these attributes to the previous studied Gypsum Valley megaflap to test the differential sediment loading model proposed for initiation of megaflap formation. This model predicts that the sediment source proximal megaflap of Fisher Valley should have started rotation earlier, contain a coarser-grained, siliciclastic-dominated, thicker stratal succession, as well as have wider lateral extent than the sediment source distal megaflap of Gypsum Valley.

The Fisher Valley and Gypsum Valley megaflaps formed in the Late Paleozoic in the Ancestral Rocky Mountains system of the Paradox Basin of Utah and Colorado. They are both formed by strata of the Pennsylvanian Honaker Trail Formation and the Permian Lower Cutler Formation, although the Fisher Valley megaflap is about twice as close to the sediment source (20 km) from the Uncompahgre Uplift as Gypsum Valley (40 km). Thicker packages of sediment were deposited on the northeastern side of the Fisher Valley salt wall than the southwestern side, beginning in Honaker Trail time and continuing through Cutler Formation deposition, whereas significant differential sediment loading at Gypsum Valley takes place during Upper Cutler deposition. The timing of megaflap rotation was determined by the stratigraphic position of a significant angular unconformity across the megaflap. At both Fisher Valley and Gypsum Valley this is documented at the Mid-Cutler unconformity, which means that megaflap rotation started at approximately the same time at both megaflaps. Fisher Valley megaflap rotation concluded in the

Triassic during the late Moenkopi or Chinle formation deposition, based on the continued shallowing of dips.

The Fisher Valley megaflap is composed of mostly of coarse-grained siliciclastics and minor carbonates deposited in three depositional facies associations (FA): Fan Delta FA, Shallow Marine Carbonate FA and Braided Fluvial FA, each of which has several lithofacies. The stratigraphic cyclicity typically seen in the Honaker Trail and Lower Cutler formations in other parts of the Paradox Basin, including Gypsum Valley megaflap is not observed in the Fisher Valley megaflap. However, there are distinct depositional episodes defined by two marine flooding events of the Shallow Marine Carbonate FA that delineate three major phases of fan delta development in the Fan Delta FA before nonmarine Braided River FA progradation occurs.

Fisher Valley and Gypsum Valley facies differ in several ways: proportion of siliciclastics to carbonates, coarse-ness of clastics, and lateral facies changes. Carbonates at Fisher Valley occur only twice during megaflap deposition, while carbonates at Gypsum Valley occur consistently throughout the megaflap panel. Siliciclastics at Fisher Valley include a large proportion of conglomerates and conglomeratic sandstones, while coarse-grained siliciclastics and clastics as a whole are not common in Gypsum Valley. Lastly, while most Fisher Valley lithofacies are distributed throughout the megaflap in a facies mosaic, Gypsum Valley lithofacies show well defined stratigraphic cyclicity and little lateral variation. Despite all these differences in facies between the two megaflaps their overall thickness is roughly the same; Fisher Valley is 190 m thick and Gypsum Valley is 200 m thick.

The documented coeval timing of megaflap rotation suggests that rotation probably was not driven by regional differences in sediment loading. At Fisher Valley, the differential sediment load may not have been great enough during Honaker Trail deposition to initiate drape-fold

rotation, but a critical tipping point may have been reached during deposition of the Upper Cutler Formation. Another possibility is that differential loading may have been generated by differential erosional stripping off and thinning of the diapir overburden at the Mid-Cutler Unconformity.

What this outcrop analogue showed is that proximity to sediment source can have a large impact on megaflap attributes such as depositional facies, stratigraphy, and structure and that differential load-induced megaflap rotation may be achieved in several different ways besides depositional accumulation thickness variation. Future work should target testing these alternative mechanisms.

TABLE OF CONTENTS

ACKNOWLEDGEMENTS iv

ABSTRACT v

TABLE OF CONTENTS viii

LIST OF TABLES xii

LIST OF FIGURES xiii

1. INTRODUCTION 1

1.1 MEGAFLAPS 1

1.2 PARADOX BASIN MEGAFLAPS 5

1.3 STUDY OBJECTIVES 7

1.4 METHODS 7

1.5 SIGNIFICANCE 8

2. GEOLOGIC BACKGROUND 9

2.1 TECTONIC EVOLUTION OF THE PARADOX BASIN 9

2.2 PARADOX BASIN STRATIGRAPHY 11

2.3 FISHER VALLEY SALT WALL 16

2.4 GYPSUM VALLEY SALT WALL 19

3. FISHER VALLEY MEGAFLAP 22

3.1 MEGAFLAP FACIES 26

3.1.1 HONAKER TRAIL 28

3.1.1.1 FAN DELTA FACIES ASSOCIATION 28

3.1.1.1.1 LAMINATED MICACEOUS SANDSTONE (LMS) LITHOFACIES 29

3.1.1.1.2 CROSS-BEDDED TO CROSS-LAMINATED MICACEOUS SANDSTONE (XBXL) LITHOFACIES 33
3.1.1.1.3 MASSIVE EXTENSIVE CONGLOMERATIC SANDSTONE (MECS) LITHOFACIES 37
3.1.1.1.4 GRANULE-COBBLE CONGLOMERATE (GCC) LITHOFACIES 40
3.1.1.1.5 SOFT-SEDIMENT DEFORMED MICACEOUS SANDSTONE (SSD) LITHOFACIES 45
3.1.1.1.6 BURROWED MICACEOUS SANDSTONE (BMS) LITHOFACIES 47
3.1.1.1.7 HONAKER TRAIL FORMATION ENVIRONMENTAL INTERPRETATION 49
3.1.1.2 SHALLOW MARINE CARBONATE FACIES ASSOCIATION 52
3.1.1.2.1 IRREGULARLY BEDDED DOLOMITIC MUDSTONE (IBDM) LITHOFACIES 53
3.1.1.2.2 CRINOIDAL WACKESTONE-PACKSTONE (CWP) LITHOFACIES 56
3.1.1.2.3 FUSULINID PACKSTONE (FP) LITHOFACIES 59
3.1.2 CUTLER FORMATION 61
3.1.2.1 LAMINATED MICACEOUS SANDSTONE (LMS) LITHOFACIES 62
3.1.2.2 CROSS-BEDDED SANDSTONE (XBS) LITHOFACIES 64
3.1.2.3 MASSIVE SANDSTONE (MS) LITHOFACIES 67
3.1.2.4 FINE-GRAINED RED SANDSTONE (FGR) LITHOFACIES 69
3.1.2.5 BURROWED MICACEOUS SANDSTONE (BMS) LITHOFACIES 71
3.1.2.6 PINSTRIPED ORANGE SANDSTONE (POS) LITHOFACIES 73
3.2 MEGAFLAP STRATAL ARCHITECTURE 75

3.3 MEGAFLAP STRUCTURE 79
3.2.1 THE NORTHWEST FOLD 82
3.2.2 THE SOUTHEAST FOLD 87
3.2.3 COLLAPSE BLOCK 88
4. DISCUSSION 92
4.1 ORIGIN OF FISHER VALLEY MEGAFLAP NORTHWEST FOLD 92
4.2 FISHER VS. GYPSUM VALLEY MEGAFLAPS: TESTING THE DIFFERENTIAL SEDIMENT LOADING HYPOTHESIS 93
4.2.1 TIMING OF MEGAFLAP ROTATION 94
4.2.2 MEGAFLAP FACIES 95
4.2.3 INTERPRETATION OF FACIES TRENDS 105
4.2.4 MEGAFLAP THICKNESS 106
4.2.5 MEGAFLAP LATERAL EXTENT 107
4.2.6 TESTING THE DIFFERENTIAL LOAD HYPOTHESIS 107
5. CONCLUSIONS 109
5.1 THE FISHER VALLEY MEGAFLAP 109
5.1.1 THE FISHER VALLEY MEGAFLAP FACIES 109
5.1.2 THE FISHER VALLEY MEGAFLAP STRUCTURE 110
5.2 FISHER VS. GYPSUM VALLEY MEGAFLAPS 111
5.2.1 FISHER VS. GYPSUM VALLEY MEGAFLAP FACIES 111
5.2.2 MEGAFLAP VARIABILITY 111
REFERENCES 113
APPENDIX 120

VITA 121

LIST OF TABLES

Table 1: Facies associations and lithofacies of the Honaker Trail and Cutler Formations……...28

Table 2: Lithofacies of the Fan Delta FA……...….29

Table 3: Lithofacies of the Shallow Marine Carbonate Facies Association……...…….52

Table 4: Lithofacies of the Braided River Facies Association……..…..62

Table 5: Stereonet data of the northwest fold……....…..84

Table 6: Gypsum Valley facies associations ……....100

Table 7: Comparison of Fisher Valley and Gypsum Valley facies …...……..…..102

Table 8: Comparison of Fisher Valley and Gypsum Valley features….…….…..103

Table 9: Comparison of Fisher Valley and Gypsum Valley facies associations and lithofacies…104

LIST OF FIGURES

Figure 1: Diagram of a megaflap…….…….2

Figure 2: Models of megaflap rotation……..……..……..…3

Figure 3: Sandbox model of megaflap rotation…….……4

Figure 4: Overview map of the Paradox Basin……6

Figure 5: The Paradox Basin stratigraphic column and Penn-Perm depositional environments...15

Figure 6: Geologic map of the Fisher Valley salt wall 17

Figure 7: Cross-section of the Fisher Valley salt wall 18

Figure 8: Geologic map of the Gypsum Valley salt wall..... 20

Figure 9: Seismic line through the Gypsum Valley megaflap 21

Figure 10: Geologic map and cross section of the Fisher Valley Megaflap 24

Figure 11: Drone image over the megaflap 25

Figure 12: Locations of measured sections on the megaflap. 26

Figure 13: LMS field photos…….…….……31

Figure 14: LMS photomicrographs…….. ……..…...32

Figure 15: XBXL field photos ..... ……...35

Figure 16: XBXL photomicrographs……..... 36

Figure 17: MECS field photos……. ……..……39

Figure 18: GCC field photos..... 42

Figure 19: GCC field photos, carbonate clasts. 43

Figure 20: SSD field photos..... 46

Figure 21: BMS field photos..... 48

Figure 22: The BMS lithofacies..... 51

Figure 23: IBDW field photos 54

Figure 24: IBDW photomicrographs 55

Figure 25: CWP field photos.. 57

Figure 26: CWP photomicrographs 58

Figure 27: FP field photos and photomicrograph. 60

Figure 28: LMS outcrop photos 63

Figure 29: LMS photomicrographs..... 64

Figure 30: XBS outcrop photos. 66

Figure 31: MS outcrop photos. 68

Figure 32: MS photomicrographs 68

Figure 33: FGR outcrop photos. 70

Figure 34: FGR photomicrographs 71

Figure 35: BMS outcrop photos..... 72

Figure 36: POS outcrop photos..... 74

Figure 37: POS lithofacies micrographs 74

Figure 38: Fence Diagram of the Fisher Valley Megaflap 79

Figure 39: Fisher Valley facies map 81

Figure 40: A drone still of the NW termination of the megaflap..... 83

Figure 41: Stereonet of the NW fold……...85

Figure 42: Geologic map of the NW fold……86

Figure 43: The southeastern termination of the megaflap.. 87

Figure 44: The relationship between the megaflap, diapir, and collapse block..... 88

Figure 45: The Paradox Formation outcrop adjacent to the megaflap..... 89

Figure 46: Collapse block strata. 90

Figure 47: Collapse block strata. 91

Figure 48: Collapse block strata. 92

Figure 49: Hinge migration model..... 93

Figure 50: Fence diagram transect between Fisher and Gypsum 97

Figure 51: Locations of Gypsum Valley measured sections 98

Figure 52: The fence diagram between Fisher and Gypsum Valley…...……..……..…….99

Figure 53: Outcrop photos of Gypsum Valley marine facies …….……..…101

Figure 54: Gypsum Valley terrestrial facies photos ……...…..…101

1. INTRODUCTION

1.1 MEGAFLAPS

Megaflaps are panels of steeply dipping to overturned strata that extend kilometers up the side of a salt diapir or equivalent weld (Giles and Rowan, 2012; Rowan et al., 2016; Figure 1). These stratal packages were originally deposited on top of a salt body as either prekinematic overburden, roof over inflated salt, or roof over an early passive diapir that later rotated to the salt body flank as the salt rose, with little stretching and thinning of the stratal panel (Rowan et al., 2016). There are two end-member models for megaflap rotation: halokinetic drape fold and contractional (Rowan et al., 2014; 2016). In the halokinetic drape fold model, drape folding related to salt rise and downbuilding leads to rotation whereas in the contractional model, regional compressional stress forces salt rise and megaflap rotation (Rowan et al., 2014; 2016; Figure 2). Megaflap rotation may also be caused by a combination of these processes.

Ferrer et al. (2016) utilized physical sandbox models to show that halokinetic drape fold megaflaps could be initiated by differential sediment loading on the flanks of inflated salt or passive diapirs (Figure 3). Rapid, load-driven subsidence on one flank creates asymmetric brittle failure at the edge of the inflated salt body, leading to diapiric breakthrough and initiation of megaflap rotation during passive salt diapir rise (Rowan et al., 2016).

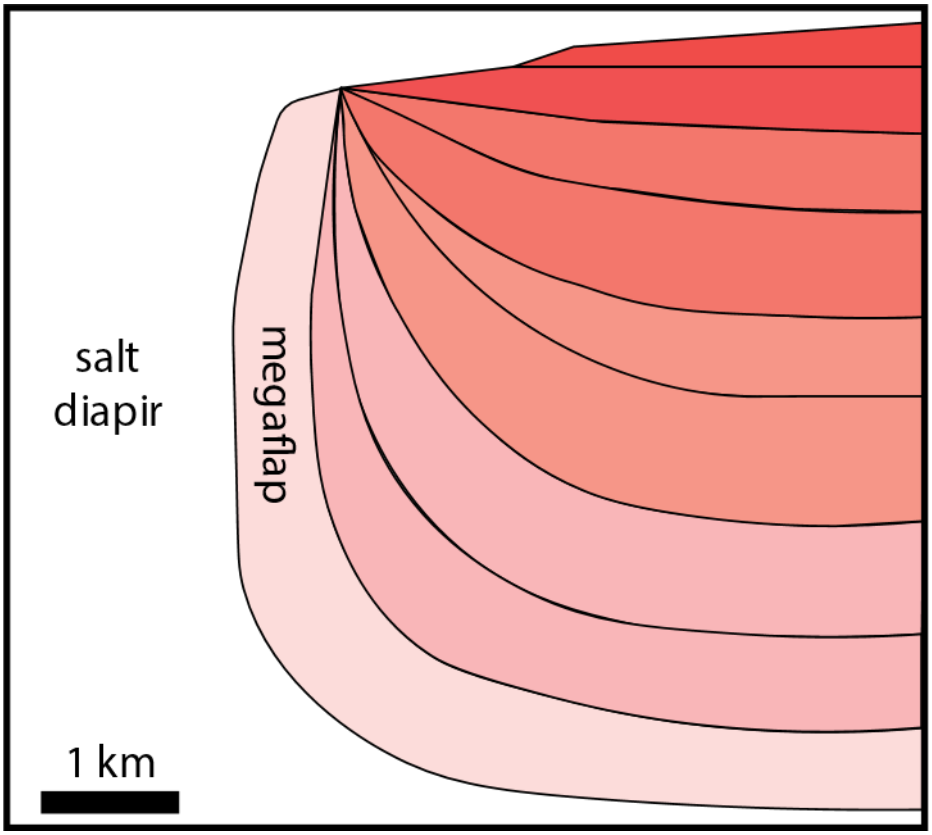

Figure 1: A schematic diagram of a megaflap. Modified from Rowan et al. (2016).

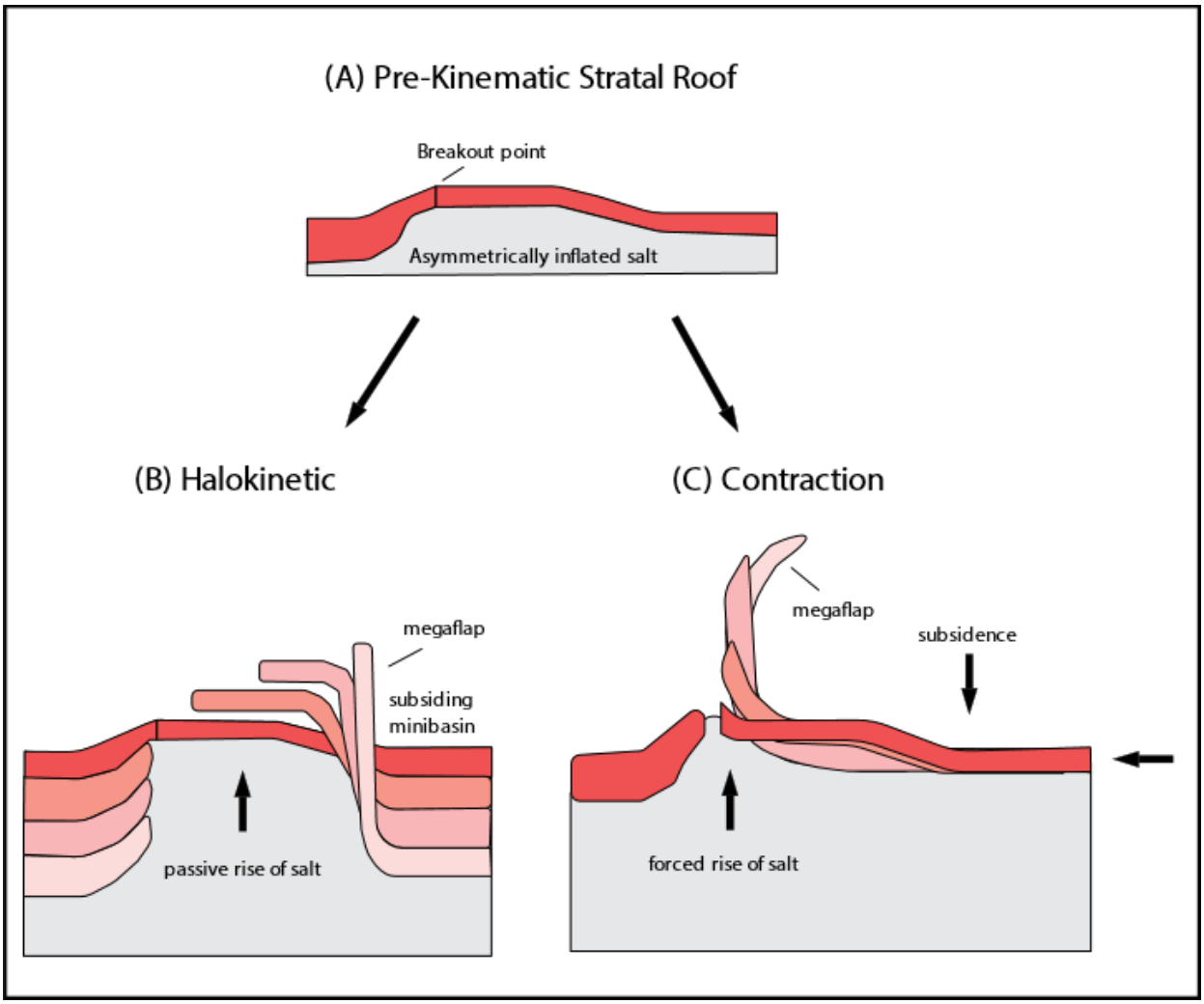

Figure 2: The two end-member models of megaflap rotation. (A) The first stage of megaflap formation, where asymmetrically inflated salt allows for the asymmetric breakage of roof strata. (B) After the breakage of roof strata in a non-compressional system, passive salt rise creates halokinetic drape folding. (C) After the breakage of roof strata in a compressional system, contraction drives the rise of salt, rotating the megaflap to vertical. Modified from Rowan et al. (2014).

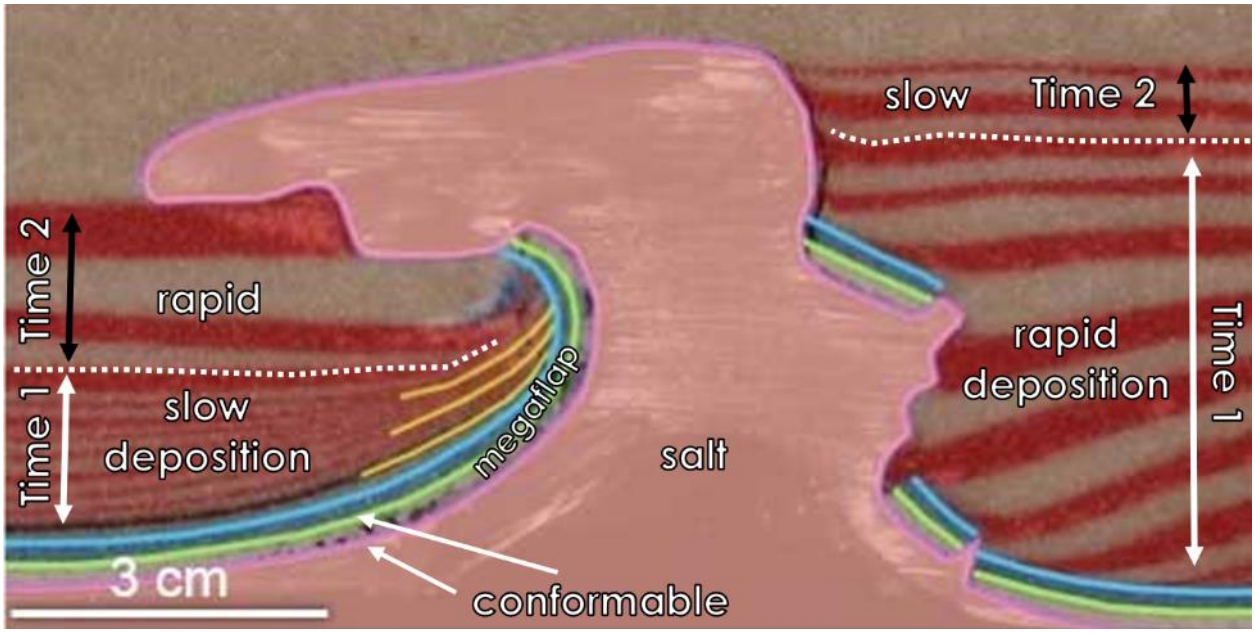

Figure 3: Sandbox model of megaflap rotation driven by differential sediment loading. During Time 1, sediment was deposited faster on the right, creating asymmetry in the salt body and allowing for roof strata to be halokinetically drape folded on the left. Modified from Ferrer et al. (2016).

1.2 PARADOX BASIN MEGAFLAPS

Megaflaps have been identified at several salt walls in the Paradox Basin in Utah and Colorado (Deatrick et al., 2015, Mast, 2016; Giles et al., 2017; Thompson et al., 2018)**,** including Fisher Valley, Sinbad Valley, Moab Valley**,** and Gypsum Valley (Figure 4). The same stratigraphic units form the megaflap stratal panel at all four salt walls: the Pennsylvanian Honaker Trail Formation and Permian Cutler Formation. Megaflap siliciclastics in both formations are primarily sourced from the nearby (20-40 km) Uncompahgre Uplift, which bounds the northeastern margin of the Paradox Basin. Because there is no evidence for shortening in the Paradox Basin during the Late Paleozoic (Ge, 1996), it can be inferred that these megaflaps formed by halokinetic drape folding (Rowan et al., 2014; Figure 2).

Trudgill (2011) used sequential structural restorations of the Paradox Basin salt walls and associated minibasins to show that the Cutler Formation (Undifferentiated) represents a basinward (southward) prograding sequence that filled minibasins proximal to the Uncompahgre before distal. Therefore, the sediment derived from rise of the Uncompahgre Uplift could have produced a differential sediment load that initiated drape fold rotation of the Paradox Basin megaflaps. If this were the case, the sediment-source-proximal megaflaps (Fisher and Sinbad Valleys) should have started megaflap rotation earlier than the distal salt wall megaflaps (Gypsum and Moab Valleys).

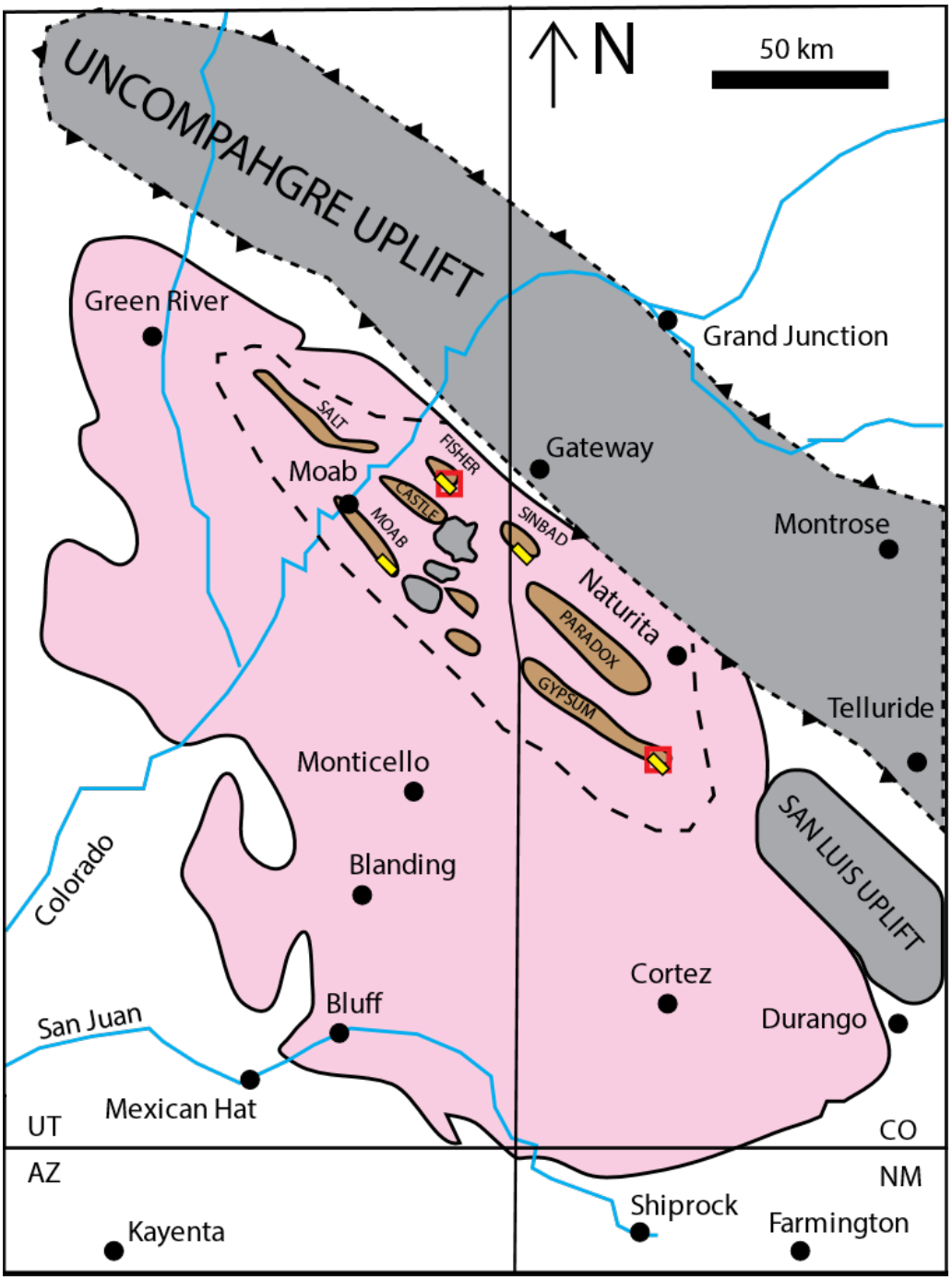

Figure 4: Overview map of the Paradox Basin, which is defined by the extent of salt deposition (pink). The salt walls (brown) are confined to the proximal NE side of the basin. Megaflaps are shown as yellow rectangles. The Fisher and Gypsum megaflap map areas are outlined in red. Modified from Trudgill et al (2011) after Barbeau (2003), Thompson et al. (2018), and Mast (2016).

1.3 STUDY OBJECTIVES

This study examines the sedimentologic, stratigraphic, and structural attributes of the Fisher Valley megaflap in Utah, which is depositionally proximal to the Uncompahgre Uplift, and compares these features to those documented (Deatrick et al., 2015) for the depositionally distal Gypsum Valley megaflap in Colorado. The chief objective of this research is to understand how salt wall proximity to sediment source affects relative timing of megaflap formation and variability of the sedimentologic, stratigraphic, and structural attributes between megaflaps in the same salt system. I expected the two megaflaps to have differences in average siliciclastic grain size, proportion of marine carbonates to siliciclastics, megaflap thickness, megaflap lateral extent, and timing of megaflap rotation. Specifically, I predicted that: 1) The sediment-source-proximal Fisher Valley megaflap would have started to rotate earlier than the sediment-source-distal Gypsum Valley megaflap due to differential sediment loading, 2) The proximal Fisher Valley megaflap strata would be siliciclastic dominated and have coarser-grained facies than those of the distal Gypsum Valley megaflap, 3) The proximal Fisher Valley megaflap would be thicker than the distal Gypsum Valley due to proximity to clastic source, and 4) The proximal Fisher Valley megaflap would have a wider lateral extent due to source proximity.

1.4 METHODS

The sedimentologic, stratigraphic, and structural attributes of the Gypsum Valley megaflap of Colorado are documented by Deatrick et al. (2015). In this study, the same data was collected for the Fisher Valley megaflap in Utah. Using a Brunton compass, tablet with QGIS, and Android FieldMove Clino, I mapped the facies of the Fisher Valley megaflap at a 1:10,000 scale. Using Doelling's (2002) map as a guide, I defined unit contacts and mappable facies and collected strike and dip measurements of bedding planes. With a Jacob's staff and Brunton compass, I measured

stratigraphic sections at well-exposed, strategic positions on the megaflap and recorded at the 1:100 scale at ~200 m intervals. Finally, samples were collected for thin section preparation and analysis to augment petrographic descriptions.

1.5 SIGNIFICANCE

The Paradox Basin is an ideal study location for understanding the origin and nature megaflaps due to its salt tectonics, petroleum production, and well exposed and easily accessible megaflap outcrops. The black shales of the Paradox Formation have served as source rocks for the Honaker Trail and Cutler formation reservoirs that have produced more than 400 million barrels of oil and 1 trillion cubic feet of gas from salt diapir related traps (Baars and Stevenson, 1982; Hite et al., 1984; Nuccio and Condon, 1996). Much of our knowledge about the formation and attributes of megaflaps is sourced from Gulf of Mexico seismic imagery, where they were originally recognized (Giles and Rowan, 2012). Often megaflaps are unpredictably encountered post drilling, because they may not be properly seismically imaged even by the best modern technology due to their vertical nature and common position beneath allochthonous salt bodies (Rowan et al., 2016). For this reason, outcrop analogues are important to characterize megaflaps to understand how they affect trap morphology (Rowan et al., 2016) and how they relate to halokinetic processes.

2. GEOLOGIC BACKGROUND

2.1 TECTONIC EVOLUTION OF THE PARADOX BASIN

The Paradox Basin is part of the Ancestral Rocky Mountains (ARM), a series of basins and uplifts that formed across the western United States during the Pennsylvanian and Permian (Figure 4). The ARM's mechanism of formation has been debated due to its distance from plate margins and lack of magmatism (Curtis, 1958; Kluth and Coney, 1981; Pitman III and Andrews, 1985; McKenzie, 1978; Barbeau, 2003). The ARM has been interpreted to be the foreland of the Ouachita-Marathon thrust system, as Laurentia and Gondwana collided to form Pangea in the Greater Ancestral Rocky Mountains (GARM) system (Kluth and Coney, 1981; Barbeau, 2003; Kluth and DuChene, 2009). Ye (1996) proposed that the tectonics of the ARM could be attributed to shallow-angle subduction, which would explain the distance to the nearest plate margin, but this idea falters in the lack of ARM magmatism (Dickinson and Lawton, 2003). Dickinson and Lawton (2003) suggest that ARM did form distally to the Ouachita-Marathon system, but as an accommodation to a space problem created during the formation of Pangea. Leary et al. (2017) proposed that since the ARM mainly shows evidence of northeast-southwest-oriented compression (Ye et al., 1996; Hoy and Ridgway, 2002; Barbeau, 2003), that ARM development was mainly driven by transpressional stress from the southwestern margin of Laurentia. Ouachita-Marathon deformation—and deformation at the Nevada margin—may have contributed to ARM tectonics but were likely not the primary drivers (Leary et al., 2017).

The Paradox Basin is in the "classic" ARM, in southwestern Colorado and southeastern Utah (Kluth and DuChene, 2009). The basin boundaries are generally defined by the extent of the Pennsylvanian Paradox Formation salt (Baars and Stevenson, 1981). It is 190 km across by 265 km long with an elongate axis oriented NW-SE, roughly parallel to the trend of its neighboring

high, the Uncompahgre Uplift (Baars and Stevenson, 1981; Kluth and DuChene, 2009). The basin is asymmetric, with the deepest part skewed toward the Uncompahgre Uplift and containing a series of NW-SE trending, elongate salt walls (Barbeau, 2003). It is now generally accepted that the basin formed due to lithospheric flexure associated with the load produced by overthrusting of the crystalline block uplift of the Uncompahgre, which fits the context of the larger ARM system (Barbeau, 2003). While there is not much ARM-associated folding in the Paradox Basin outside the salt walls, evidence of ARM contraction is found in the crystalline basement involved high-angle thrusts/reverse faults present along the western margin of the Uncompahgre Uplift (Frahme and Vaughn, 1983; White and Jacobson, 1983; Barbeau, 2003; Trudgill, 2011).

Paradox Basin salt walls have been interpreted to be aligned with pre-existing, northeast-dipping, normal faults in the basement (Baars, 1966; Ge, 1996; Doelling, 2002; Trudgill et al., 2004; Trudgill, 2011) and 2D seismic work supports this idea (Kluth and DuChene, 2009; Trudgill and Paz, 2009; Trudgill, 2011). Northeast-southwest basement faults created the sharp truncations of the salt walls (Trudgill, 2011). Initiation of salt wall formation is thought to be driven by the sediment loading of the Cutler Formation (Undivided; Figure 5), with the northern salt walls generally initiated before the southern (Trudgill, 2011). Diapirism began during deposition of the Pennsylvanian (Missourian-Virgilian) Honaker Trail Formation with growth peaking during Permian Cutler Group deposition and concluding in the Late Jurassic with Chinle Formation deposition (Trudgill, 2011).

After the conclusion of ARM tectonics and Permian peak of salt tectonics, relatively minor deformation occurred during the Sevier and Laramide orogenies, mostly in the form of reactivations and overprinting of structures including the salt walls (Baars and Stevenson, 1981; Mankowski et al., 2002; Kluth and DuChene, 2009; Trudgill and Paz, 2009). Baars and Stevenson

(1981) suggests that the salt acted like a “bowl of jelly,” reducing the effect later tectonics had on the salt structures. Kluth and DuChene (2009) proposed as well that the compression was mostly absorbed by the salt, driving the salt walls up and tilting the Mesozoic strata that tops the salt valleys today. Lastly, within the last 5 million years, solution collapse of the salt walls and associated overburden created the series of NW-SE trending topographic valleys that we see in the Paradox Basin today (Trudgill, 2011).

2.2 PARADOX BASIN STRATIGRAPHY

During Pennsylvanian (Desmoinesian) time, the Uncompahgre Uplift started rising, producing 2-5 km of flexural accommodation in the proximal portions of the Paradox Basin, and the basin locally filled with very coarse-grained, conglomeratic arkosic sediments shed off the uplift in large alluvial fans (Mack and Rasmussen, 1984). However, in conjunction with the deposition of these non-marine siliciclastic sediments, to the south in the foreland, 2500 m of cyclic marine evaporites, organic-rich mudstones, and carbonates of the Paradox Formation were deposited (Barbeau, 2003; Figure 5). The Paradox Formation is composed of 29 cyclic packages of evaporites, dolostone, and black shales produced by Pennsylvanian glacioeustasy (Peterson and Hite, 1969; Dickinson et al., 1996; Nuccio and Condon, 1996). In the center of the Paradox Basin, these cyclothems can be up to 3 km thick with individual packages of halite 10s of meters thick (Nuccio and Condon, 1996; Trudgill, 2011). In the distal southwestern portion of the basin, the Paradox Formation thins to approximately 350 m of shelf carbonates and sapropelic mudrocks (Barbeau, 2003). In the proximal portion of the basin, against the Uncompahgre Uplift, the Paradox Formation interfingers with the coarse-grained siliciclastics that comprise the alluvial fans of the Undivided Cutler Formation (Barbeau, 2003; Trudgill, 2011; Figure 5).

The Pennsylvanian (Desmoinesian – Missourian) Honaker Trail Formation, first defined by Wengerd and Matheny (1958), is composed primarily of carbonates, with lesser siltstones, sandstones, and mudstones. The warm, equatorial Pennsylvanian environments of the western U.S. had three regional depositional systems: a sandy desert with extensive and complex dunes; carbonates produced by glacioeustatic sea level changes that brought marine flooding, and immature, coarse-grained fluvial/alluvial siliciclastics derived from ARM basement block uplifts, (Herman and Sharp, 1956; Peterson and Olen, 1963; Fryberger, 1980, 1984; Baars and Stevenson, 1981; Driese and Dott, 1984; Franczyk and Clark, 1994; Huffman and Taylor, 1994; Gianniny and Simo, 1996). These environments are seen in the Honaker Trail Formation in the form of a variety of cyclic carbonates and siliciclastics. Carbonates include peloidal limestone, carbonate boundstone, mud-supported skeletal limestone, grain-supported skeletal limestone, oolitic grainstone, quartz-rich dolostone, spiculitic dolomitic wackestone, and microbiotic laminate (Gianniny and Simo, 1996). Siliciclastics include fine to coarse-grained quartz sandstone, fossiliferous and non-fossiliferous siltstone, and black laminated mudstone (Gianniny and Simo, 1996). Overall, the Honaker Trail is interpreted in the southwest part of the basin as an extensive shelf with carbonate shoals that to the northeast interfingered with nonmarine fluvial systems (Barbeau, 2003).

The Cutler Formation (Undivided) refers to the coarse-grained alluvial deposits that were deposited between early Pennsylvanian (Atokan) through the mid-Permian time in the northern, proximal Paradox Basin against the front of the Uncompahgre Uplift (Figure 5). Here, they form as much as 5 km of stratigraphic section (Barbeau, 2003) and are partly correlative to the Paradox and Honaker Trail formations that were deposited in the medial and distal part of the basin to the south. In the distal part of the basin, the Honaker Trail is overlain by the Cutler Group, which

ranges from Late Pennsylvanian (Virgilian) through Late Permian in age and is subdivided into five formations including (in ascending order): Lower Cutler, Halgaito, Cedar Mesa, Organ Rock and White Rim Sandstone. The Cutler Group comprises roughly 530 meters of arkosic and quartzose sandstone and siltstone in shades of tan, orange, red, and maroon (Barbeau, 2003). These siliciclastics were deposited by fluvial and eolian systems, whereby sediment supply from the Uncompahgre Uplift became too great for sustained carbonate deposition in the Permian (Condon, 1997; Barbeau, 2003).

The Lower Triassic Moenkopi Formation sits unconformably atop the Cutler Group/Formation, with significant thickness variation across the basin, largely due to the pronounced paleotopography created by ongoing salt tectonics (Trudgill, 2011). Many of the salt walls were areas of non-deposition during deposition of the Moenkopi (Doelling and Morgan, 2000; Trudgill et al., 2004; Trudgill, 2011). The Moenkopi Formation is composed of red-yellow-brown siltstones, mudstones, sandstones, and limestones deposited in a system that ranged from subaqueous non-marine to shallow marine to shoreface to delta (Blakey, 1973). In Fisher Valley, the Moenkopi is mainly composed of dark reddish-brown sandstone, which can be distinguished from the underlying Cutler Formation by its finer grains, lesser micas and potassium feldspar, and more abundant quartz. While the Uncompahgre Uplift is still the sediment source for the Moenkopi, its topography has greatly worn down by this time (Blakey, 1973). The effect of salt tectonics on the overlying Upper Triassic Chinle Formation was similar, with angular unconformities visible locally at several of the salt walls (Doelling, 1988; Hazel, 1994; Trudgill, 2011). Minimal Chinle fluvial deposition did occur on the Uncompahgre Uplift, which did not happen for the Moenkopi Formation (Doelling, 1988; Trudgill, 2011). The Chinle Formation is composed of fluvial sandstones, conglomerates, and mudrocks (Prochnow et al., 2006), which are

not accessible in the Fisher Valley megaflap study region due to the steepness of the southwestern valley wall.

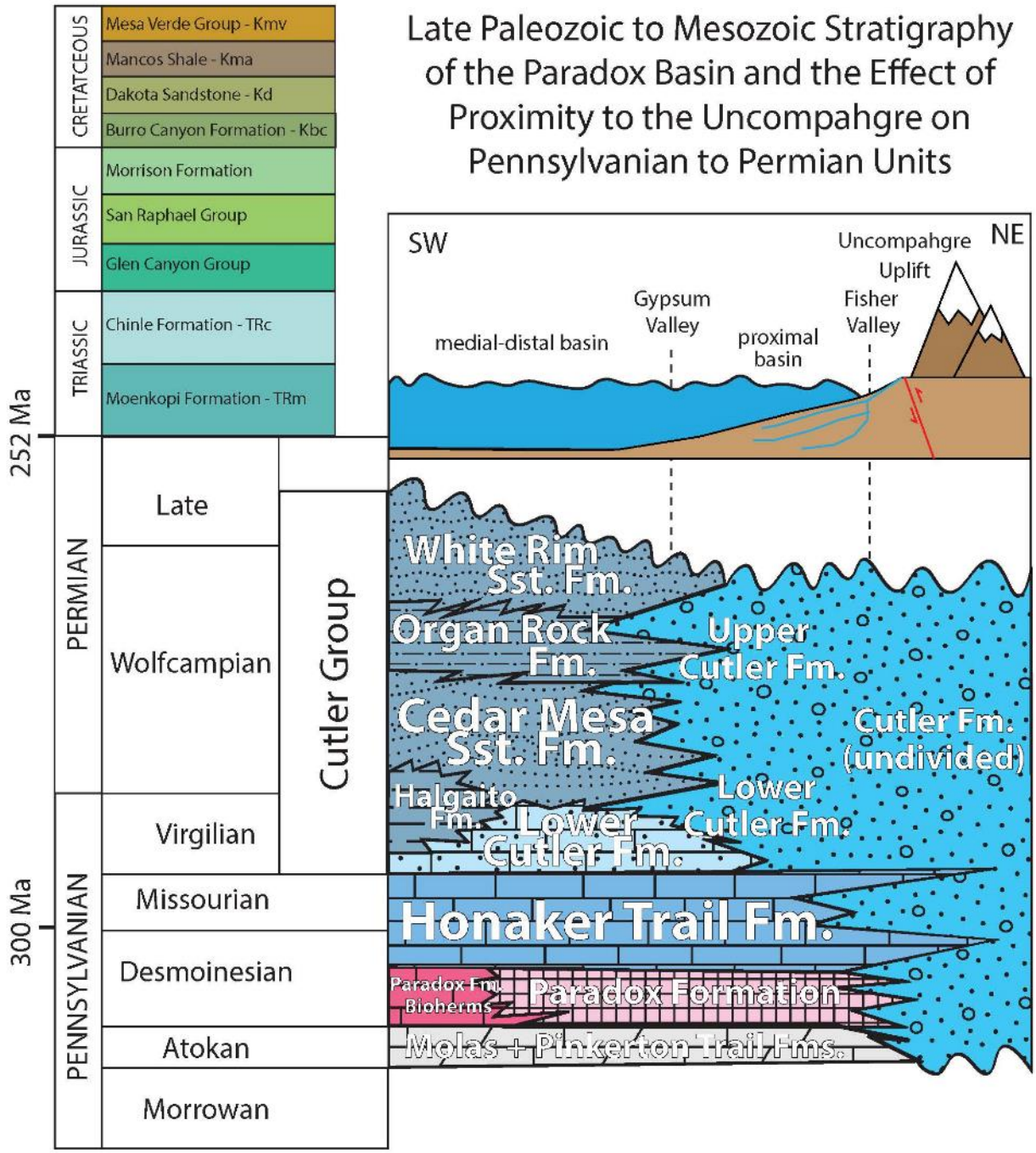

Figure 5: The Paradox Basin stratigraphic column and Penn-Perm depositional environments, modified from Barbeau (2003) and partially based on unpublished work from the Institute of Tectonic Studies. Permian-Triassic boundary age from Shen et al. (2011).

2.3 FISHER VALLEY SALT WALL

Fisher Valley salt wall is in southeastern Utah about 40 km outside the city of Moab, where it lies roughly 20 km from the Uncompahgre Uplift and is thus one of the most proximal salt walls to the sediment source (Figure 3). The exposed portion of the Fisher Valley salt wall (1.5 km by 3.5 km) is often referred to as the Onion Creek salt diapir and the creek, which runs through part of the valley, shares this name as well (Figure 6; Trudgill, 2011). Strata of Pennsylvanian through Jurassic age are exposed along the margin of the salt wall. On the southeastern side of the salt wall is an exposed megaflap composed of near-vertical Honaker Trail and Cutler formations (Figure 7). Correlative strata on the northern side of the salt wall (Figure 7) are mostly present in the subsurface and consist of gently northward dipping, but greatly expanded sections (nearly 3 km) of the Honaker Trail and Cutler (Undivided) formations established by well data (Doelling, 2002; Trudgill, 2011).

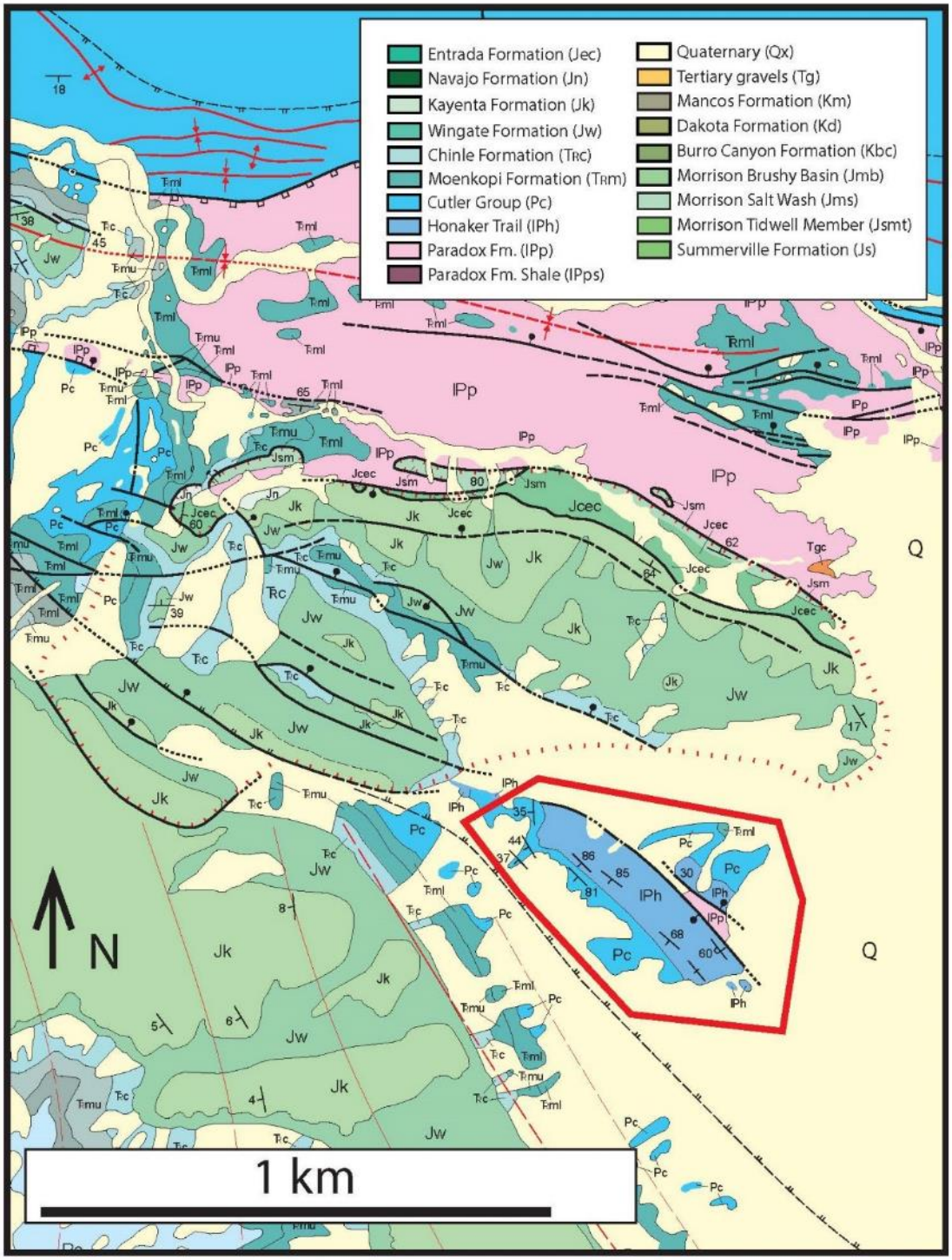

Figure 6: Geologic map of the Fisher Valley salt wall, with the megaflap outlined in red. Modified from Doelling (2002).

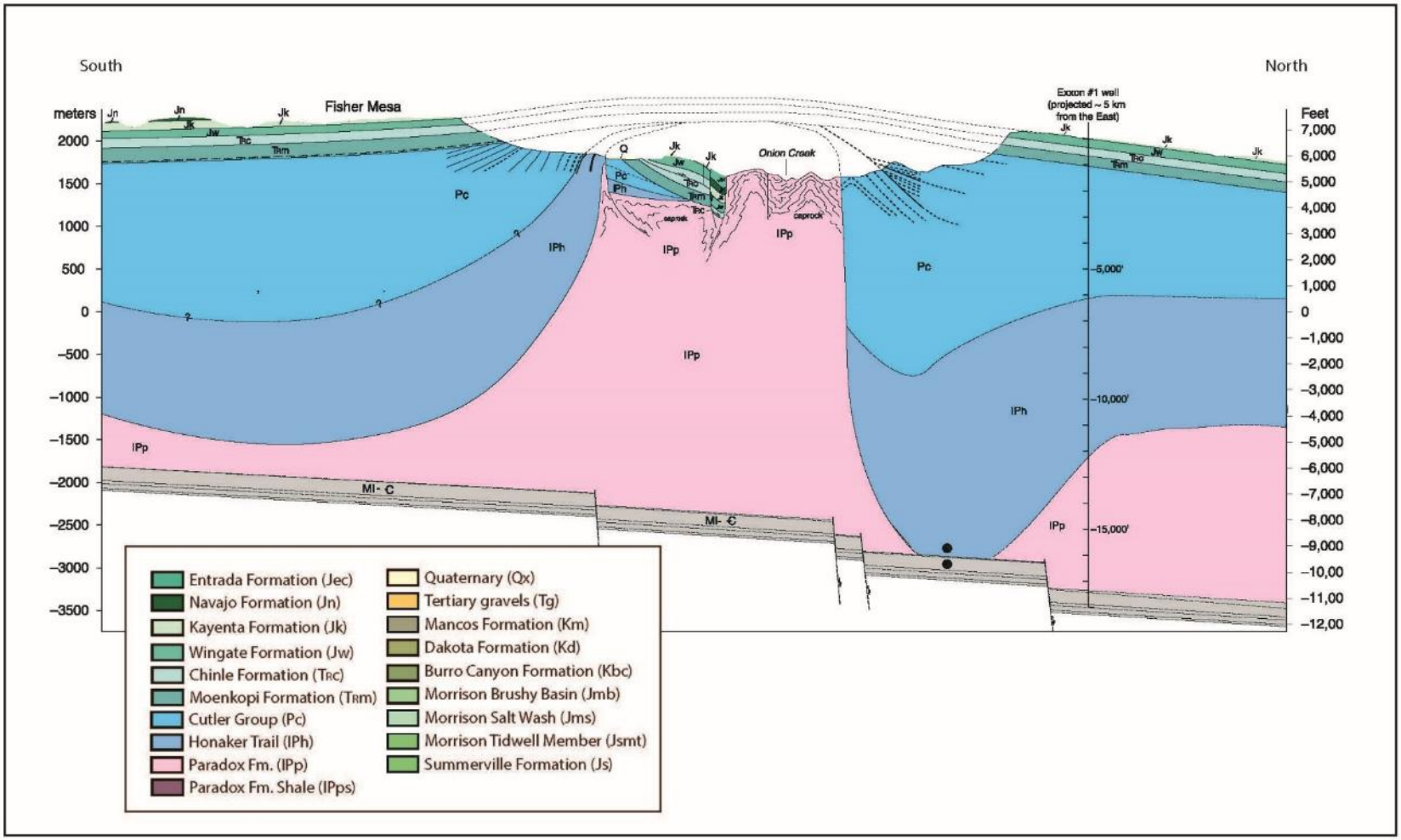

Figure 7: Fisher Valley cross-section modified from Trudgill (2011) after Doelling (2002), complied from mapping, seismic, and well data.

2.4 GYPSUM VALLEY SALT WALL

The Gypsum Valley salt wall is in southwestern Colorado, between the towns of Naturita (25 km to the NE) and Dove Creek (35 km to the SW) (Figure 4). At 40 km, it is approximately twice as far from the Uncompahgre Uplift sediment source than the Fisher Valley salt wall. The Paradox Formation is mapped at the surface in the southeastern portion of the salt wall (Figure 8), but outcrop is poor to absent, especially when compared to the dramatic outcrops of the Onion Creek diapir. Pennsylvanian through Cretaceous strata are exposed along the salt wall margins, with a megaflap of near-vertical uppermost non-evaporite Paradox, Honaker Trail, and Lower Cutler formations (Deatrick et al., 2015; Mast, 2016) to the southeast of the Paradox Formation diapiric exposure (Figure 9). Correlative strata on the northern side of the salt wall (Figure 9) are present only in the subsurface and consist of gently northward dipping, but greatly expanded sections (nearly 2 km) of the Honaker Trail and Cutler formations established by seismic and well data (Rowan et al., 2016).

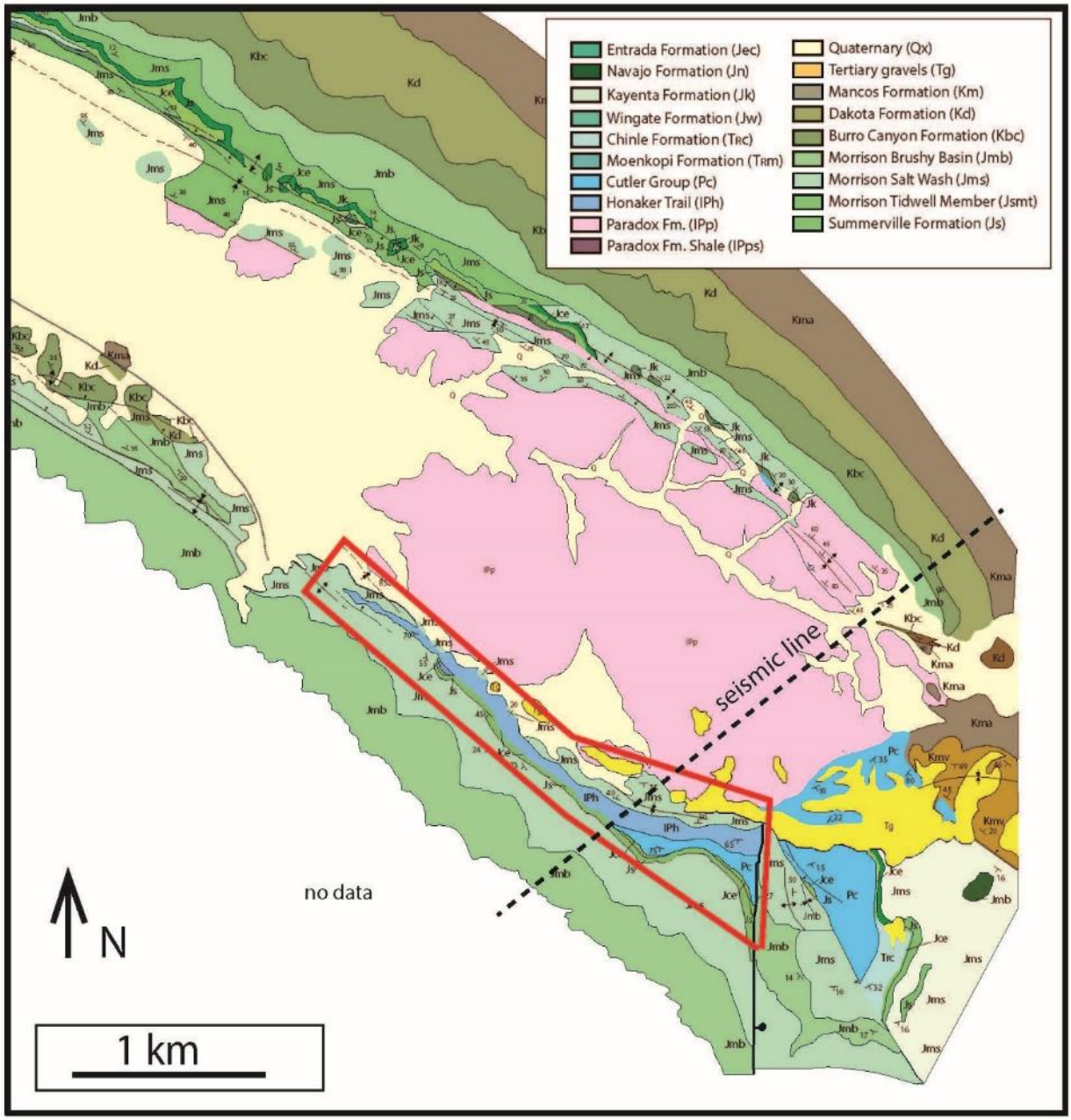

Figure 8: Geologic map of the Gypsum Valley salt wall with the megaflap outlined in red. Unpublished work of the Institute of Tectonic Studies.

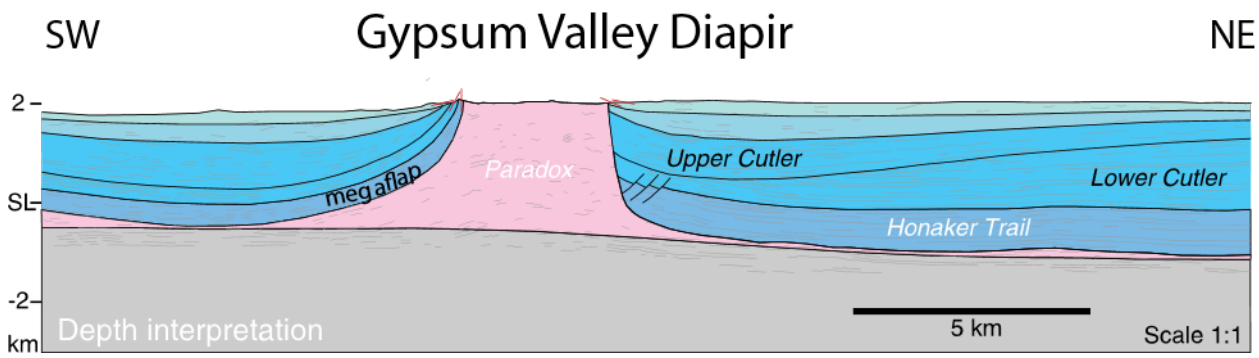

Figure 9: Interpretation of a seismic line through the Gypsum Valley megaflap. The location of the seismic line can be found in Figure 8. Modified from Rowan et al. (2016).

3. FISHER VALLEY MEGAFLAP

The Fisher Valley megaflap was mapped in detail at 1:10,000 scale (Figure 10). A few significant changes were made to Doelling's (2002) 1:100,000 map of the megaflap area:

1. The Honaker-Lower Cutler Formation contact was refined to follow the rule of V's. The base of the Lower Cutler Formation is defined as the first appaerence of dark purple, massive, medium to coarse-grained sandstone, a facies unique to Lower Cutler (Figure 11). Cutler and Moenkopi formation contacts were extrapolated between their outcrops to remove areas previously defined as Quarternary cover.
2. The Upper Cutler-Moenkopi Formation contact was moved to the northeast to the first occurance of reddish brown sandstone (which has lesser micas and potassium feldspar and greater quartz than Cutler facies) (Figure 11).
3. Doelling's most northwest outcrop of Honaker Trail Formation was not found and Cutler Formation was not found to be that extensive in this area. His mapping included a minor fold in the strata, which was found to be more extensive and tight in this study.
4. To the southeast of the megaflap, the Honaker Trail Formation was found to be more extensive than previously mapped. Additionally, changes in strike and dip were found (~20 degrees in strike an dip) in this area and have been mapped as a small fold.

The northern side or base of the megaflap is placed at the faulted contact of the Honaker Trail and Paradox formation's bedded gypsum. This contact is mostly covered along the length of the megaflap. The southern side or top of the megaflap is placed at the significant dip change within the Cutler Formation between what is designated here as Lower Cutler (> 80° dip) and Upper Cutler (< 45° dip). Six stratigraphic sections were measured (Figure 12) from the exposed

base of the megaflap to the top of the megaflap and lithologic descriptions were used to determine lithofacies types and depositional facies associations.

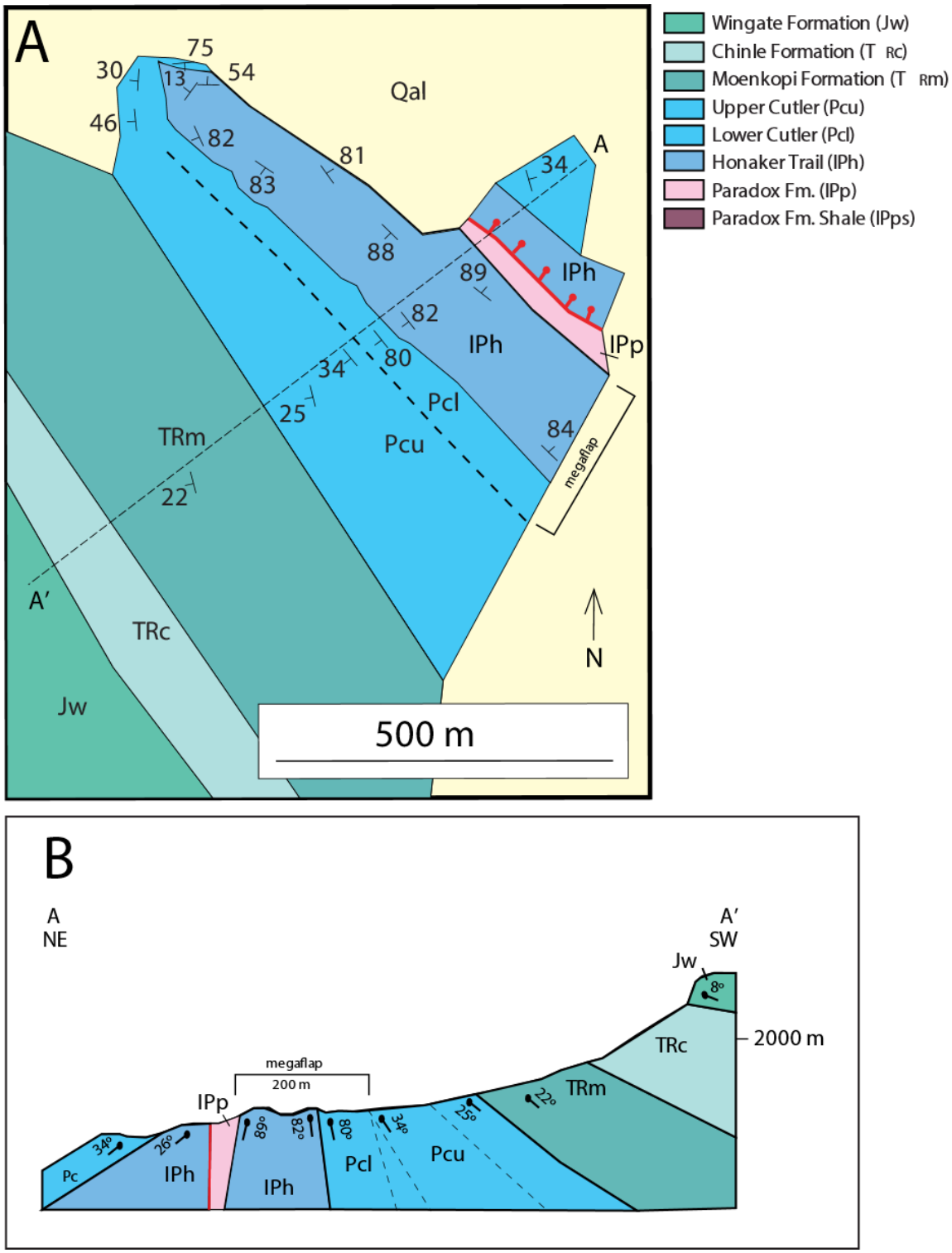

Figure 10: Geologic map (A) and cross section (B) of the Fisher Valley Megaflap, after Doelling (2002).

Figure 11: Drone image over the megaflap, showing the Honaker Trail-Lower Cutler-Upper Cutler-Moenkopi formational contacts and dip changes.

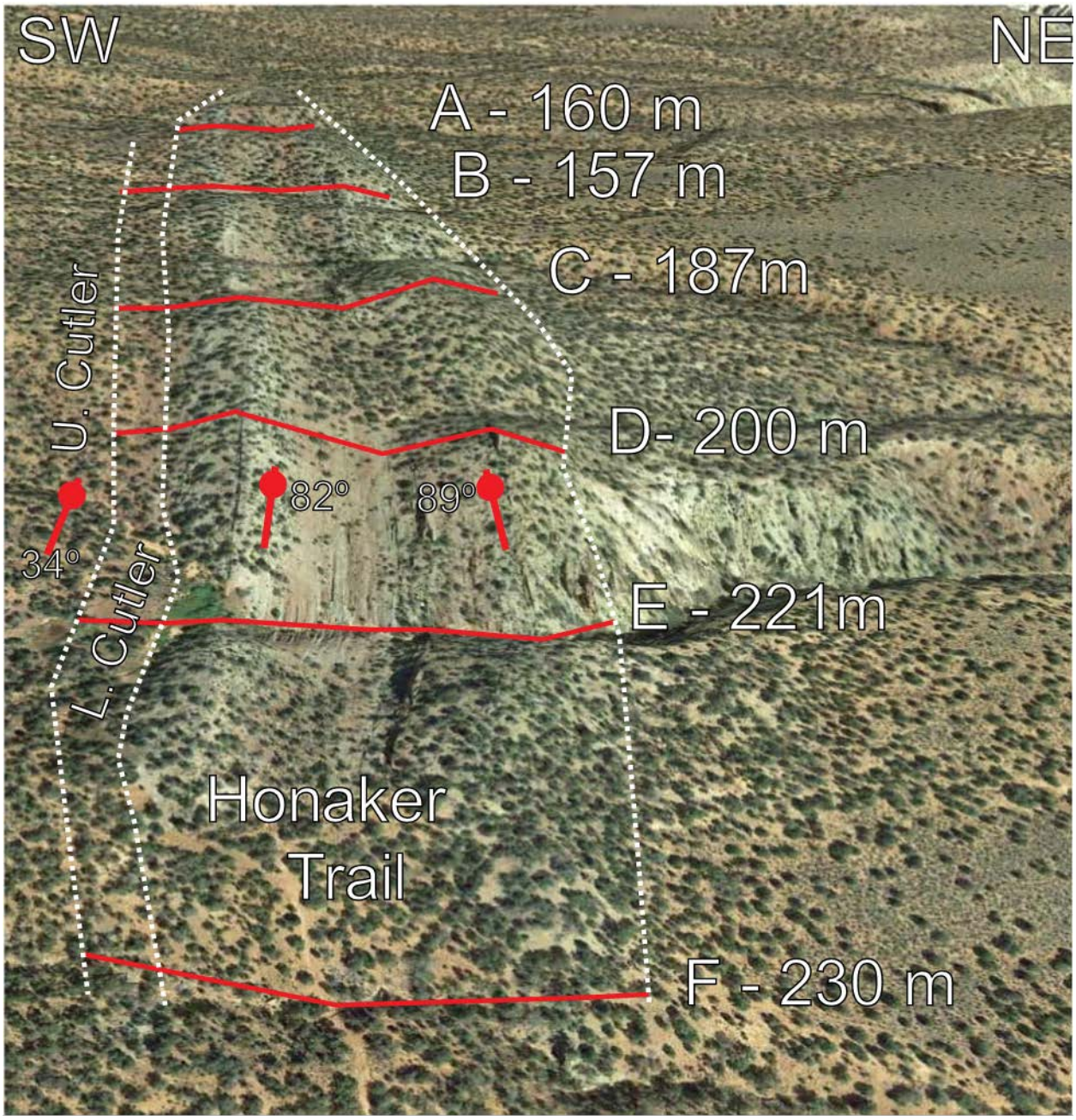

Figure 12: Google Earth image showing location of measured stratigraphic sections on the megaflap. The thickness shown is between the base of the basal Honaker Trail carbonate and the top of the top Honaker Trail carbonate.

3.1 MEGAFLAP FACIES

The Fisher Valley megaflap is composed of the Pennsylvanian Honaker Trail and Cutler formations. The Honaker Trail's carbonates are topographically expressed as two hill-forming

linear carbonate ledges, which parallel the valley walls. The Honaker Trail-Cutler contact is mapped in this study as the onset of the Cutler Formation's deep purple massive sandstones, whose beds and dirt stand out from the red of the Honaker Trail siliciclastics. Regionally, this contact is defined by the onset of abundant micas in the Cutler sandstones, but the Fisher Valley megaflap's Honaker Trail sandstones are highly micaceous as well. Lithofacies of the Honaker Trail and Cutler formations were described and interpreted within a depositional facies association framework. Two depositional facies associations were recognized within the Honaker Trail: Shallow Marine Carbonate and Fan Delta—and one was recognized in the Cutler Formation: Braided River (Table 1). An Alluvial Fan FA model is also presented as an alternative to the Fan Delta FA.

Table 1: Facies associations and lithofacies of the Honaker Trail and Cutler formations.

Facies Association	Lithofacies	Occurrence
Fan Delta	Laminated Micaceous Sandstone, Cross-Bedded to Cross-Laminated Micaceous Sandstone, Massive Extensive Conglomeratic Sandstone, Granule-Cobble Conglomerate, Soft-Sediment Deformed Micaceous Sandstone, Burrowed Micaceous Sandstone	90% of Honaker Trail Formation
Shallow Marine Carbonate	Irregularly Bedded Dolomitic Mudstone, Crinoidal Wackestone-Packstone, Fusulinid Packstone	10% of Honaker Trail Formation
Braided River	Laminated Micaceous Sandstone, Conglomeratic Cross-Bedded Sandstone, Massive Sandstone, Fine-Grained	100% of Cutler Group

3.1.1 HONAKER TRAIL

3.1.1.1 FAN DELTA FACIES ASSOCIATION

The Fan Delta Facies Association (FA) is the most common facies association in the Honaker Trail Formation, making up about 90% of the stratigraphy. The Fan Delta FA is evenly distributed from base to top of the Honaker Trail and laterally across the megaflap. The lithofacies of the Fan Delta FA are all highly micaceous and rapidly grade into one another laterally and stratigraphically, making them impractical as map units. Outcrop color ranges from a greenish-gray to white (typical of medium-grained sandstone) to red (typical of fine-grained sandstone) with bedding from < 1 cm to 1.5 m. Maximum thickness of the Fan Delta FA is about 100 meters, with the thinnest section at 10 meters. Its lithofacies are the Laminated Micaceous Sandstone (LMS), Cross-Bedded to Cross-Laminated Micaceous Sandstone (XBXL), Massive Extensive

Conglomeratic Sandstone (MEC), Granule-Cobble Conglomerate (GCC), Soft-Sediment Deformed Micaceous Sandstone (SSD), and the Burrowed Micaceous Sandstone (BMS). These lithofacies, the favored fan delta interpretation, and alternative alluvial fan interpretation, are presented in Table 2.

Table 2: Lithofacies of the Fan Delta FA, with possible Alluvial Fan model.

Lithofacies	Fan Delta Interpretation	Alluvial Fan Interpretation	Abb.	Occurrence
Laminated Micaceous Sandstone	Shelf sands	Stream-flow sheetflood	LMS	Common
Cross-Bedded-Cross-Laminated Micaceous Sandstone	Shoreface sands	Stream-flow incised channel	XBXL	Common
Massive Extensive Conglomeratic Sandstone	Debris flow	Debris flow	MEC	Common
Granule-Cobble Conglomerate	Fan delta topsets + bottomsets	Stream-flow incised channel	GCC	Common
Soft-Sediment Deformed Micaceous Sandstone	Shelf sands	Stream-flow sheetflood	SSD	Occasional
Burrowed Micaceous Sandstone	Shelf sands	Stream-flow sheetflood reworking	BMS	Occasional

3.1.1.1.1 LAMINATED MICACEOUS SANDSTONE (LMS) LITHOFACIES

Description

The Laminated Micaceous Sandstone Lithofacies is common throughout the Fan Delta FA (Figure 13). It forms depositional packages that range from a few centimeters to a few meters in

thickness and are laterally continuous along strike for 10 meters. Basal and upper contacts are sharp. LMS outcrop color ranges from shades of red (oxidized fine-grained sandstone) to greenish-gray-white (typically reduced medium-grained sandstone). Bedding thickness ranges from very thin to medium with local 3-cm lenses of ripple cross-laminated sandstone.

Beds are internally laminated reflecting both color and grain size variations as bands of medium-grained gray-white sandstone alternate with fine-grained red sandstone. Lenses of medium-grained sandstone within an overall fine-grained sandstone are typical of this unit; occasionally, these lenses may be inverse-graded. The sandstone is composed of angular grains of sorted quartz, potassium feldspar, and biotite, with subordinate glauconite and muscovite/phlogopite (Figure 14).

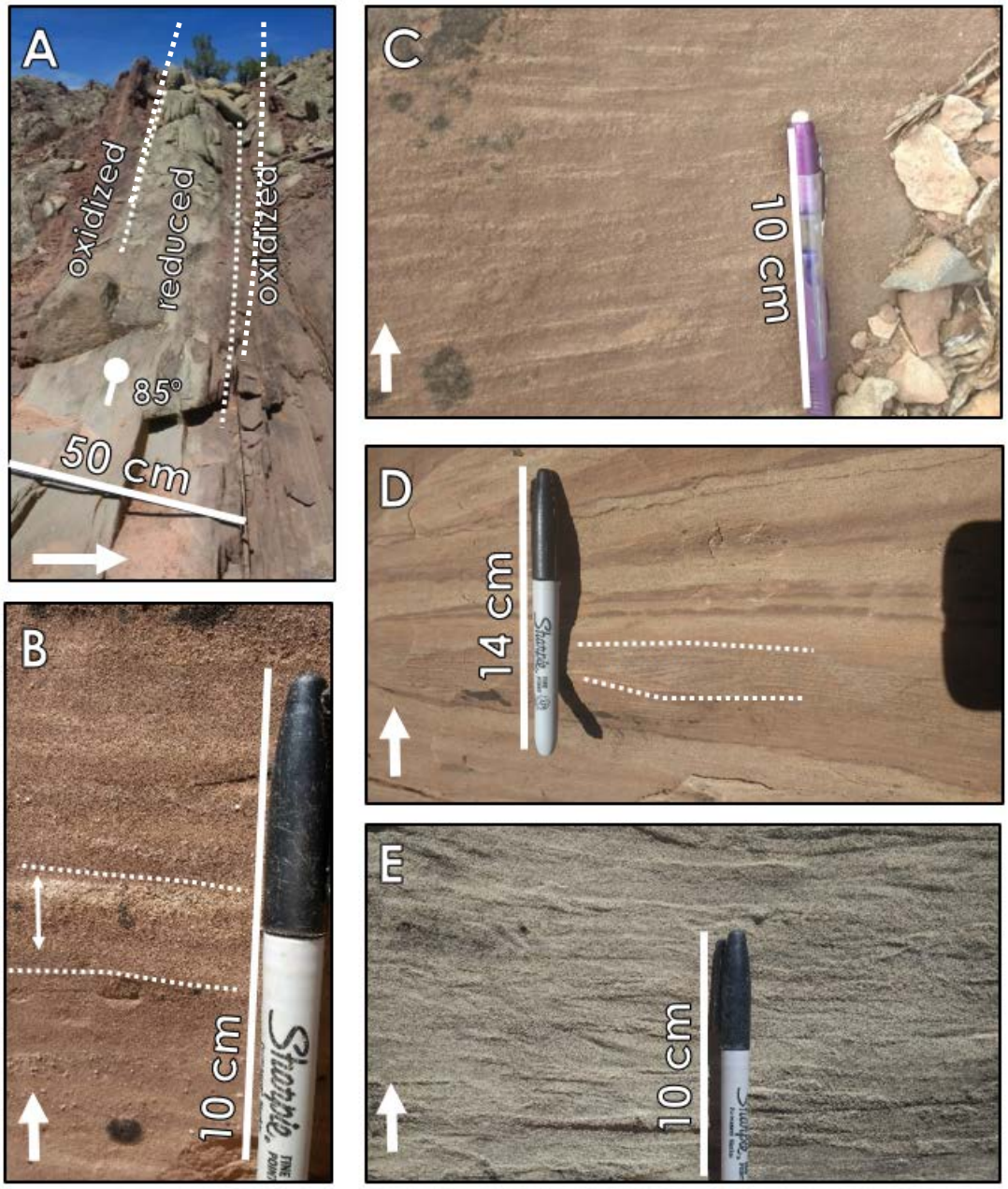

Figure 13: Outcrop photos of the Laminated Micaceous Sandstone. (A) Part of a 3-meter thick package of LMS. The central gray-white-green body is medium-grained and reduced while the surrounding red beds are fine-grained and oxidized. (B) 2.5-cm inverse-graded fine-medium-grained lens. (C) Series of white medium-grained lenses in a red fine-grained sandstone, a sequence common in the LMS. (D) Variable package of LMS with millimeter laminae to centimeter beds in fine- to medium-grained sandstone with a 3-cm ripple cross-laminated package. (E) Less common iteration of C, where the break in grain scale is smaller between the lenses and laminae.

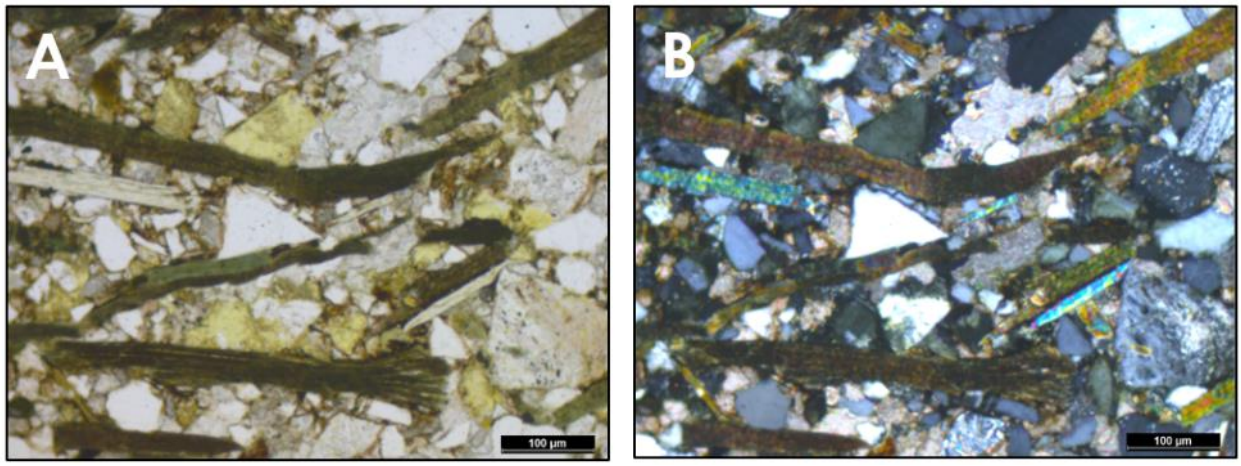

Figure 14: LMS photomicrographs with (A) in plane light and (B) in crossed polars shows the same portion of a LMS thin section, with a typical assemblage of angular potassium feldspar, quartz, and biotite, with lesser glauconite.

Interpretation

The grain composition and angularity (angular quartz, potassium feldspar, and biotite grains) indicate an immature, first generation igneous source, consistent with derivation from the nearby Uncompahgre Uplift granitic basement (Frahme and Vaughn, 1983). The laminations of this lithofacies indicate moderate flow strength in the upper flow regime while less common ripples indicate low flow strength in the lower flow regime (Fielding, 2006). Some of the laminae are lenticular and coarsen-upward, which probably represent reworking by eolian processes during periods of low water levels (Loope, 1984). Such "pinstripes" are recognized by Jordan and Mountney (2012) in the Lower Cutler Formation as well as in this study.

Mack and Rasmussen (1984) recognize laminated micaceous sandstone in their water-laid sheetflood facies association in middle to upper Cutler near Gateway, Colorado, as part of an alluvial fan model. This laminated micaceous sandstone is also associated with granule to pebble conglomerates, ripples, soft-sediment deformation, and burrowing, all seen herein; however, Mack and Rasmussen (1984) also observed laminated siltstone and root casts in their facies association, neither of which is found in the Fisher Valley megaflap Honaker Trail Fm. An alternative

interpretation for the LMS presented by Rees et al. (2017), where lithofacies “Fm” occurs via upper plane bed deposition from storm events on the innermost shelf of a larger fan delta system. The two problems with this interpretation are: 1) Rees et al. (2017) laminated sandstone is associated with massive siltstone (not documented in the megaflap) deposited during fair weather periods, and 2) Honaker Trail megaflap laminated micaceous sandstone potentially has pinstripes, which show evidence of eolian reworking, which were not recognized by Rees et al. (2017). Potentially for the Honaker Trail megaflap, either no fair weather periods occurred, or were not recorded, and eolian reworking represents periods significant regression.

3.1.1.1.2 CROSS-BEDDED TO CROSS-LAMINATED MICACEOUS SANDSTONE (XBXL) LITHOFACIES

Description

The Cross-Bedded-Cross-Laminated Micaceous Sandstone lithofacies is the most common lithofacies of the Fan Delta FA and quickly shifts laterally and through time into other lithofacies of the Fan Delta FA (Figure 15). It is usually lenticular in shape as it pinches out within 1-3 meters once it begins to thin. Packages may be traced for 10-15 meters before such thinning occurs. The lithofacies is typically no thinner than 0.5 m. Erosional truncations are often observed within the unit and at its base as it may erode into the underlying unit. It may also be erosionally truncated at its top. It has ripples and dunes, with dunes up to 1.5 meters thick and the exposure of the lithofacies is typically no thicker than this. Outcrop color ranges from greenish-gray-white (typical of medium-grained sandstone) to red (typical of fine-grained sandstone). Weathering patterns may give it a striped appearance. Bedform ripples may be symmetrical or asymmetrical, indicating both bi- and unidirectional flow. Some supercritical ripples are observed. Bedform ripples may be intermixed with dune forms.

The sand is fine- to medium-grained, moderately- to poorly-sorted, dominated by angular quartz, potassium feldspar, and biotite (Figure 16). Accessory grains include sandstone lithic clasts and glauconite.

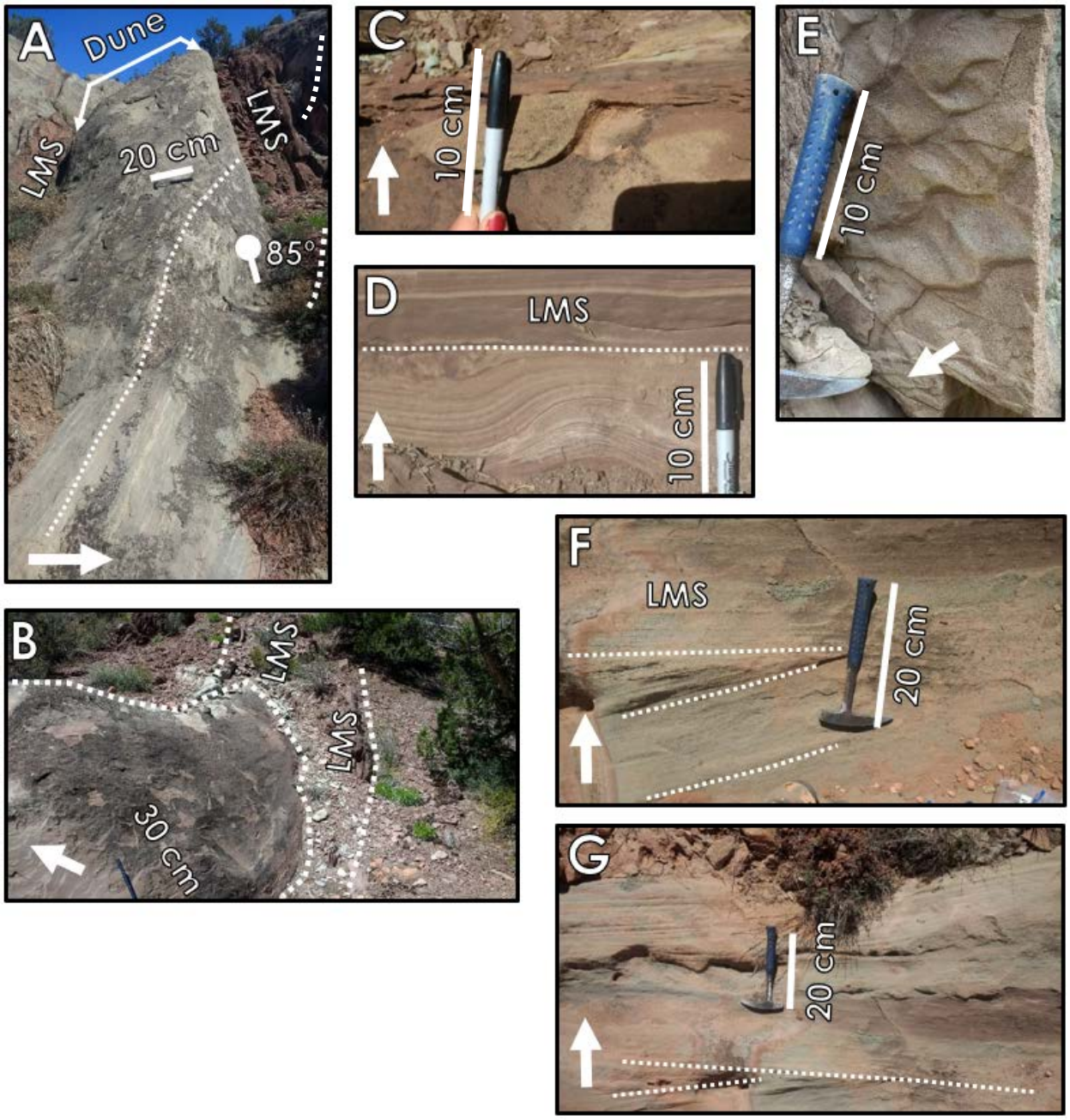

Figure 15: Cross-bedded and cross-laminated micaceous sandstones of the XBXL lithofacies. (A) A 1.5 m thick dune package with under- and over-lying sharp contacts with LMS. (B) A 1 m dune eroding 0.5 m into the underlying LMS. (C) A 5-cm scour into LMS, overlain by LMS. (D) A supercritical ripple sharply overlain by LMS. (E) Asymmetric ripples on the top of a bedding plane. (F) A dune sharply truncated by LMS. (G) A complex sequence of XBXL interbedded with LMS: From base, a dune sharply overlain by LMS, which is eroded into by ripples followed by LMS that pinches out to the left. Ripples erode the second LMS package and then most LMS follows.

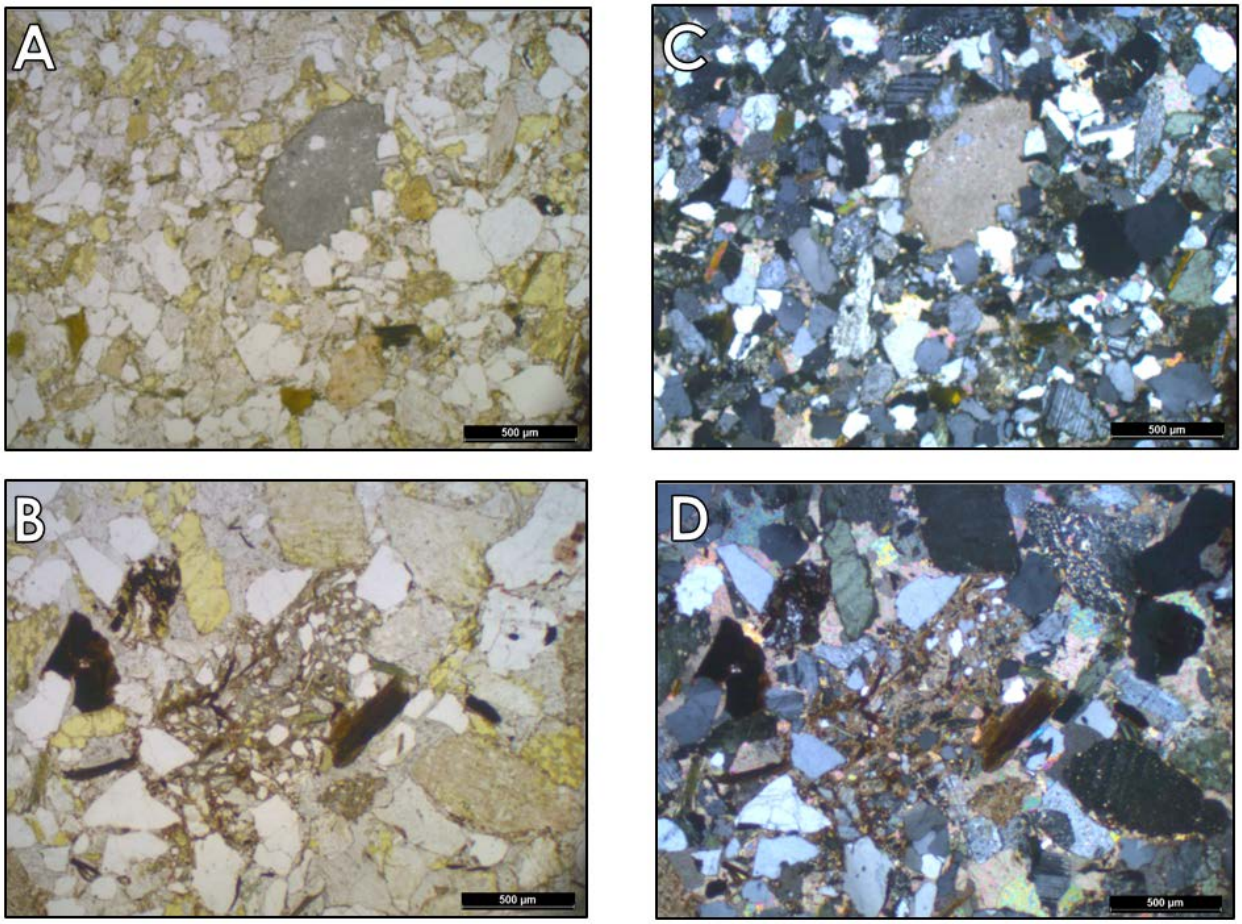

Figure 16: XBXL photomicrographs in plane light (A, B) and cross-polars (C, D). (A, C) shows a rounded lithic clast with minor quartz in a matrix of angular quartz, potassium feldspar, biotite, and glauconite. (B, D) shows an angular lithic clast with abundant quartz in a matrix of angular quartz, potassium feldspar, biotite, and glauconite.

Interpretation

The XBXL lithofacies demonstrates an environment with variable high-energy processes (Fielding, 2006). Cross-beds can be up to 1.5 m thick, but cross-laminae may be only a few centimeters tall, showing variable water depth from very shallow to quite deep (Fielding, 2006). Erosional scours vary as well: a few centimeters into the underlying unit to more than a meter. The depositional environment would have been sediment-choked to form supercritical ripples (Ashely, Southyard, and Boothroyd, 1982). Immature clast composition and angularity indicates close proximity to the Uncompahgre source terrane (Frahme and Vaughn, 1983). Further evidence

of erosive power is in the presence of lithic clasts derived from within the basin (Colburn and West, 1981).

The XBXL is similar to some of the lithofacies recognized in Mack and Rasmussen (1984)'s braided stream and sheetflood facies associations. In their braided stream FA, they found abundant trough cross-bedded sandstone and in their sheetflood FA, rippled sandstone. However, both were associated with siltstone—not observed herein—and more closely associated with other lithofacies—conglomerates, soft-sediment deformation, burrowing—than each other. A close association between dunes and ripples is what defines the XBXL and a better comparison would probably be to the Rees et al. (2017) "Sp" lithofacies, which contain cross-beds and ripples that are interpreted as a high energy lower shoreface environment. The only "missing piece" to the Rees et al. Sp lithofacies are mud drapes, which are not observed in the megaflap.

3.1.1.1.3 MASSIVE EXTENSIVE CONGLOMERATIC SANDSTONE (MECS) LITHOFACIES

Description

The Massive Extensive Conglomeratic Sandstone comprises about 10% of the Honaker Trail Formation but is located in only two positions within the stratigraphy: about 20 meters above the basal carbonate and about 10 meters below the basal carbonate (Figure 17). Most often, there is no more than 10 meters below the basal carbonate exposed, so this portion of the lithofacies is rarely observed. Above the basal carbonate, the unit pinches in and out laterally with an average thickness of 3 meters, reaching up to 6 meters thick. The unit is very well outcropping; in the vertical beds, where it may reach thicknesses of 10 meters.

Despite the impressive outcrops, the unit is poorly consolidated, making sample collection difficult. Angular granule and gravel clasts of potassium feldspar will readily rain off the unit and

the conglomeratic sandstone matrix will crumble. The lithofacies is similar to the composition of the Granule-Cobble Conglomerate, but what sets it apart is its scale: the GCC is rarely more than 2 m thick, while the MECS is usually at least 3 meters thick, and laterally that 3 meters becomes 6 meters.

Bedding of the MECS is not apparent; it appears to be on the scale of the unit itself, up to 6 meters thick. Grading or reverse grading is not apparent, nor are any sedimentary structures of any form. The weathering of this body rounds the rock and the surface may be coated in lichen.

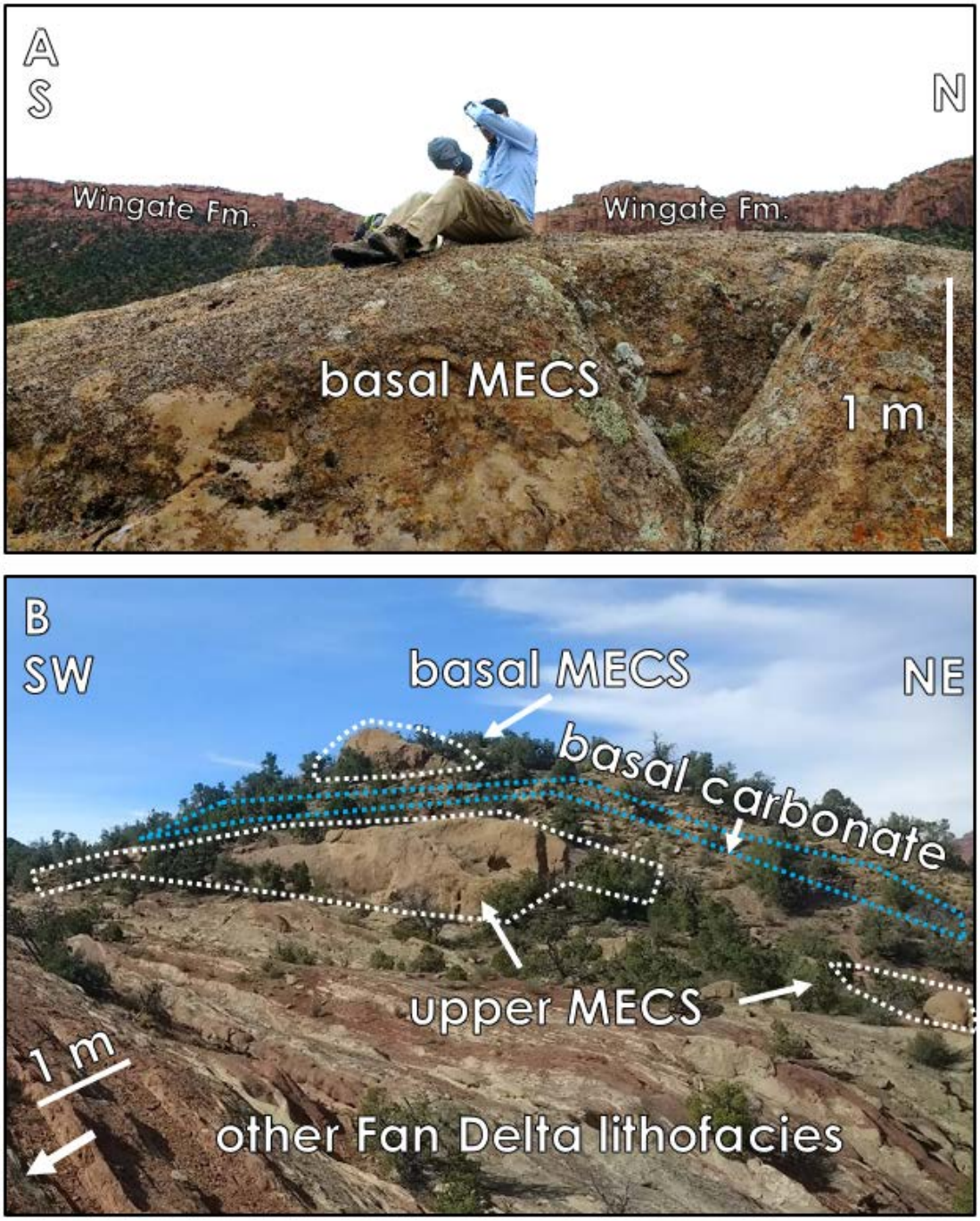

Figure 17: Outcrops of the MECS. (A) is one of the only MCS outcrops below the basal carbonate. This outcrop is the same MECS body as "basal MECS" in (B). (B) Basal and upper MCS, divided by (but not in contact with) the basal carbonate of the Shallow Marine FA. Between the MECS and carbonate and throughout the rest of the image is the Fan Delta FA. Upper MECS here pinches in and out again, which is typical of the unit.

Interpretation

The MECS is curious in its restricted position within the section, only occurring at two times during Honaker Trail deposition. It has no bedding and contains abundant clasts of angular granule - gravel potassium felspar in a matrix of coarse-grained micaceous sandstone. In its two levels in the section, it forms broad bodies that pinch in and out laterally. The massive nature of the body suggests rapid deposition (Kneller and Branney, 1995), while the lenticular shape suggests filling of a channel.

Lack of bedding also permits an interpretation of a debris flow process for deposition (Mack and Rasmussen, 1984; Kneller and Branney, 1995). Mack and Rasmussen (1984) and Sweet (2017) describe similar debris flows from Cutler outcrops 15 km northeast of Fisher Valley (near Gateway, CO). They inferred debris flows based on the large and poorly sorted clast sizes as well as the lack of bedding. Again, near Gateway, Soreghan et al. (2009) also recognized a massive granule conglomerate in their Granule Conglomerate Facies. The Granule Conglomerate Facies is laterally extensive, 1-12 m thick, sharp basal and upper contacts, and may be at best only crudely stratified, which is very similar to the MECS. Soreghan et al. (2009) interpreted this facies as being deposited from hyperconcentrated flood flows or HFFs, which would allow for the massive nature of the body and deposition by a single event. With this interpretation of deposition, Soreghan et al. (2009) suggests a braided river. Regardless of whether the MECS was deposited by a debris flow or hyperconcentrated flood flow, its body shape suggests that it was filling in a channel due to its lateral pinching and swelling.

3.1.1.1.4 GRANULE-COBBLE CONGLOMERATE (GCC) LITHOFACIES

Description

The Granule-Cobble Conglomerate Lithofacies is common and widespread throughout the section, however its packages are thin, typically no more than a meter and often only a few tens of

centimeters (Figure 18). The base of the conglomerate (when exposed) is erosional and locally has erosional relief of a few centimeters to a half meter into the underlying strata. Deeper scours have larger clasts. The basal erosional contact is usually with the Laminated Micaceous Sand Lithofacies, as is the upper sharp contact. Packages of Conglomerate Lithofacies and LMS may be stacked on top of one another. Single conglomerates are typically thicker than the stacked packages. Unlike the Massive Extensive Conglomeratic Sandstone, this lithofacies is not laterally extensive for more than 5 meters and is typically only 2-3 meters wide.

Clast size ranges from granule to cobble. Sorting is poor to very poor. The matrix is medium to very coarse-grained micaceous sandstone. Some of the conglomerates have a distinctive break in clast size between the clasts and matrix; however, others show a full continuum of grain sizes. Clast composition is varied. The most common granule to gravel clasts are potassium feldspar, while pebble to cobble clasts are typically sandstone and carbonate. Rarer clasts include quartz (granule-gravel), intrusive igneous/metamorphic (pebble-cobble), and crinoid fragments. The clasts are typically angular, excluding the quartz and crystalline rocks, which are rounded, and some sandstones and carbonates, which are sub-angular to sub-rounded. Carbonate clasts of the GCC lithofacies are diverse, ranging from mudstones to packstones with fossil assemblages of fusulinids, gastropods, and/or phylloid algae (Figure 19).

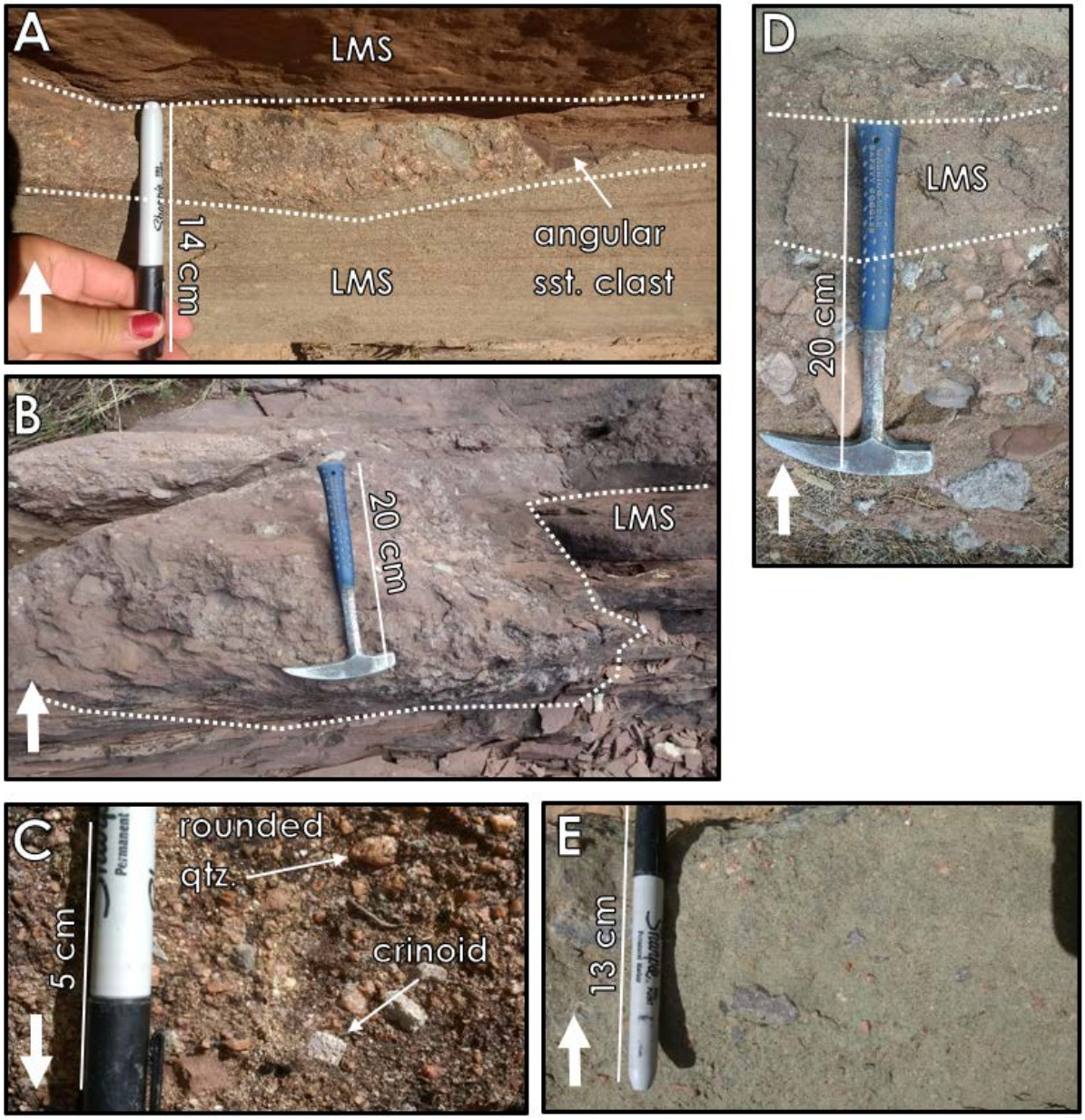

Figure 18: Varieties of the GCC Lithofacies. (A) A 6-cm poorly sorted conglomerate lens of granule-gravel angular potassium feldspar and rounded quartz with some pebble-cobble angular sandstone clasts. The lens erodes into the underlying LMS and is sharply overlain by LMS. (B) A poorly sorted GCC Lithofacies erodes 30 cm into the underlying LMS. (C) A close view of a granule-gravel section of the unit, with abundant angular potassium feldspar and lesser rounded quartz and crinoid clasts. (D) Two packages of GCC interbedded with LMS. The basal conglomerate is dominated by sub-rounded to sub-angular carbonate and sandstone pebbles and cobbles. The upper carbonate has granules and gravels of potassium feldspar and quartz. (E) A massive section of GCC with few and scattered clasts of potassium feldspar, quartz, and sandstone.

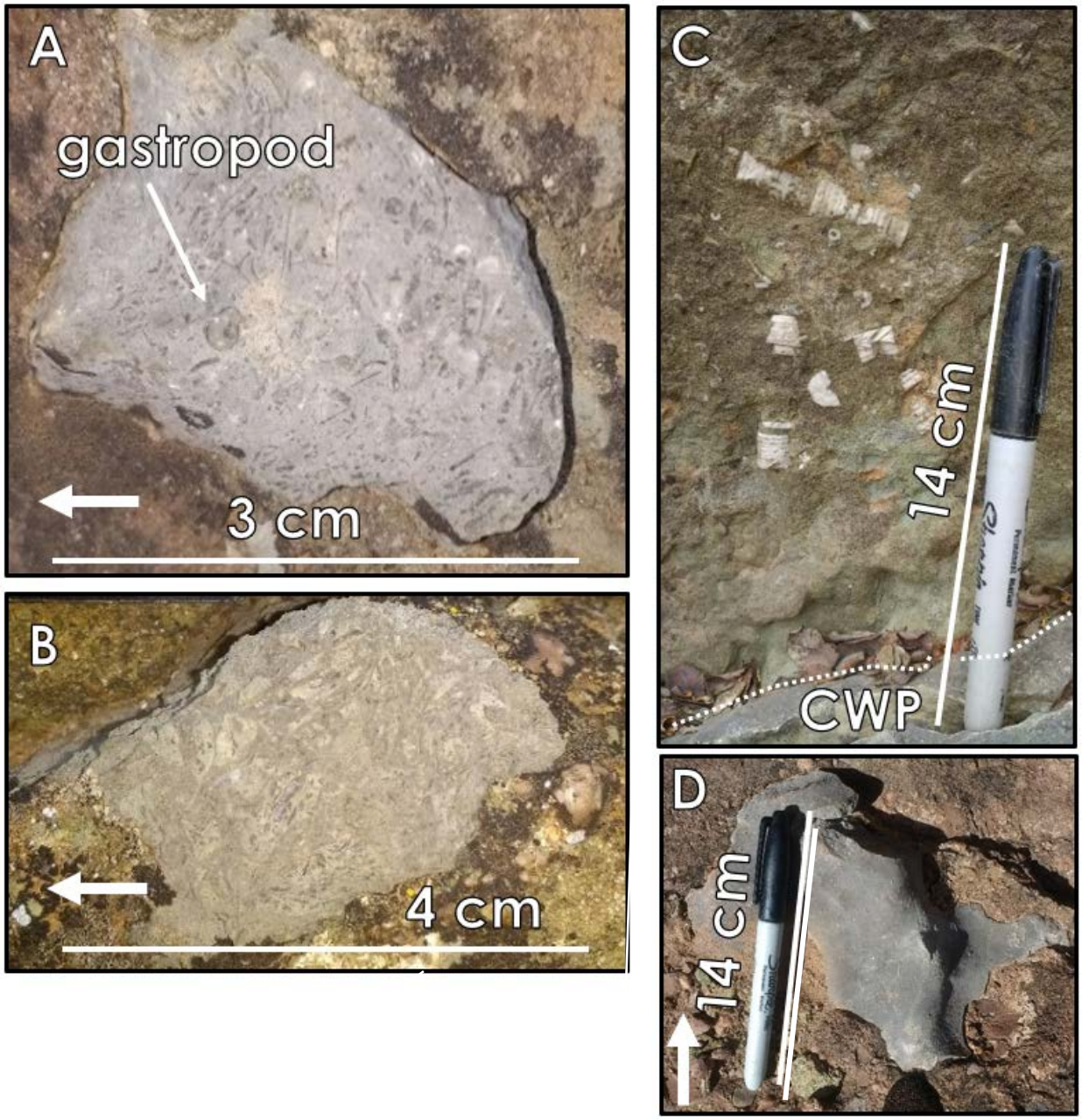

Figure 19: Carbonate clasts of the GCC Lithofacies. (A) A 3-cm, sub-rounded, phylloid algae/gastropod packstone clast. (B) A 4-cm, sub-rounded fusulinid packstone clast. (C) Crinoid stem and fragment clasts ripped up from the underlying Crinoid Wackestone-Packstone. Up is directly into the image. (D) A 15-cm, rounded carbonate clast.

Interpretation

The GCC lithofacies is the most erosive of the FA. Like the XBXL lithofacies, it has deep scours and Uncompahgre-derived sand grains, but it is also erosive with its abundant, large

intraclasts of carbonate and sandstone (Colburn and West, 1981). Additionally, it has rounded pebbles to cobbles of Uncompahgre-derived granite and quartz, as well as granules and gravels of potassium feldspar (Frahme and Vaughn, 1983). The channel-form geometry implies that these were not sheetflood deposits, but that the GCC was deposited from channelized flows (Mack and Rasmussen, 1984). Poor sorting indicates short transport distance and variable current energy and rapid deposition (Frahme and Vaughn, 1983).

Elston et al. (1962) found similar carbonate conglomerates in a Salt Valley probable Cutler unit that unconformably overlaid middle Honaker (formerly the Paradox Member). Figure 4 shows the location of Salt Valley, which is slightly more distal than Fisher and further to the northwest. The clasts were mostly well-rounded, with some sub-rounded to angular pebbles, and many had identifiably Mississippian fossils (Elston et al., 1962), though the non-fossiliferous clasts were similar to top Honaker Trail. Elston et al. (1962) hypothesized that the Mississippian clasts came from the northwestern end of the Uncompahgre Uplift while probable Honaker Trail clasts came from Pennsylvanian carbonates exposed by the rising salt. These Pennsylvanian carbonates could also come from bioherms eroded during lowstand, like those observed by Gianniny and Miskell-Gerhart (2009) near Durango, Colorado. They described Pennsylvanian phylloid algal bioherms, which could produce clasts like those seen in Figure 19-A. Such bioherms could be eroded during lowstand and recycled in the depositional system (Elston et al., 1962).

In their Salt Valley study, Elston et al. (1962) interpreted their carbonate conglomerate lithofacies as at least partly fluvial. Disregarding the carbonate clasts, the GCC is also similar to a Mack and Rasmussen (1984) Cutler conglomerate that they recognized in their channelized streamflood facies association. Alternatively, the GCC could have been deposited in a fan delta's topsets or bottomsets (Rees et al., 2017).

3.1.1.1.5 SOFT-SEDIMENT DEFORMED MICACEOUS SANDSTONE (SSD) LITHOFACIES

Description

The Soft-Sediment Deformed Lithofacies is common, though not particularly thick (typically 5-20 cm) or laterally extensive (less than 3 meters) (Figure 20). It appears throughout the Fan Delta FA both laterally and stratigraphically. It is typically seen in association with the Laminated Micaceous Sandstone Lithofacies, with which it forms sharp basal and upper contacts. This lithofacies is defined by its soft-sediment deformation structures, typically in the form of dewatering structures. These structures are often easily recognizable as alternating bands of red (fine-grained sandstone) and greenish-gray-white (medium-grained sandstone) that have been deformed. The red portions may preferentially weather recessively and the lighter-color portions stick out in wiggly bands. The red-white banding may not always occur and more rarely, the deformation will take place in just the medium-grained sandstone. The break in grain size between colors may be greater or less, making the banding less obvious.

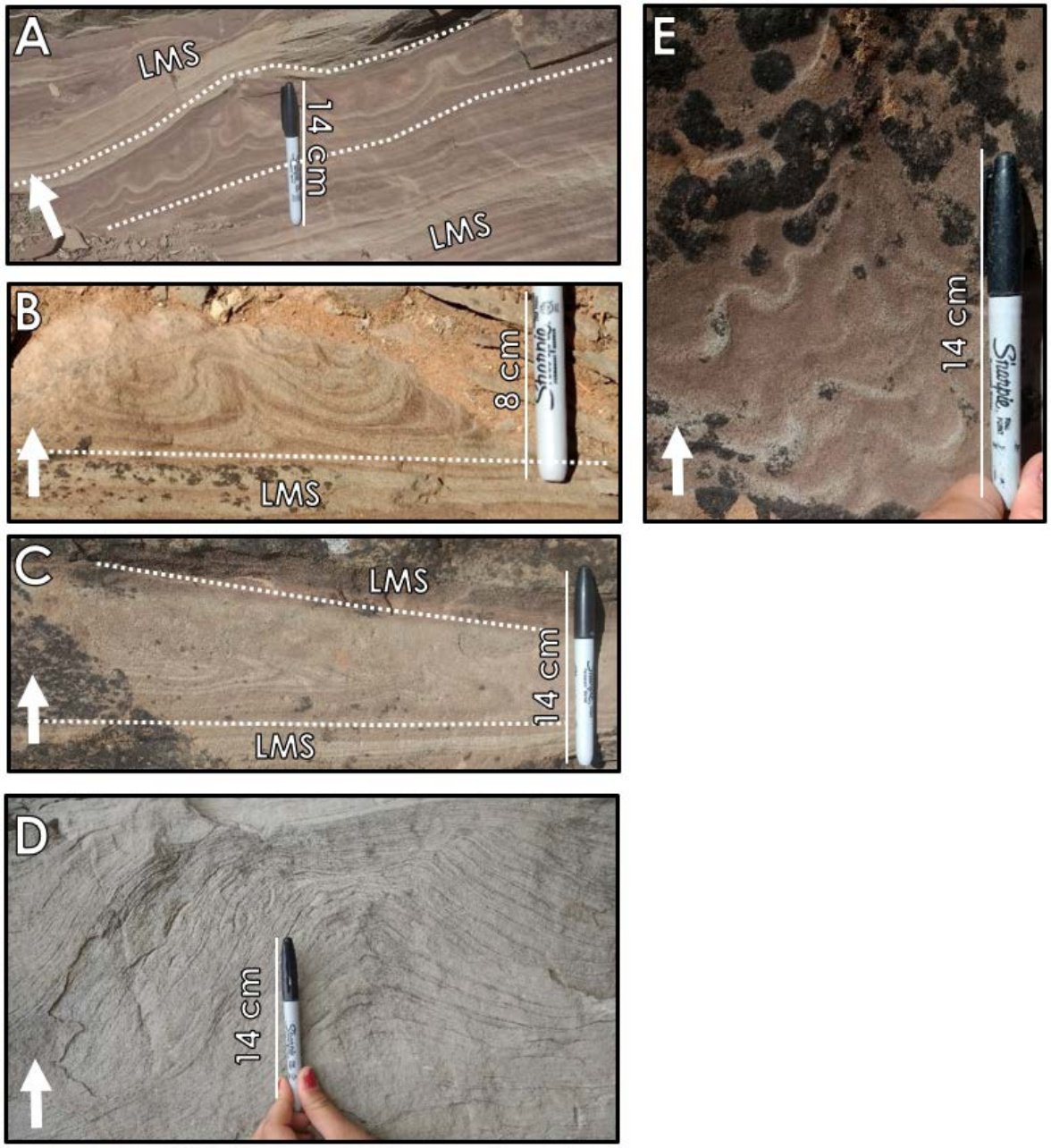

Figure 20: Forms of soft sediment deformation in the SSD lithofacies. (A) A typical outcrop of SSD: SSD is 8 cm thick and under- and overlain sharply with LMS. (B) The most typical morphology and color (red and white) of the SSD's dewatering structures. (C) An uncommon presentation of soft sediment deformation in the SSD. (D) A less common dewatering structure; there is no significant break in grain size (all medium-grained) and no striking difference in color. (E) One of the best examples of how the SSD commonly occurs in fine-grained red sandstone that preferentially weathers compared to its gray, medium-grained laminae.

Interpretation

Soft-sediment deformation often indicates repeated rapid input of sediment on to unlithified, water-saturated sediment; however, it may also be a result of seismicity (Owen et al., 2011; Owen and Moretti, 2011). Mack and Rasmussen (1984) recognize soft sediment deformation in their Cutler Formation sheetflood facies. This Cutler sheetflood facies also contains laminated micaceous sandstone, granule to pebble conglomerates, ripples, and burrowing—features that are also associated with the SSD of the Fisher Valley megaflap. Due to its close relation with the LMS, the possibility that the SSD is a shelf sand should also be considered.

3.1.1.1.6 BURROWED MICACEOUS SANDSTONE (BMS) LITHOFACIES

Description

The Burrowed Micaceous Sandstone Lithofacies (BMS) is very similar to—and associated with—the Laminated Micaceous Sandstone Lithofacies (Figure 21). The sandstone is fine- to medium-grained, red to greenish-gray-white, and thinly to very thinly bedded. The trace fossil behavior may be difficult to impossible to observe without breaking open the apparently LMS along a bedding plane. The BMS is evenly-distributed throughout the section, but rare and only obvious upon close inspection. Typically, it exists in zones within the LMS as several, 2-centimeter beds intermixed with the laminated sandstone. It may be traceable along strike for 3-5 meters, though it is not obvious. Both vertical and horizontal burrows are observed, though horizontal are far more common.

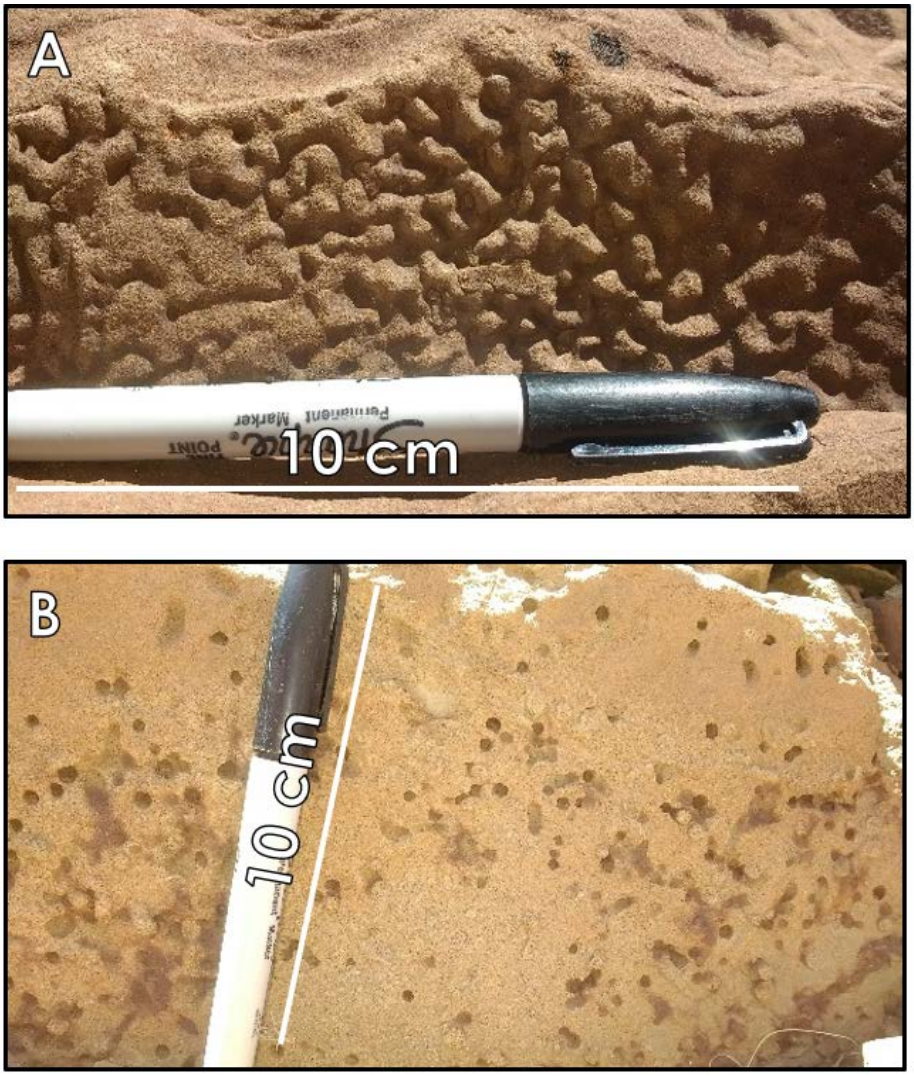

Figure 21: The BMS lithofacies. (A) Horizontal burrows in medium-grained sandstone. Up is directly out of the image. (B) Vertical burrows in medium-grained sandstone. Up is directly out of the image.

Interpretation

Burrowing indicates low environmental stress, where there is sufficient oxygen, tolerable salinity, and enough time for colonization (Taylor and Goldring, 1993). Since the BMS facies is relatively rare in occurrence and thin in extent, we can assume that at least one of these factors was often lacking during megaflap deposition. The BMS facies is very similar to the LMS in aspects beyond its organism activity, and like the LMS, Mack and Rasmussen (1984) recognize it in the Cutler Formation Undifferentiated near Gateway, CO. Here it is associated with not only

laminated micaceous sandstone, but granule to pebble conglomerates, ripples and soft-sediment deformation. Due to its close relation with the LMS, the BMS should also be considered as a possible shelf sand.

3.1.1.1.7 HONAKER TRAIL FORMATION ENVIRONMENTAL INTERPRETATION

The Fisher Valley megaflap Honaker Trail is unusual when compared to its regional makeup due to its high proportion of coarse-grained siliciclastics, which requires a closer examination of its depositional environment. Presented here are two models for the siliciclastic lithofacies detailed above: alluvial fan and fan delta. In the alluvial fan model, Honaker Trail siliciclastics mimic those of the Cutler Formation Undifferentiated deposited near Gateway, CO (Mack and Rasmussen, 1984). The MECS is an alluvial fan debris flow, XBXL and GCC are incised channel flows, and LMS, BMS, and SSD are sheetflood facies. In an alternative fan delta model not based off previous work in the Paradox, the MECS is still a debris flow, but deposited mid-fan. The XBXL is shoreface sands, the GCC deposited in fan delta topsets and bottomsets. Finally, the LMS, BMS, and SSD are deposited in the shelf. A summary of these ideas is presented in Figure 22.

One would want to make the case for the megaflap's Honaker Trail mimicking nearby sedimentation of comparable age, but the alluvial fan model struggles to account for the carbonates that are indeed present in the megaflap. Massive, non-Waltherian, transgressive-regressive changes would have to take place very quickly to account for the lack of environments intermediate to an alluvial fan and an open marine shelf (Gianniny and Simo, 1996). Such changes are observed, especially in the Pennsylvanian with ongoing high amplitude, rapid glacioeustatic changes (Gianniny and Simo, 1996), and have been documented in in the Honaker Trail

Formation; however, it should be noted that this is not the norm (Soreghan and Dickinson, 1994; Gianniny and Simo, 1996).

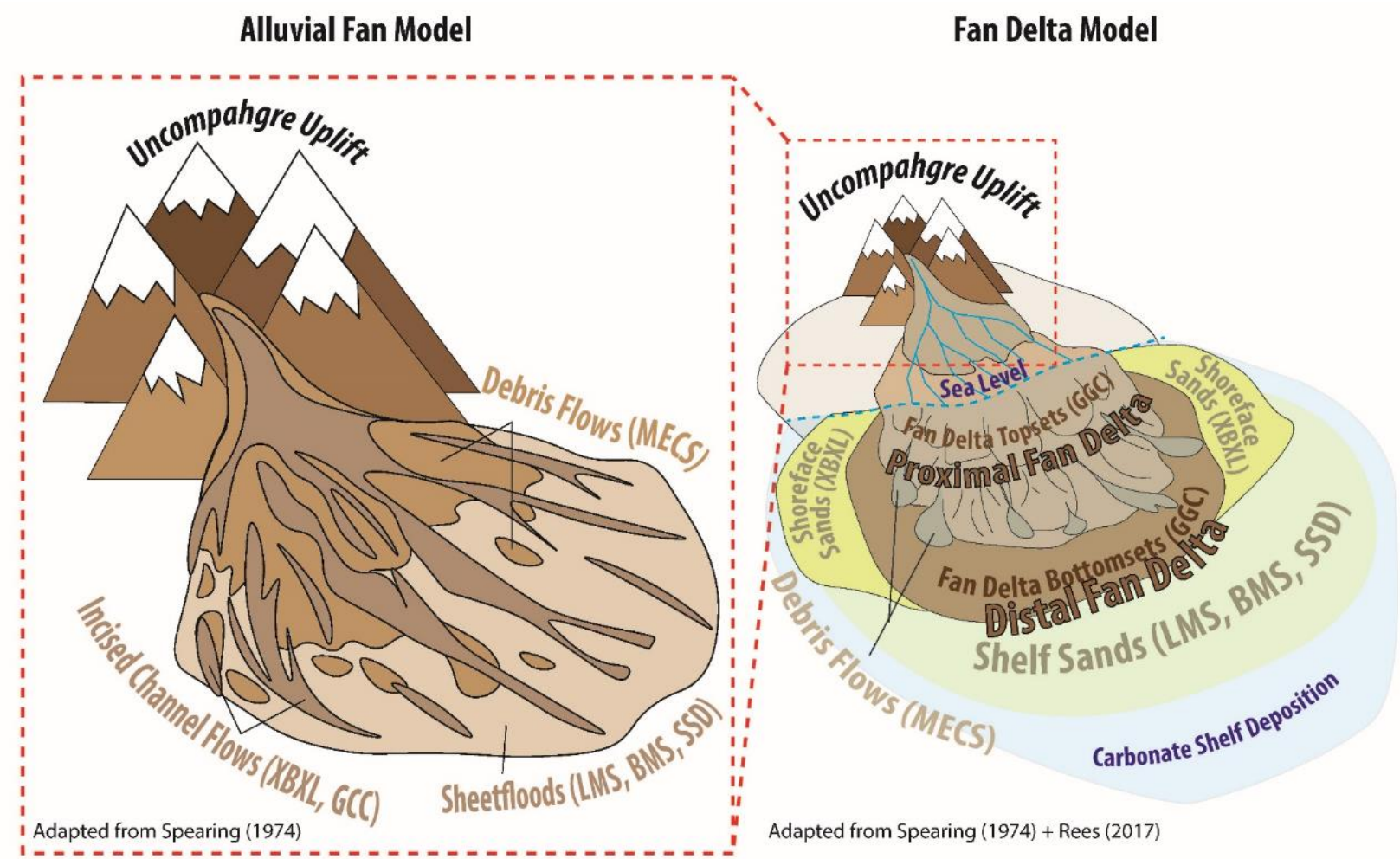

Figure 22: Two models of interpretation for the Honaker Trail megaflap.

3.1.1.2 SHALLOW MARINE CARBONATE FACIES ASSOCIATION

The Shallow Marine Carbonate Facies Association (SMFA) forms two resistant carbonate ridges within the Honaker Trail of the megaflap: the first about 10 meters from the base of the section (referred to as basal carbonate unit) and the second about 10 meters from the top of the section (referred to as upper carbonate unit). These carbonate units, each 6-12 meters thick, are easily traced laterally across the megaflap and contain abundant normal marine invertebrate fossils such as crinoids, brachiopods, and bryozoans. They are under- and overlain by the Fan Delta FA. The contact with the overlying Fan Delta FA is typically erosional. Table 3 lists the lithofacies that comprise the SMFA.

Table 3: Lithofacies of the Shallow Marine Carbonate Facies Association. *FP is never observed in the Basal Carbonate unit.

Lithofacies	Interpretation	Abbreviation	Occurrence
Irregularly Bedded Dolomitic Mudstone Lithofacies	Shelf	IBDM	Common
Crinoidal Wackestone-Packstone Lithofacies	Shelf	CWP	Common
Fusulinid Packstone Lithofacies	Shelf	FP	Common*

3.1.1.2.1 IRREGULARLY BEDDED DOLOMITIC MUDSTONE (IBDM) LITHOFACIES

Description

The Irregularly Bedded Dolomitic Mudstone lithofacies is one of the most common carbonate lithofacies (Figure 23). It is typically laterally extensive along strike for up to 50-100 meters but may also change laterally through gradational lithofacies shifts. Unit thickness ranges from 0.5 m to 6 m. When its upper contact is visible, the contact is erosional and with the Fan Delta FA, GCC lithofacies. The lower contact is undulating but appears conformable with other carbonate lithofacies; it is not otherwise seen due to cover. The IBDM is gray, nodular, lacks obvious bedding planes, and has few fossils. It may be interbedded with any of the other carbonate lithofacies. Although it's a dolomitic mudstone, it may have abundant calcite cement filled vugs. It commonly has black chert nodules or stringers that may extend laterally for 1-3 meters. Locally the mudstone contains abundant sand-sized grains of quartz, potassium feldspar, and biotite, which are angular and sorted to poorly sorted (Figure 24).

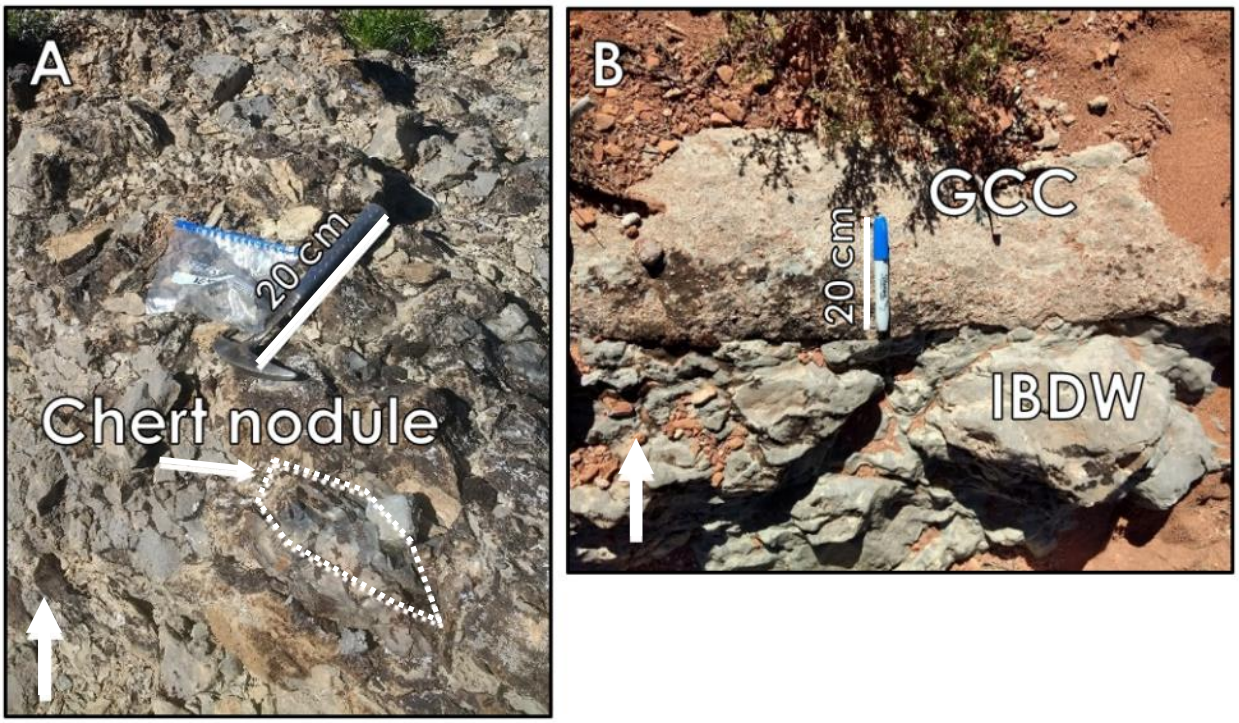

Figure 23: Outcrop photos of the IBDW. (A) Typical IBDW with some 5-10-cm black chert nodules. (B) Typical erosional upper contact (when exposed) with the GCC Lithofacies of the Fan Delta FA

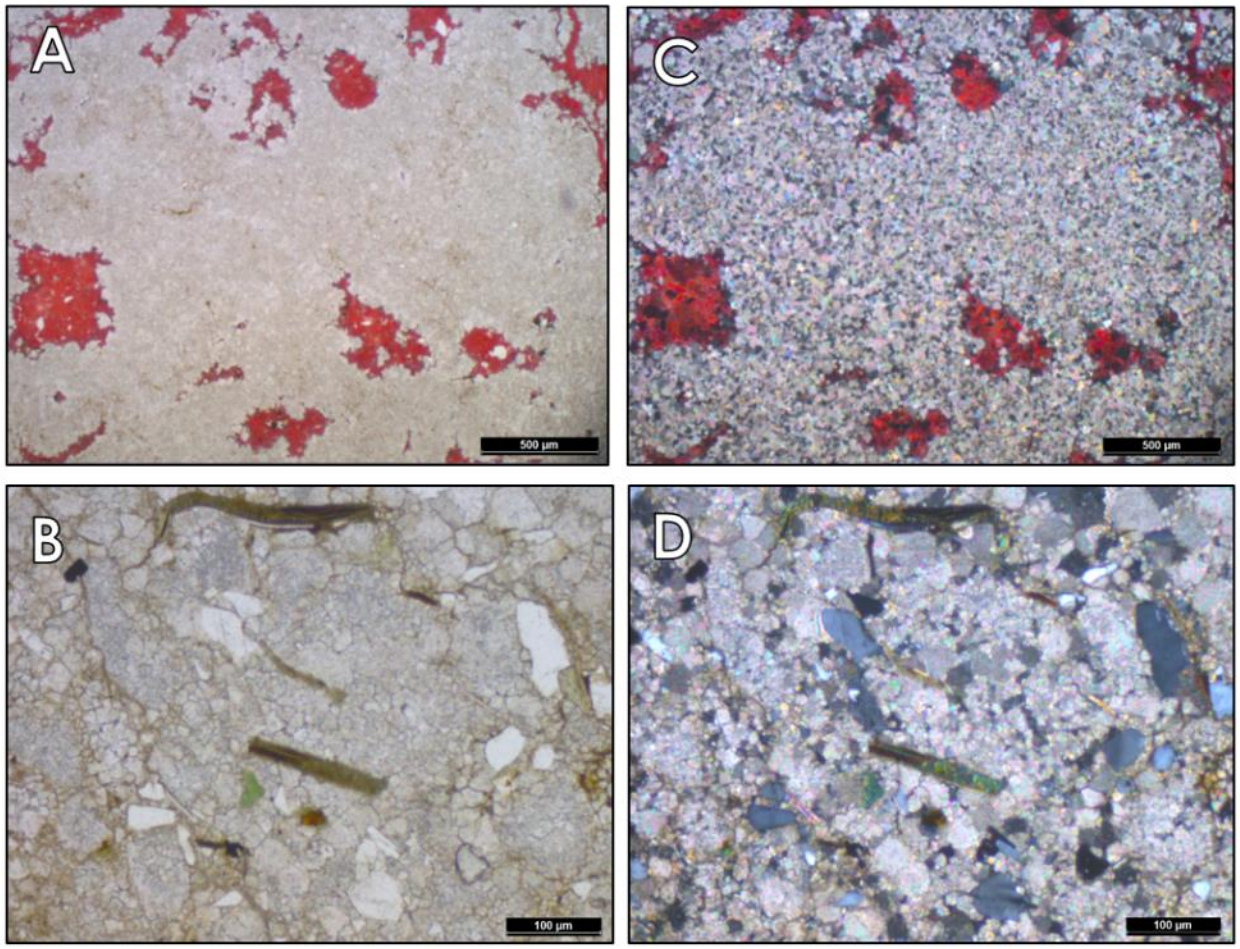

Figure 24: Photomicrographs of the IBC, which show greater variability than in outcrops. Left photos are plane light; right are under crossed polars. (A) Dolomite micrite with calcite-cemented pores. (B) Dolomite with angular grains of quartz, potassium feldspar, and biotite.

Interpretation

The irregular, patchy, wavy bedding and lack of sedimentary structures suggests a large amount of bioturbation (Byers, 1977). Grammer et al. (1996) describes carbonate bioturbation in his Honaker Trail Intermediate Facies-Diverse (IF-D), but this bioturbation is accompanied a moderate amount of broken skeletal grains, including crinoids, brachiopods, fusulinids, and bryozoans, all seen in other lithofacies of the Fisher Valley megaflap's Shelf FA. Bioturbation without fossils may be indicative of a dysaerobic environment (Byers, 1977). Grammer et al.'s (1996) environmental interpretation for the Intermediate Facies-Diverse was a low to moderate

energy shelf with circulation conditions conducive to a diverse faunal assemblage. One model for the IBCW—which is associated with the full fossil assemblage of Grammer et al. (1996)—is that circulation conditions were poor and severely restricted fauna.

3.1.1.2.2 CRINOIDAL WACKESTONE-PACKSTONE (CWP) LITHOFACIES

Description

The Crinoidal Wackestone to Packstone is another common lithofacies of the Shallow Marine Carbonate FA (Figure 25). Typical lithofacies thickness ranges from 0.5 m to 6 meters. It is typically laterally extensive for up to 100 meters along strike but may also change quickly through gradational lithofacies shifts. The most abundant fossils are crinoid columnals that range in size from millimeters to a centimeter in diameter and may be present as single columnals and/or articulated stalks. The crinoids of this facies are also found in the Fan Delta Facies Association and are interpreted to have been eroded and deposited in the overlying sandstone with carbonate clasts. Other fossils may be present, including brachiopods and sponges, though these are rare in outcrop. In thin section, brachiopod and bryozoan fragments are relatively common and as well as trilobites, scleractinian corals, and fusulinids, which are much less common (Figure 26).

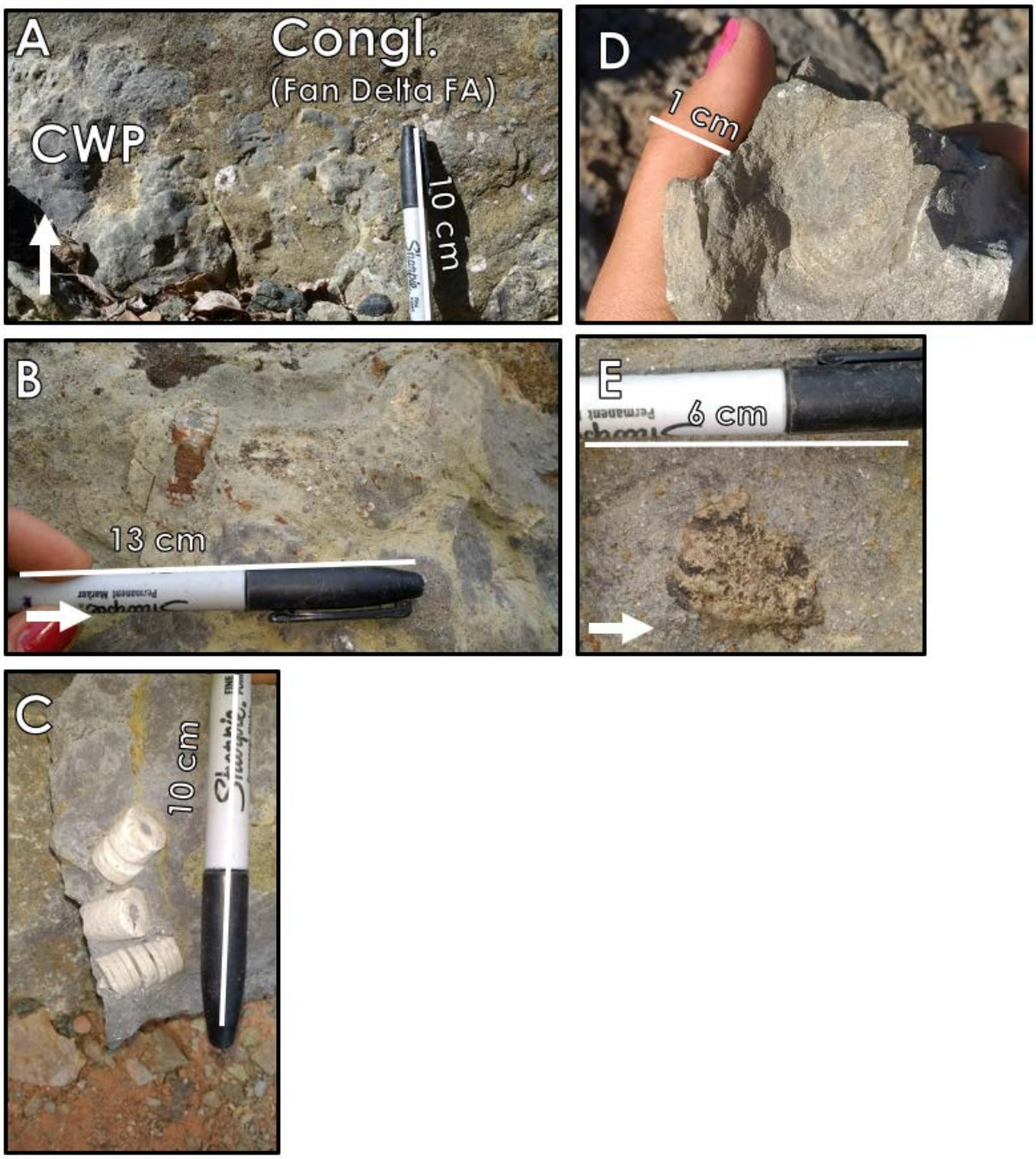

Figure 25: Outcrop photos and photomicrograph of the CWP. (A) Erosional contact between CWP and the Conglomerate of the Fan Delta FA, with ripped-up CWP. (B) 1.5-cm crinoid stem and 1-2-mm crinoid fragments. (C) Crinoid stems can be quite large (2-cm diameter) as seen in this freed chunk of CWP. (D) 2.5-cm brachiopod, an occasional accessory to the CWP. (E) Sponge, an occasional accessory to the CWP. (F) Photomicrograph of the CWP with fossil fragments including brachiopods.

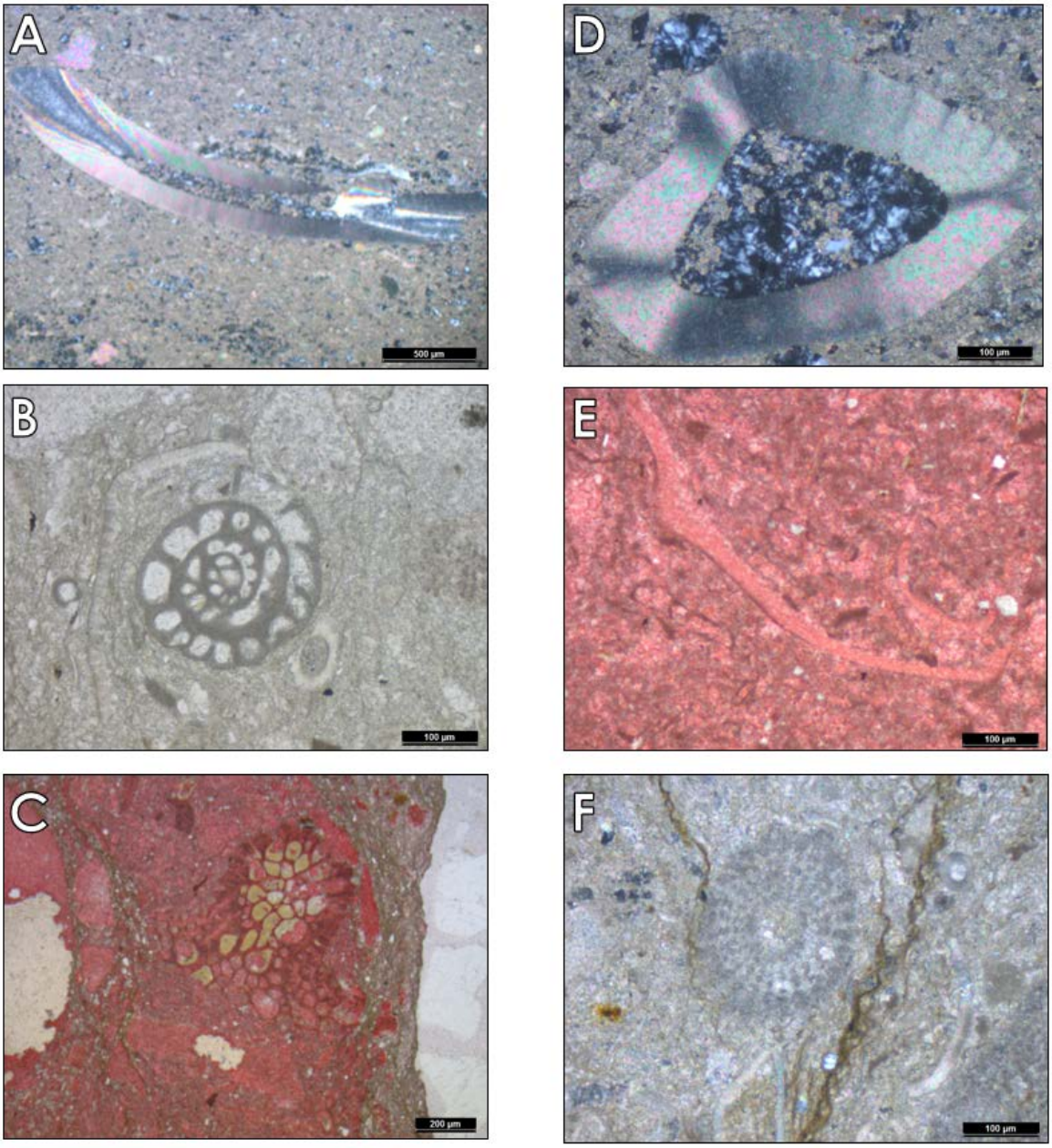

Figure 26: Photomicrographs of the CWP lithofacies. While crinoids are abundant and dominate in hand sample and thin section, the CWP does have accessory fossils. (A) A trilobite fragment. (B) Fusulinids are never found in basal carbonate or CWP in hand sample but may be occasionally found under the microscope like this fusulinid in the CWP basal carbonate. (C) A bryozoan. Bryozoan fragments are common in the CWP; sections as well-preserved as this are rare. (D) A trilobite from the same sample as A. (E) A brachiopod fragment, relatively common in the CWP, at least under the microscope. (F) Echinoid spine.

Interpretation

The CWP is relatively similar to Grammer et al.'s (1996) Intermediate Facies-Diverse (IF-D), which he observed in the Honaker Trail of southeastern Utah along the San Juan River (Figure 4). The ID-F is a wackestone to packstone with a diverse fossil assemblage of crinoids, brachiopods, forams including fusulinids, molluscs, bryozoans, and subordinate phylloid algae. The CWP is dominated by crinoids, but also includes subordinate brachiopods, fusulinids, and bryozoans—as well as other fauna indicative of diversity (trilobites, scleractinian corals). Grammer et al. (1996) also describes thin to medium-scale bedding (consistent with CWP), the presence of sand grains mostly in the form of quartz (consistent), and rare cross-bedding (not observed). Overall, the CWP is very similar to the IF-D. Grammer et al. (1996) interprets the IF-D as a low to moderate energy shelf with good circulation. This interpretation of the CWP is consistent with the IBDW, which is interpreted as restricted IF-D. Another facies comparison can be achieved with Gianniny and Simo's (1996) Skeletal Limestone-Mud Supported lithofacies, observed near Mexican Hat, Utah, slightly west of Grammer et al.'s 1996 study. The Skeletal Limestone-Mud Supported is a wackestone to packstone dominated by crinoids, brachiopods, peloids, and quartz grains, with subordinate bryozoans, brachiopods, and phylloid algae. Like the CWP, many of Gianniny and Simo's (1996) crinoids are articulated stems, as opposed to merely fragments. Gianniny and Simo (1996) interpret their lithofacies as similarly to Grammer et al (1996), though Gianniny and Simo (1996) suggest that their lithofacies may also be present in the dysaerobic zone as the shelf starts to drop off. This interpretation would fit with the CWP's association with the IBDW, which is likely dysaerobic based on lack of fossils.

3.1.1.2.3 FUSULINID PACKSTONE (FP) LITHOFACIES

Description

The Fusulinid Packstone Lithofacies is less common than the other carbonate lithofacies and is not present in the basal carbonate unit of the Shallow Marine FA (Figure 27). Weathered color is a medium-gray and maximum thickness of this package is typically no more than 10-20 cm, although may be laterally extensive for up to 50 m. Gradual facies shifts are not observed with the Fusulinid Packstone; its contacts with other units are covered. It contains abundant fusulinids in a lime mud matrix, with some angular, sorted quartz grains and minor fossil debris.

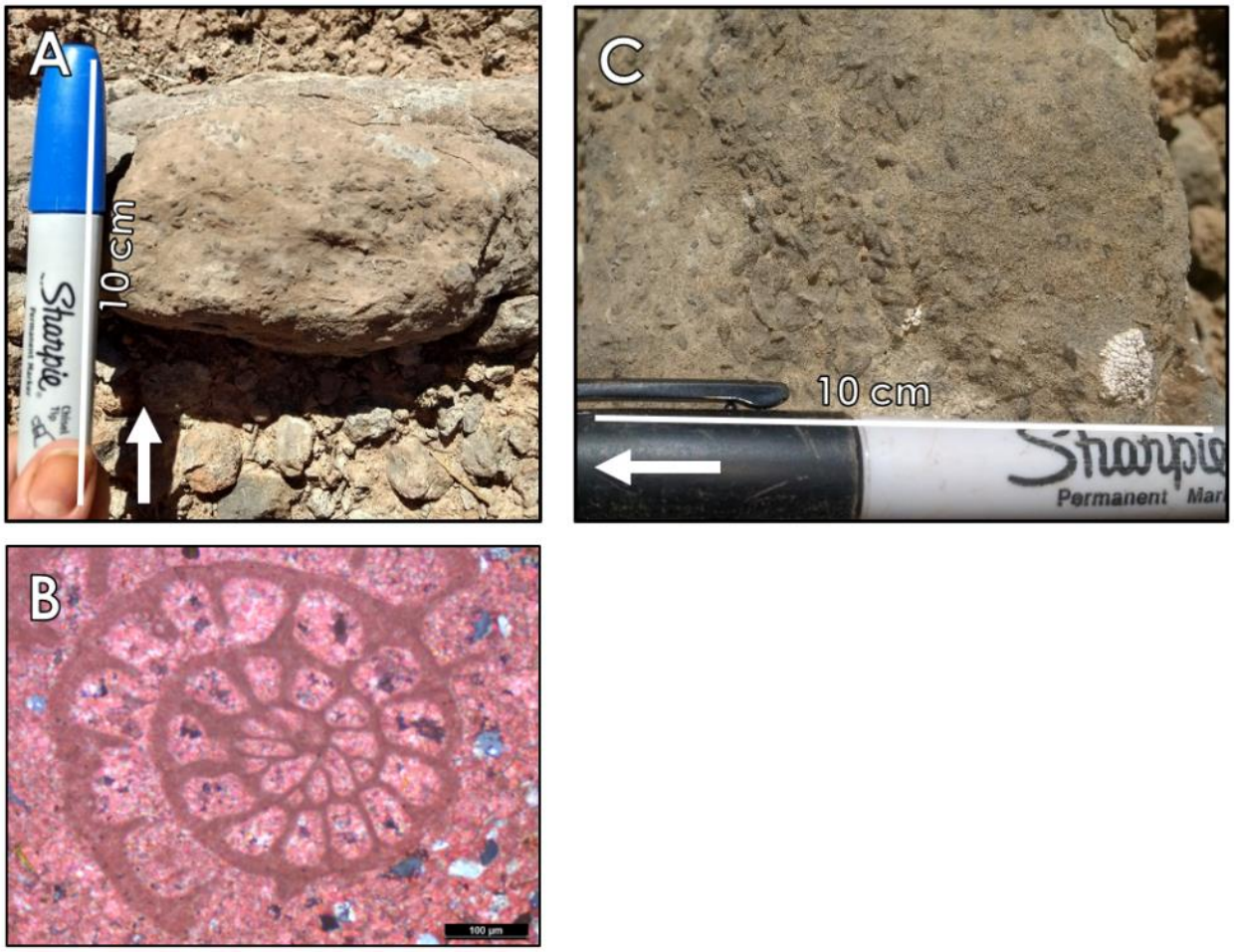

Figure 27: Outcrop photos and photomicrograph of the FP lithofacies. (A) Typical outcrop exposure of the FP. (B) Photomicrograph of a fusulinid. (C) Thin section photomicrograph of a fusulinid grain (stained /plane light).

Interpretation

The FP is similar to Grammer et al.'s (1996) Skeletal Capping Facies-Fusulinid lithofacies, a wackestone to packstone, with abundant fusulinids and other minor fauna. The FP also bears similarity to Gianniny and Simo's (1996) Skeletal Limestone-Grain Supported, which is a grainstone dominated by fusulinids with lesser peloids and skeletal fragments. Both authors interpreted their lithofacies as a low to moderate energy shelf.

3.1.2 CUTLER FORMATION

While the Fisher Valley megaflap's Honaker Trail Formation shows the stratigraphic interplay between an alluvial fan delta and shallow marine depositional system, the Lower Cutler Formation is a purely nonmarine, complex braided river system with local eolian reworking into small dunes. There are no carbonate strata and no evidence of marine influence. The transition from Honaker Trail to Cutler Formation facies is abrupt and obvious based on color, as deep reds and pale greenish-gray-whites of the Honaker Trail sandstones abruptly shift to the deep purple sandstones of the Lower Cutler Formation, with no overlap or gradational transition. Even the local red rocks within Fisher Valley Cutler Formation are distinct from those of the Honaker Trail in that they are a more vibrant red and have white reduction spots. The lithofacies of the Fisher Valley megaflap's Cutler Formation fit a single facies association—the Braided River Facies Association—which has several lithofacies: Laminated Micaceous Sandstone, Cross-Bedded Sandstone, Massive Sandstone, Bedded to Cross-Bedded Sandstone, Burrowed Micaceous Sandstone, and Pinstriped Orange Sandstone (Table 4).

Table 4: Lithofacies of the Braided River Facies Association.

Lithofacies	Interpretation	Abbreviation	Occurrence
Laminated Micaceous Sandstone	Floodplain	LMS	Common
Conglomeratic Cross-Bedded Sandstone	Channel	CXB	Common
Massive Sandstone	Bioturbated floodplain	MS	Common
Fine-Grained Red Sandstone	Channel	FGR	Common
Burrowed Fine-Grained Red Sandstone	Floodplain	BFGR	Occasional
Pinstriped Orange Sandstone	Floodplain reworking	POS	Occasional

3.1.2.1 LAMINATED MICACEOUS SANDSTONE (LMS) LITHOFACIES

Description

The Laminated Micaceous Sandstone lithofacies (LMS) is traceable along strike for no more than 10 m, due to alluvial cover (Figure 28). Basal contacts are typically sharp; upper contacts vary from sharp to gradational. Outcrop color ranges from tan to brown to red. Laminated Micaceous Sandstone of the Cutler Formation has a crucial difference from the LMS of Honaker Trail Formation: grain size. Cutler LMS is medium to coarse-grained with conglomeratic lenses. The clasts of these conglomerates are diverse but are most commonly rounded pebbles of quartz and rounded cobbles of intrusive igneous and metamorphic rock, with lesser granules and gravels of angular potassium feldspar. Sand-sized grains are composed of quartz, potassium feldspar, and biotite (Figure 29). Locally flame structures are present.

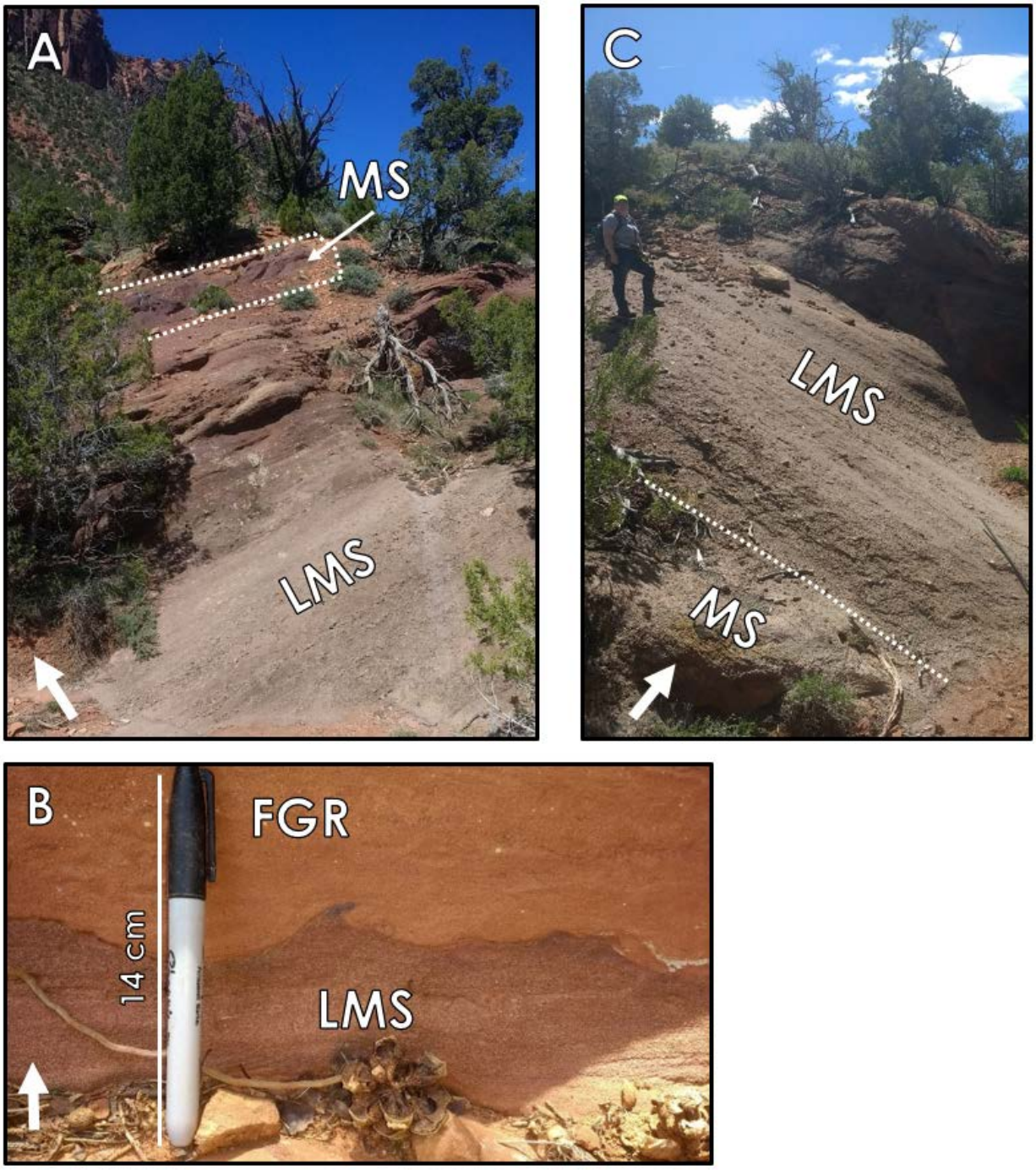

Figure 28: Outcrop photographs of the Laminated Micaceous Sandstone Lithofacies (LMS). (A) A typical succession of varied LMS with gravel-pebble lenses near the base. Deep purple LMS near top. (B) A rare exposed contact between LMS & MS facies in the Cutler Fm. LMS is overlain by FGR. Flame structures mark the contact between the distinctly deep red LMS and orangey-red FGR. (C) Massive Sandstone overlain by LMS, which has gravel-pebble lenses.

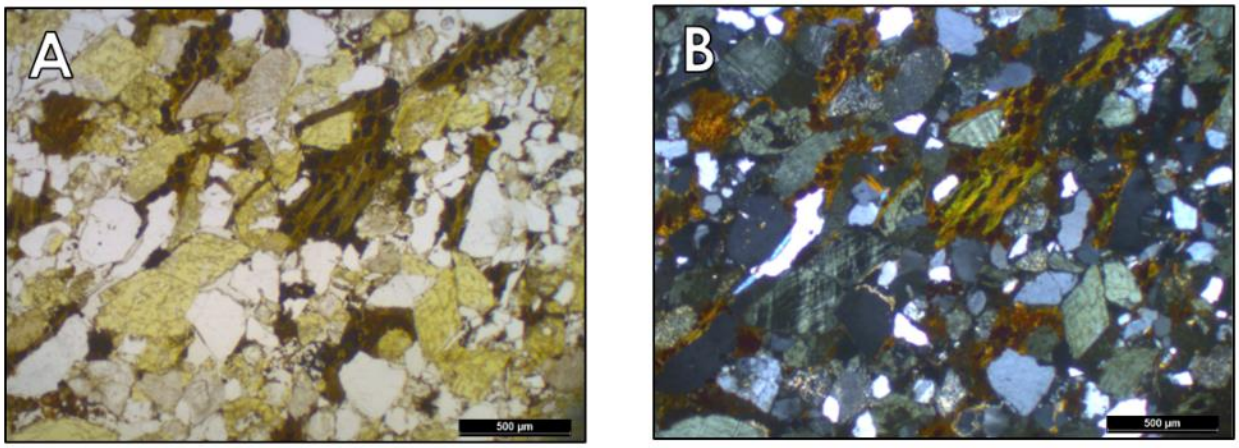

Figure 29: Photomicrographs of the LS lithofacies. (A) is plane light and (B) is under crossed polars. The unit is dominated by potassium feldspar, quartz, and biotite.

Interpretation

The LMS has lower to upper plane beds, indicating moderate energy capable of moving pebbles and cobbles (Fielding, 2006). Rapid deposition is supported by the presence of flame structures (Dasgupta, 1998). LMS grain composition is angular and immature, derived from the nearby Uncompahgre uplift and probable recycled Honaker Trail siliciclastics (Frahme and Vaughn, 1983). Mack and Rasmussen (1984) recognize laminated micaceous sandstone with soft-sediment deformation in their water-laid sheetflood facies association in the Cuter Formation near Gateway, CO. Similar to the LMS, the sheetflood facies has red to orange outcrop color, thickness from half a meter to 12 meters, and an association with granule to pebble conglomerates, burrowing, and soft-sediment deformation. A distinctive difference between the two lithofacies is that the sheetflood facies at Gateway commonly has root traces, while the LMS in the megaflap does not. Mack and Rasmussen (1984) interpreted periods of depositional quiescence in their sheetflood facies, but a major portion of the evidence for breaks in deposition was that they saw evidence of soil formation with root traces, which the LMS does not have.

3.1.2.2 CROSS-BEDDED SANDSTONE (XBS) LITHOFACIES

Description

Due to alluvial cover, the Cross-Bedded Sandstone lithofacies (XBS) may be traced along strike for only 10 m at most. Basal and upper contacts are typically erosional. It is evenly distributed both laterally and stratigraphically. This lithofacies is a red to white, medium to very coarse-grained, cross-bedded, sorted, micaceous sandstone to granule-gravel conglomerate. Conglomerate clasts are dominantly angular potassium feldspar, with subordinate rounded quartz. The sandstone matrix is composed of quartz, potassium feldspar, and micas. Cross beds are typically half a meter thick. It is distinctly different from the Honaker Trail's Cross-Bedded-Cross-Laminated Micaceous Sandstone in its grain size; while Honaker Trail cross-beds are fine- to medium-grained, Cutler cross-beds are medium to very coarse-grained sandstone or even true granule-gravel conglomerates (Figure 30).

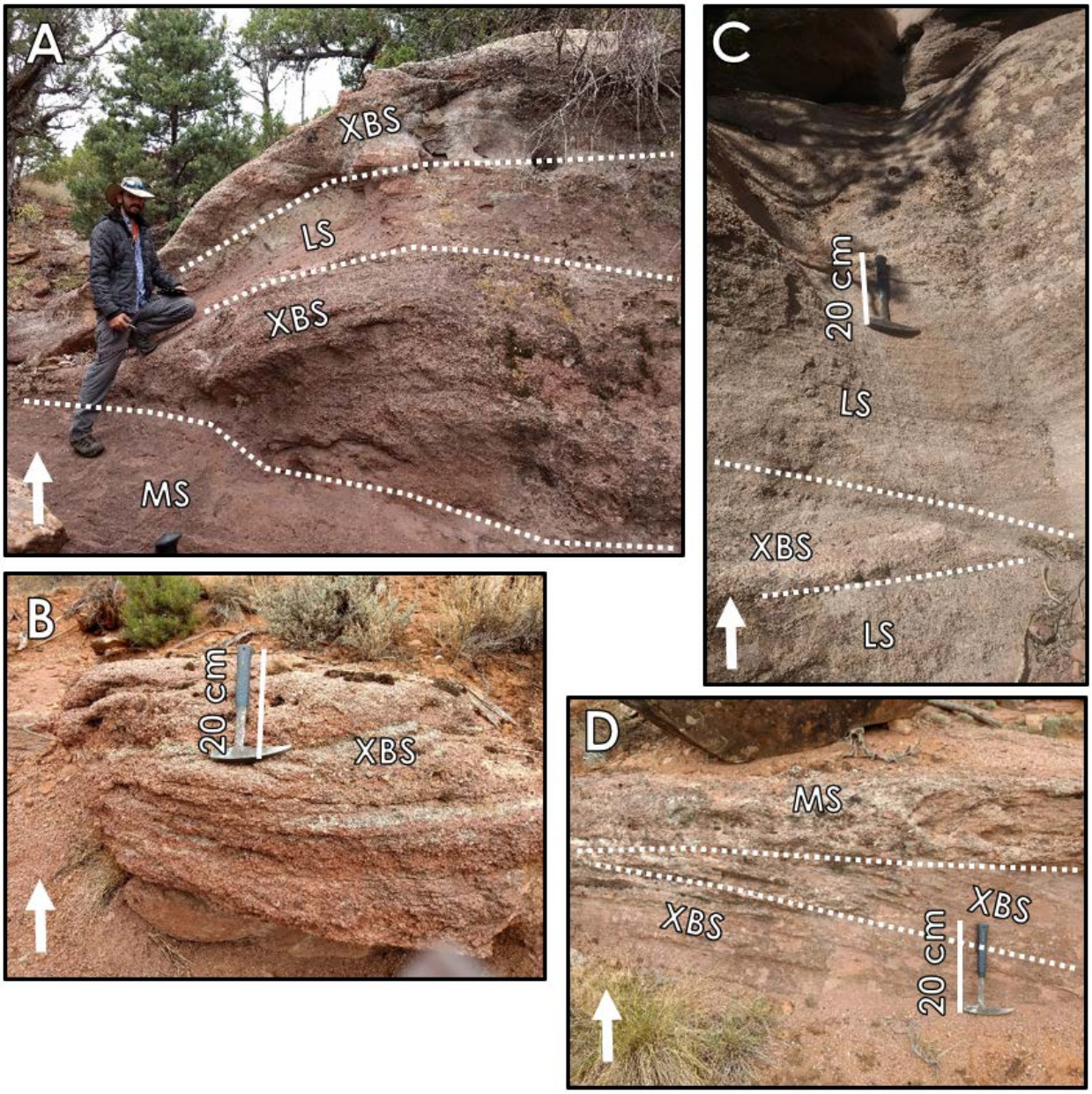

Figure 30: XBS lithofacies outcrop photos. (A) A typically complex outcrop with basal MS eroded into by the XBS. LS roughly overlies XBS before being truncated by XBS. (B) Very coarse sandstone to granule-gravel conglomerate, cross-bedded. Such coarse cross-beds are typical of the XBS and distinctly different from any Honaker strata. (C) Basal LS overlain by XBS, which is sharply truncated by LS. (D) Cross-beds of XBS that coarsen upward before deposition of very coarse to granule-gravel MS.

Interpretation

The XBS lithofacies is high energy with its dunes and commonly very coarse-grained sandstones and granule-gravel conglomerates (Fielding, 2006). The dominant clast in the conglomerates is potassium feldspar, indicating very rapid shedding off the Uncompahgre Uplift as some dunes are mostly composed of feldspar granules (Frahme and Vaughn, 1983). Mack and Rasmussen (1984) recognize similar facies in the Cutler at Gateway in their Braided-Stream Facies: grain size from fine-grained sand to granules, trough cross-beds, and lenses of coarser-grained sediment. In their interpretation, the dunes are deposited in the braided river channels during high water conditions (Williams, 1971; Mack and Rasmussen, 1984).

3.1.2.3 MASSIVE SANDSTONE (MS) LITHOFACIES

Description

The Massive Sandstone (MS) lithofacies is common, though easily covered by alluvium and probably more extensive than it appears. Laterally it is expressed at the surface as zones that grade in and out of deep purple dirt, but true outcrop may be traced for no more than 10 m laterally. It is massive, micaceous, brown to deep purple with white reduction spots. The lithofacies is a medium to very coarse-grained, massive sandstone with well-rounded pebbles and cobbles of intrusive igneous and metamorphics and pebbles of rounded quartz and potassium feldspar and angular to sub-angular granules and gravels of potassium feldspar and quartz (Figure 31 and 32). It may occasionally have extremely large (> 20 cm) out-sized clasts of sandstone (Figure 31-C).

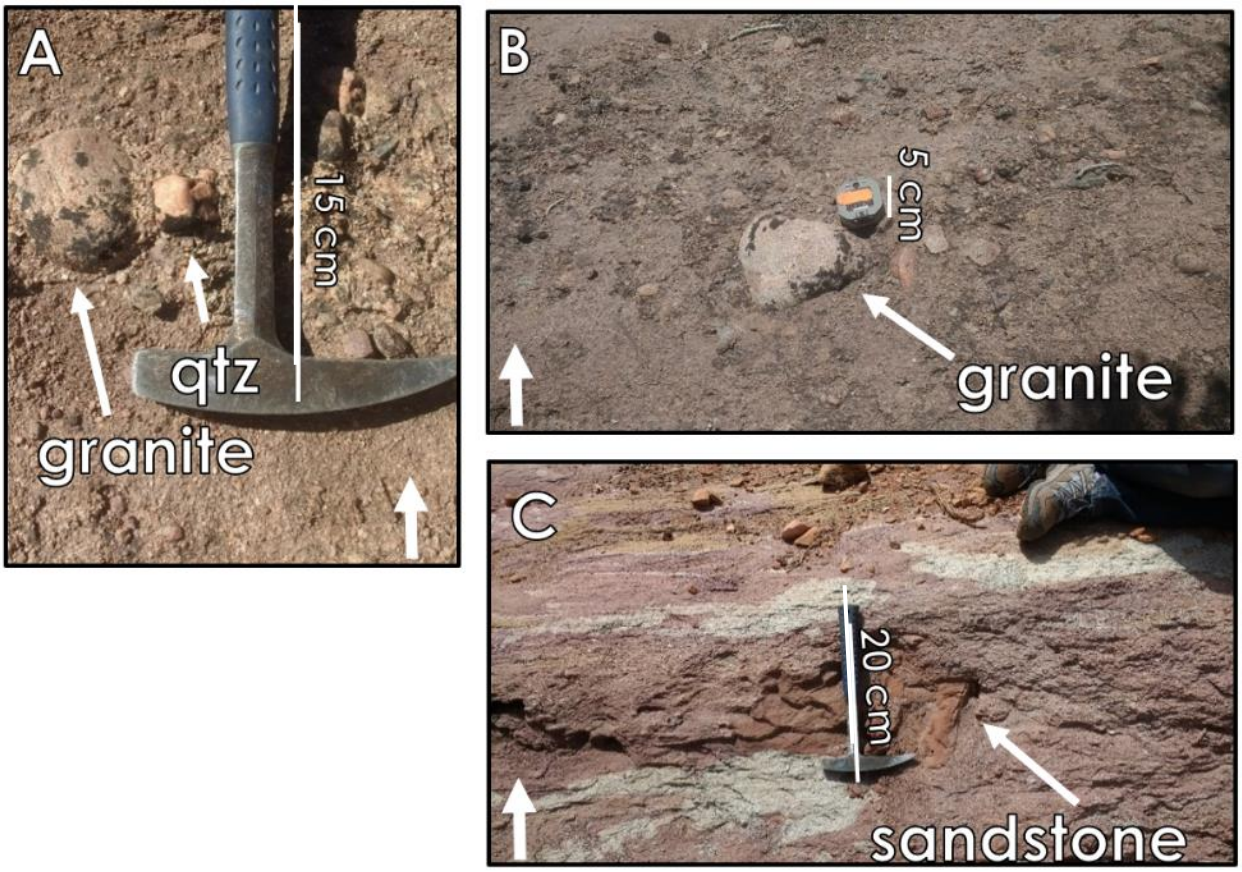

Figure 31: MS lithofacies outcrop photos. (A) A very coarse sandstone with rounded pebbles of quartz and cobbles of granite. (B) A rounded 10-cm granite clast. (C) A 25-cm wide sandstone clast supported by coarse to very-coarse-grained matrix of the Massive Sandstone.

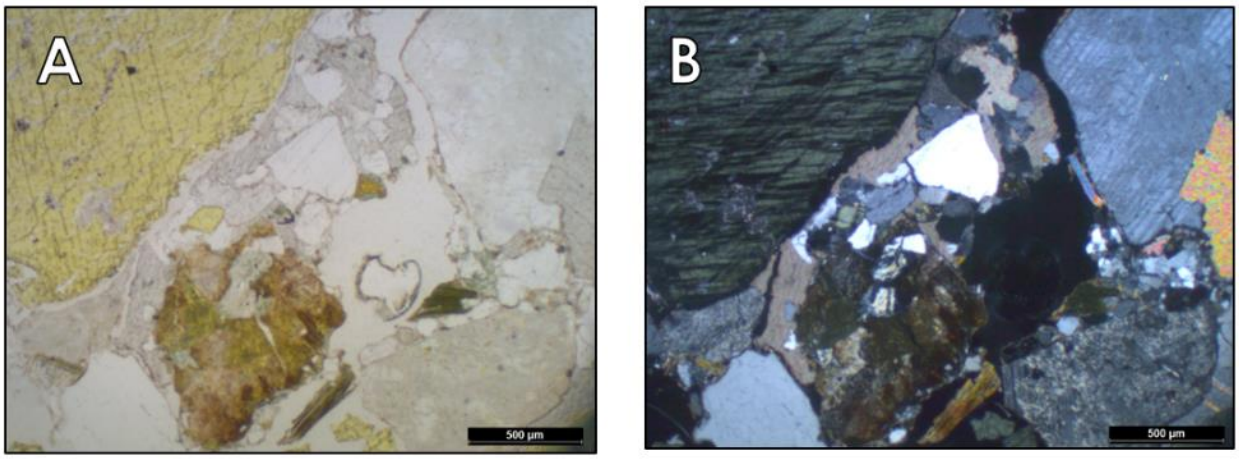

Figure 32: Photomicrographs of the Massive Sandstone lithofacies with (A) in plane light and (B) in crossed polars. MS is dominated by potassium feldspar, quartz, and biotite as seen here.

Interpretation

The structureless nature and poor sorting of this coarse-grained lithofacies, suggests deposition under laminar flow in a concentrated debris flow (Mack and Rasmussen, 1984). Mack and Rasmussen observe Cutler Formation debris flows near Gateway, where boulder-sized clasts are not uncommon. The MS has some near boulder-sized clasts (Figure 31-C) and the reason it may not have more may simply be a matter of proximity to the source; while Fisher Valley may be proximal to the Uncompahgre Uplift, Mack and Rasmussen's 1984 study was undertaken directly adjacent to the frontal fault of the Uncompahgre.

3.1.2.4 FINE-GRAINED RED SANDSTONE (FGR) LITHOFACIES

Description

The Fine-Grained Red Sandstone (FGR) lithofacies thickness ranges from 10 cm to 8 m. Laterally, it can be extensive and traced up to 50 m, which is unusual for the megaflap's Cutler units. Bedding thickness ranges from very thin to thick beds. The lithofacies is a fine-grained, red to tan, micaceous, laminated sandstone, which commonly displays white reduction spots. Bedding ranges from very thin to very thick, with thick to very thick beds and cross-beds most common. Grains are sorted, sub-rounded quartz, potassium feldspar, biotite, and glauconite (Figure 33, 34).

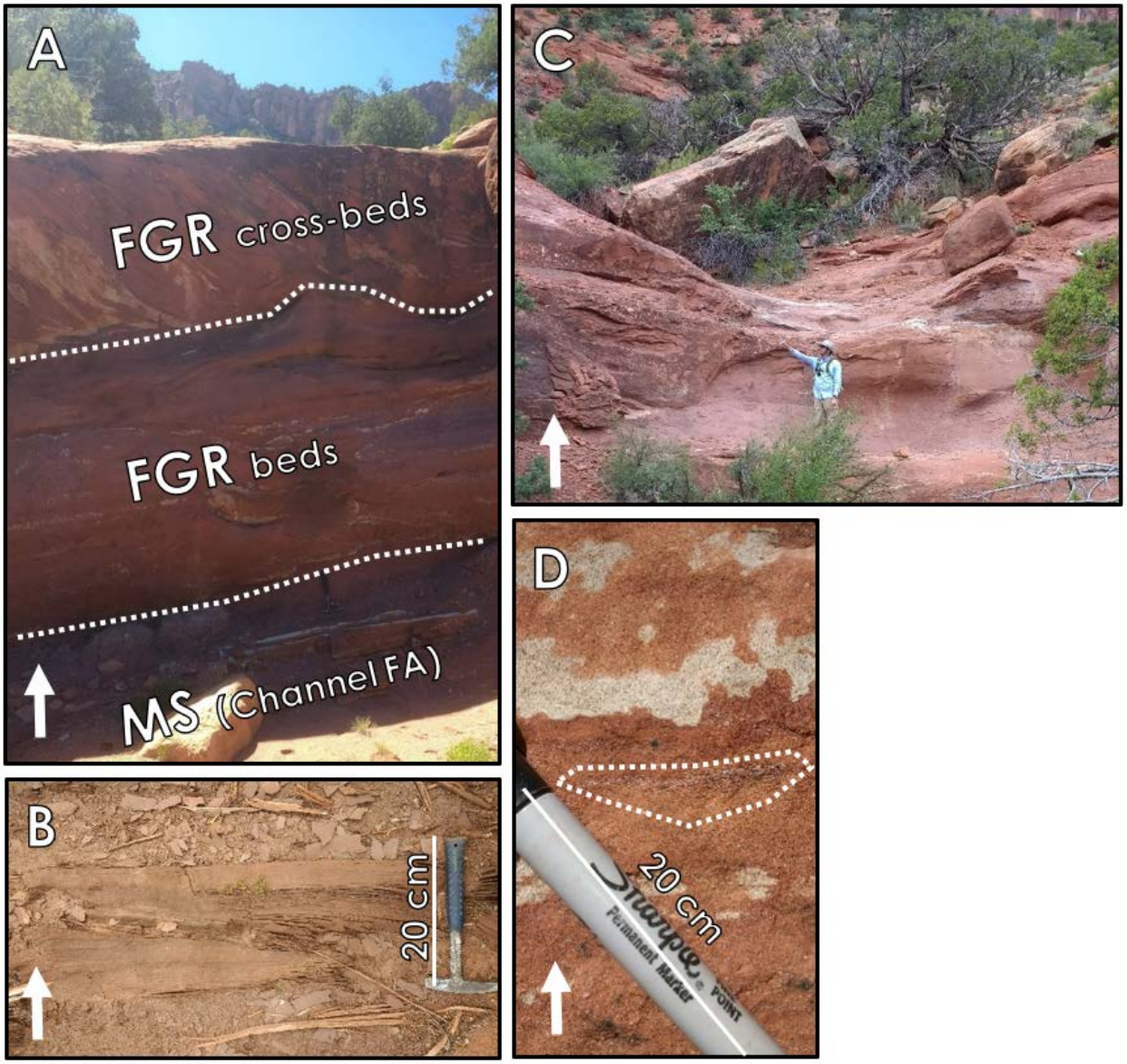

Figure 33: FGR Lithofacies outcrop photos. (A) Massive Sand is overlain by bedded FGR, which is overlain by cross-bedded FGR. (B) FGR may be thin to very thinly bedded occasionally. (C) This entire outcrop photo is FGR, showing how thick and extensive the unit may be. (D) FGR may sometimes have medium to coarse-grained lenses in its fine- to medium-grained sandstones.

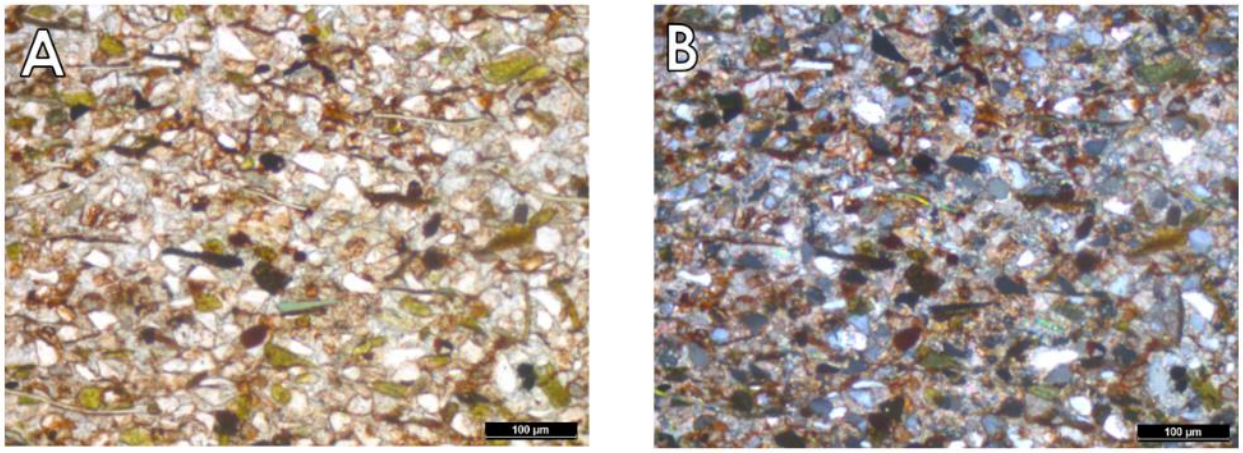

Figure 34: FGR photomicrographs; A is plane light with B in crossed polars. Sorted, sub-rounded quartz, potassium feldspar, biotite, and glauconite.

Interpretation

The FGR is finer-grained and better sorted than other Cutler units and appears to be more oxidized. It has lower to upper plane beds, indicating moderate energy capable of moving pebbles and cobbles (Fielding, 2006). Its most comparable facies, like the LMS, is Mack and Rasmussen's (1984) sheetflood facies association laminated sandstone in the Cutler near Gateway. It should be noted that FGR and LMS are assigned different lithofacies for a reason—FGR is red, fine-grained, sub-rounded, well-sorted, and thickly bedded, while LMS variably colored, medium-grained, angular, unsorted, and medium-bedded. Clast composition is comparable, but the FGR sandstone appears to be less immature than its LMS counterpart.

3.1.2.5 BURROWED MICACEOUS SANDSTONE (BMS) LITHOFACIES

Description

This unit is very similar to the burrowed lithofacies of the Honaker Trail Formation. Unit thickness ranges from 10-20 centimeters and there are no observable contacts. It may be traced along strike for no more than 2-3 meters, but it usually outcrops in gullies, so it can be inferred to be more laterally continuous. It is a very fine- to medium-grained, micaceous, laminated sandstone

disrupted by burrowing (Figure 35). Burrows are horizontal, typically 1/3 cm in diameter, and irregularly wind and cross-cut one another on bedding planes.

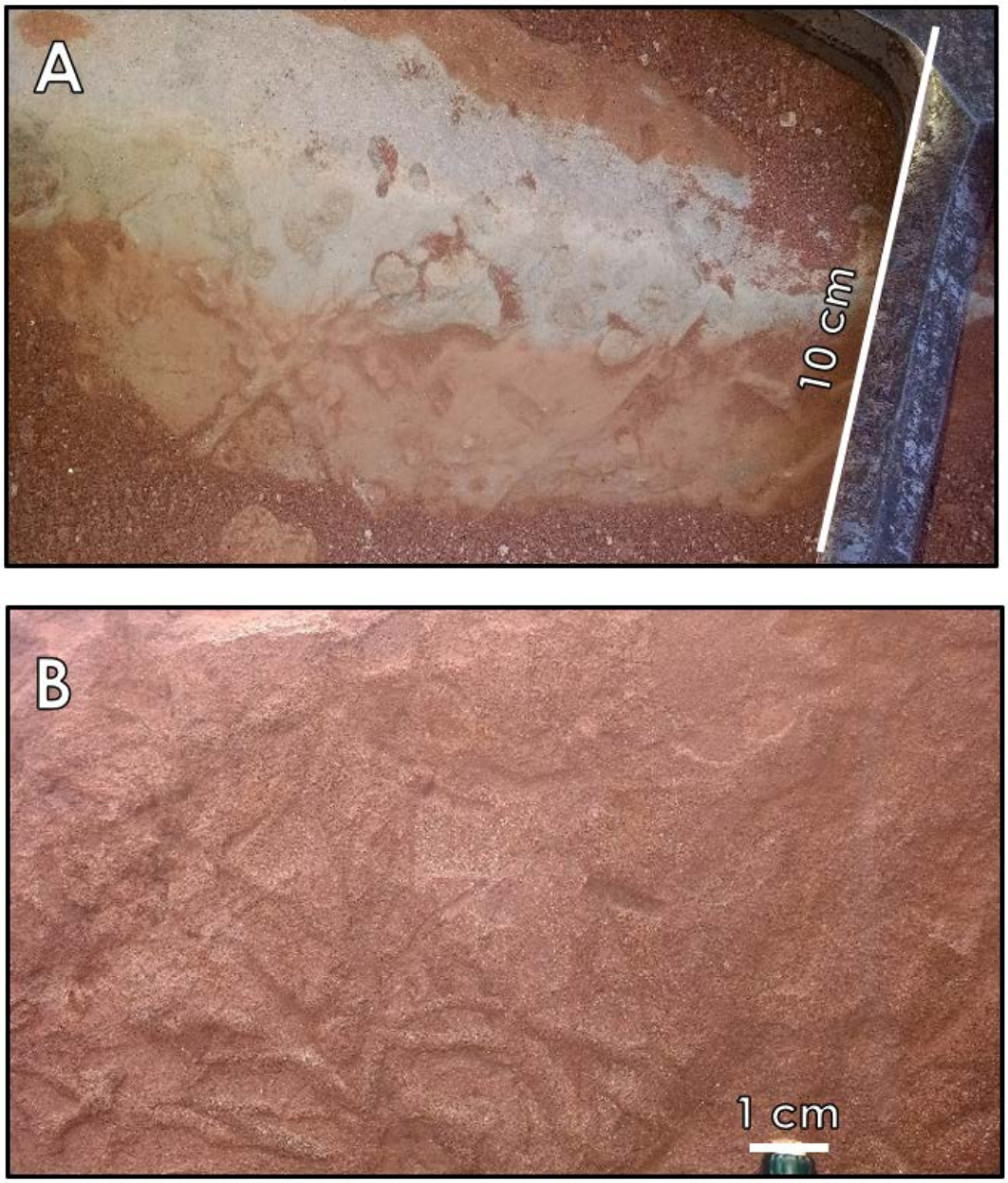

Figure 35: Horizontal burrows in the BMS. (A) A fine-grained interval of horizontal burrows on the top of a bedding plane. (B) A medium-grained interval with obvious micas and heavy burrowing.

Interpretation

Burrowing necessitates a lack of environmental stress, with sufficient oxygen, tolerable salinity, and enough time for colonization (Taylor and Goldring, 1993). Like the BMS of the Honaker, the BMS in Cutler Formation is both rare and thin; we can assume that at least one of the factors for burrowing was often lacking during megaflap deposition. The Cutler BMS facies is very similar to the Cutler LMS in aspects beyond its organism activity, and like the LMS, Mack and Rasmussen (1984) recognize a similar unit in the Cutler near Gateway in their sheetflood facies.

3.1.2.6 PINSTRIPED ORANGE SANDSTONE (POS) LITHOFACIES

The Pinstriped Orange Sandstone comprises about 5% of the Cutler Formation. Maximum unit thickness is less than 1 m. Contacts with other units are not observed due to alluvial cover. Bedding thickness ranges from thin to medium. Laterally, it may be traced for 5 to 10 m. It is a very fine- to medium-grained orange sandstone with coarsening-upward, lenticular laminae. Grains include sorted, angular quartz, potassium feldspar, biotite, and hematite (Figure 36, 37).

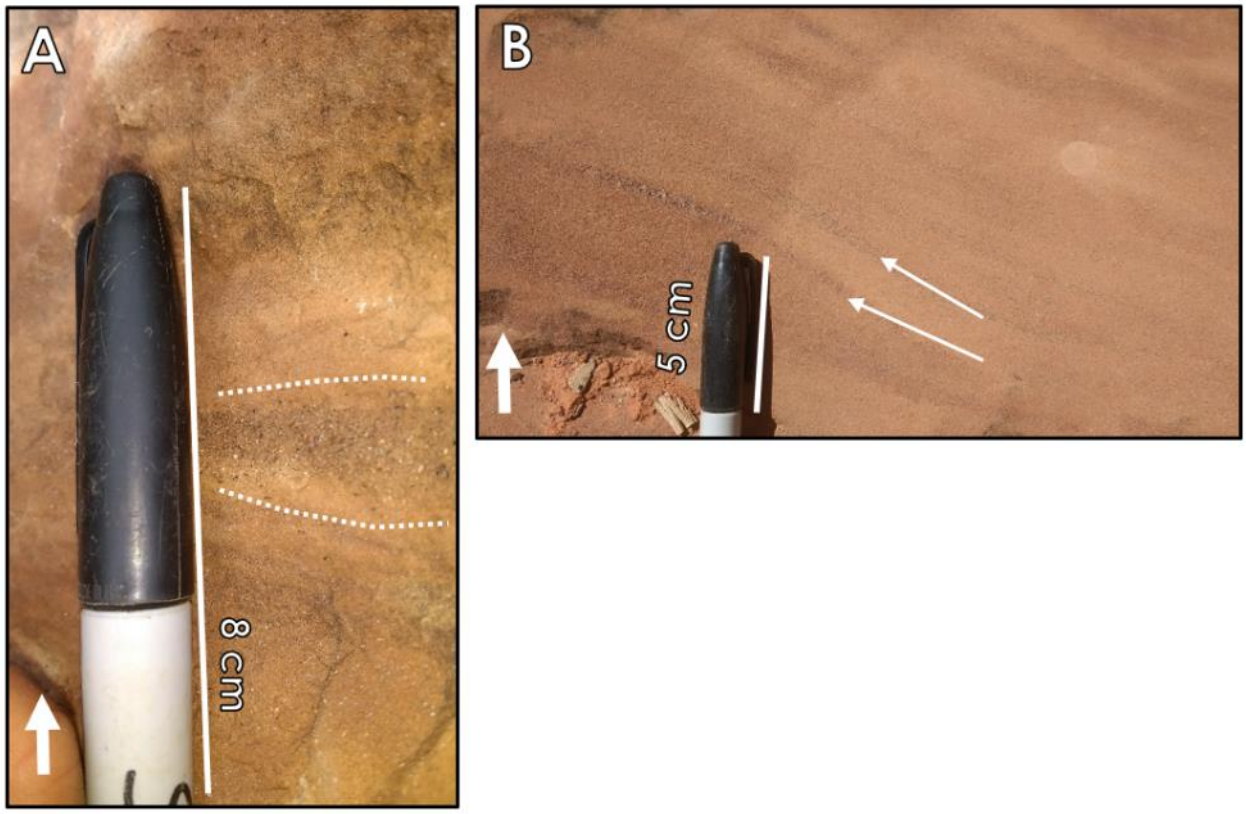

Figure 36: POS outcrop photos. (A) A coarsening-upward lens or "pinstripe," medium-grained in otherwise fine-grained, orange sandstone. (B) A series of coarsening-upward lenses, medium-grained in otherwise fine-grained, orange sandstone.

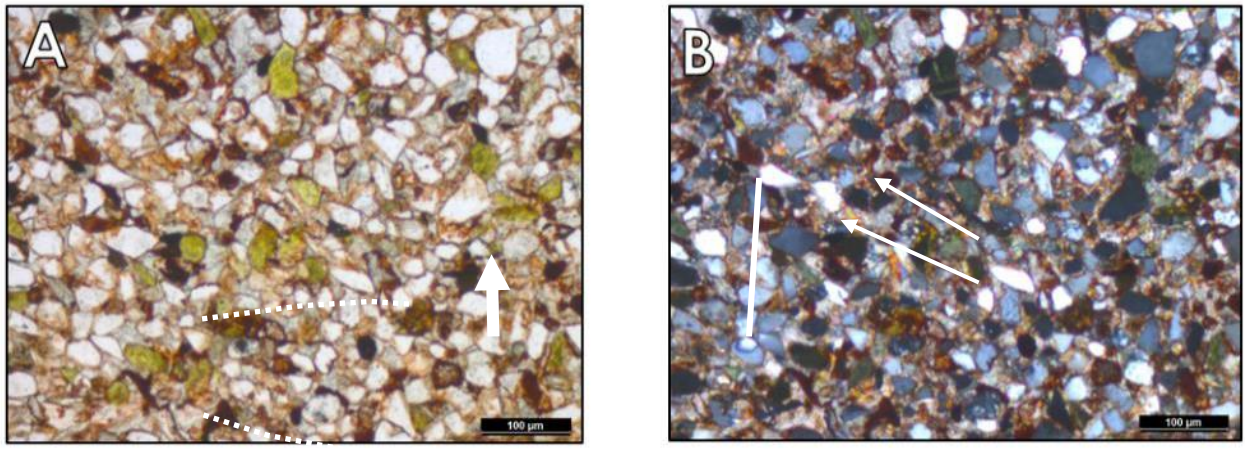

Figure 37: POS lithofacies micrographs with A in plane light and B crossed polars. Sorted, angular quartz, potassium feldspar, biotite, and hematite.

Interpretation

This lithofacies is likely eolian because of its pinstripes, which are reverse graded, lenticular-shaped lenses typical of eolian processes (Loope, 1984), which occur consistently and frequently). Jordan and Mountney (2012) have documented such pinstripes in their eolian facies association elsewhere in the Paradox Basin in the Lower Cutler Formation.

3.2 MEGAFLAP STRATAL ARCHITECTURE

The Honaker Trail and Lower Cutler facies of the Fisher Valley megaflap lack the stratigraphic cyclicity typically exhibited by these formations in other parts of the Paradox Basin (Gianniny and Simo, 1996). However, two marine flooding events of the Shallow Marine Carbonate FA do interrupt the siliciclastic deposition of the marginal marine Fan Delta FA and nonmarine Braided River FA (Figures 38 and 39; Appendix A, Figure 1). These marine flooding events delineate three major phases of fan delta development in the study area, referred to here as: Fan Delta FA 1, Fan Delta FA 2, and Fan Delta FA 3 (Figure 38).

Fan Delta FA 1 forms the basal part of the megaflap, sitting nonconformably on the underlying Fisher Valley salt diapir (Figure 38). Fan Delta FA 1 is roughly 27 m thick across the megaflap and contains predominately fine-grained sandstone lithofacies (LMS, XBXL, BMS, and SSD) and lesser conglomeratic lithofacies (GCC). Section D contains a local 10 m thick lense of channel-fill conglomeratic debris flow (MECS lithofacies). The relatively consistent thickness and lack of abundant coarse-grained channelized and debris flow facies indicates deposition on the distal margin of the fan delta system (Figure 22; Rees et al., 2017).

Fan Delta FA 1 is abruptly overlain by a 2-5 m thick resistant ledge of Shallow Marine Carbonate FA composed of IBDW and CWP wackestones and packstones. The basal contact is not observed due to cover, while the upper contact is sharp. This distinctive Honaker Trail lower carbonate represents the first marine flooding event (MFE1) in the study area. This transgression

was likely rapid as the underlying Fan Delta FA 1 contact is abrupt with no transitional facies to demonstrate a progressive deepening succession. This widespread and uniform transgression is easily correlated across the study area and has no significant lateral thickness or facies changes, suggesting little depositional relief on the underlying Fan Delta FA 1.

Fan Delta FA 2 conglomerates (GCC) abruptly and erosionally overly MEF1. When observed, this contact is erosional, with MEF1 fossil fragments reworked into the GCC. The succession of Fan Delta FA 2 lithofacies that follows ranges from 70 - 140 m thick, which represents significant thinning from southeast to northwest across the 1 km long megaflap exposure (Figure 38). In addition to the dramatic thinning, Fan Delta FA 2 contains a thick (up to 10 m) zone of massive debris flow (MECS lithofacies) that can be traced across almost the entire megaflap. However, the MECS lithofacies is not found on the northwest end of the megaflap (Sections A and B) where the Fan Delta FA 2 is thinnest (Figures 38 and 39). The lenticular MECS bodies pinch and swell across the megaflap, as best captured in a 10 m thick MECS package which rapidly pinches out to coarse-grained sandstones. All other lithofacies of the Fan Delta FA also occur in Fan Delta FA 2, including the LMS, XBXL, GCC, BMS, and SSD. These lithofacies are difficult to trace laterally for more than 10 - 20 m and they do not exhibit patterns of succession through time. By far, the LMS and XBXL lithofacies are the most common, followed by GCC. GCC is more common in the thicker measured sections towards the southeastern end of the megaflap than in the thinner sections to the northwest. The dominance of coarse-grained debris flow facies along with large thickness changes is consistent with proximal fan-delta front depositional systems (Gobo et al., 2015).

Fan Delta FA 2 is abruptly overlain by a 5 to 10 m thick resistant ledge of Shallow Marine Carbonate FA; this transition comes without progressively deepening facies shifts in the upper Fan

Delta FA 2. This Shallow Marine Carbonate FA represents a second marine flooding event (MFE2). MEF2 is much thicker and more variable in thickness across the megaflap than the carbonate units of MFE1, probably representing greater topographic relief on Fan Delta FA 2 sediments. The lower contact of MFE1 is not observed and the upper contact is abrupt and erosional. MFE1 contains IBCW and CWP wackestones and packstones, as well as Fusulinid Packstone (FP), which is not documented in the lower carbonate unit.

Just as the Fan Delta FA 2 abruptly capped MEF1, Fan Delta FA 3 of the upper Honaker Trail caps MFE2. The contact is abrupt and erosional. Fan Delta FA 3 is no more than 20 m thick and is mostly covered by modern alluvium, trees, and shrubbery. The upper contact is also abrupt and erosional, and it marks the beginning of the progradation of the Braided River FA, which ends the deposition of marine and marginal marine environments in the study area. The Braided River FA of the Lower Cutler Formation is no more than 20 m thick and is composed of conglomeratic, medium- to coarse-grained sandstones (LMS, SSD, BMS, XBS) and fine- to medium-grained sandstones (FGR, POS). The angular unconformity between Lower Cutler and Upper Cutler (the Mid-Cutler angular unconformity) marks the top of the megaflap succession.

3.2.1 MEGAFLAP SEQUENCE STRATIGRAPHY

The facies association stacking patterns and their attributes were used to define five depositional sequences within the Fisher Valley megaflap. The basal contact of the megaflap with the underlying Fisher Valley salt diapir forms Sequence Boundary 1 and Fan Delta FA 1 forms the lower part of the megaflap depositional Sequence 1 (Figure 38). Fan Delta FA 1 is abruptly overlain by MFE1 on a Transgressive Surface (TS), which defines Fan Delta FA 1 as the Lowstand Systems Tract (LST) of Sequence 1 (Cataneanu et al., 2011). MFE1 is abruptly and erosionally overlain by Fan Delta FA 2, which demonstrates an abrupt basinward shift in depositional facies,

delineating Sequence Boundary 2 and defining the lower shallow marine carbonate of the megaflap as the Transgressive Systems Tract (TST) of Sequence 1 (Cataneaunu et al., 2011).

Fan Delta FA 2 is abruptly overlain by MFE2 on a TS, defining Fan Delta FA 2 as the LST of Sequence 2. MFE2 is abruptly and erosionally overlain by Fan Delta FA 3, which represents another abrupt basinward shift in depositional facies, delineating Sequence Boundary 3 and defining the upper shallow marine carbonate unit (MFE2) in the megaflap as the TST of Sequence 2.

Fan Delta FA 3 of the Honaker Trail is abruptly overlain by the Braided River FA of the Lower Cutler Formation. The lack of gradational intertonguing between the Fan Delta FA 3 and Braided River FA suggests this is not a progradational Waltherian facies progression (Coe et al. 2002; Cataneanu et al., 2011). In addition, the stark color changes between the Lower Cutler fluvial beds and the Honaker Trail fan delta strata suggests a change in detrital provenance, representing the LST of a new depositional sequence (Sequence 4) and a Sequence Boundary 4 at the contact (Lawton et al., 2003). Finally, the angular unconformity at the top of the megaflap delineates Sequence Boundary 5 and the top of Sequence 4.

Depositional Sequences 1 through 4 display overall progradation whereby the shallow marine carbonates and marginal marine fan delta complexes of the Honaker Trail give rise to the braided fluvial succession of the overlying Cutler Formation. This stratigraphic architecture is consistent with Trudgill's (2011) seismic and well log interpretation of basinward progradation of Uncompahgre-derived siliciclastics towards the distal part of the Paradox Basin during this time period.

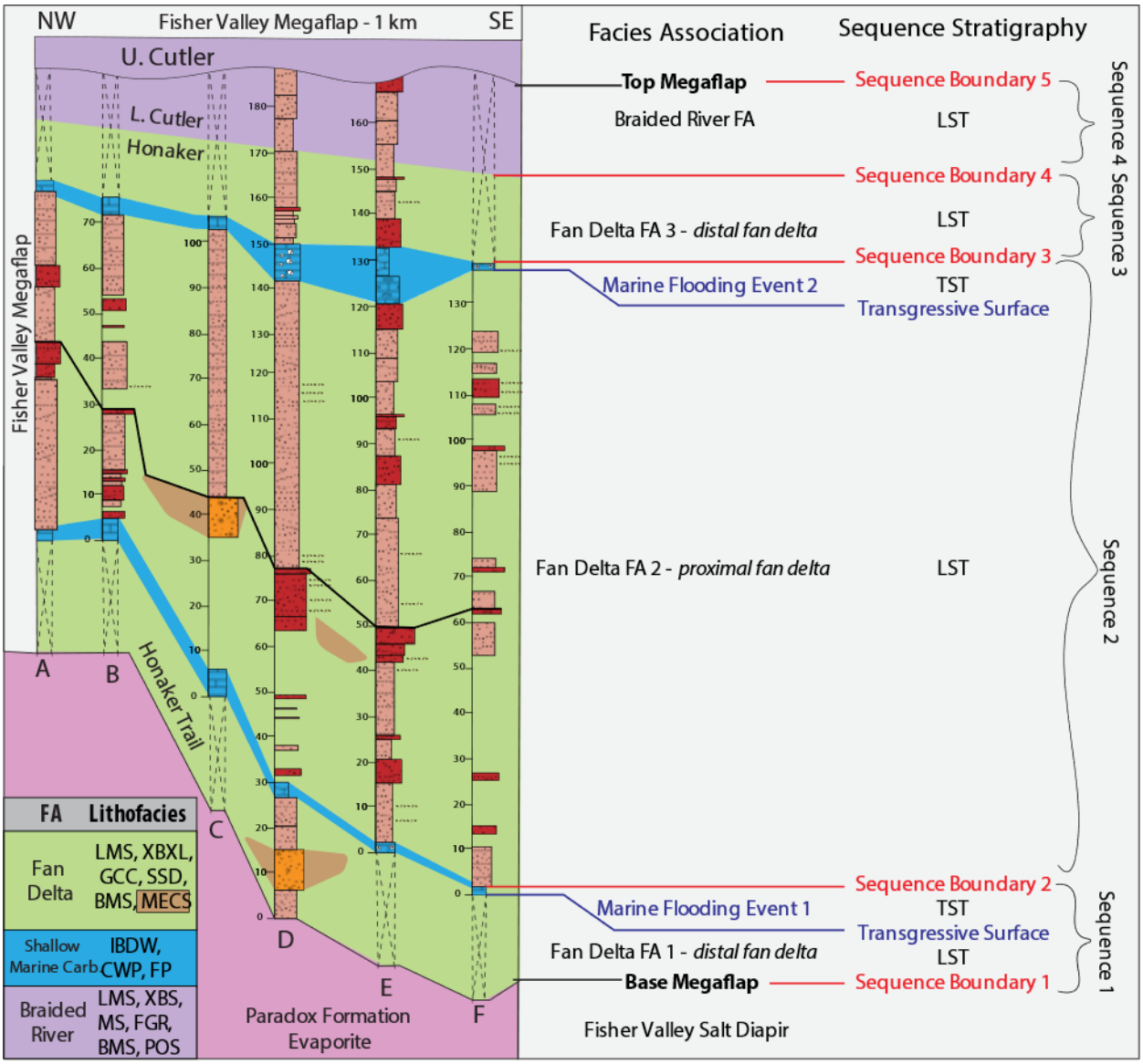

Figure 38: Fence diagram of the Fisher Valley megaflap facies associations and sequence stratigraphic interpretation. Sections are at 200 m spacing and span the width of the megaflap. Dotted portions represent areas where section was mapped, but not measured due to cover. The southeasternmost section shows the last occurrence of basal Shallow Marine Carbonate FA. The locations of the stratigraphic sections are shown in Figure 39.

3.3 MEGAFLAP STRUCTURE

Mapping of the Fisher Valley megaflap was based on modifications and additional detailed data added to the Doelling (2002) basemap. A few significant changes were made to Doelling's

map: the location of the Honaker-Cutler contact, Cutler-Moenkopi contact, the NW termination of the megaflap, and the SE termination of the megaflap. The Honaker-Cutler contact was refined, while the Cutler-Moenkopi contact was significantly moved resulting in thinning of the extent of the Cutler Formation. Doelling's 2002 map shows a slight bend to the NW of the Honaker and Cutler strata, but this study documented a very tight fold terminating the NW end of the megaflap, such that the top Honaker Trail folds around to face the base Honaker Trail. Figure 39 displays the results of the detailed facies mapping. I have subdivided the study area into three distinct structural domains: 1) Northwest Fold, 2) Southeast Fold, and 3) Collapse Block.

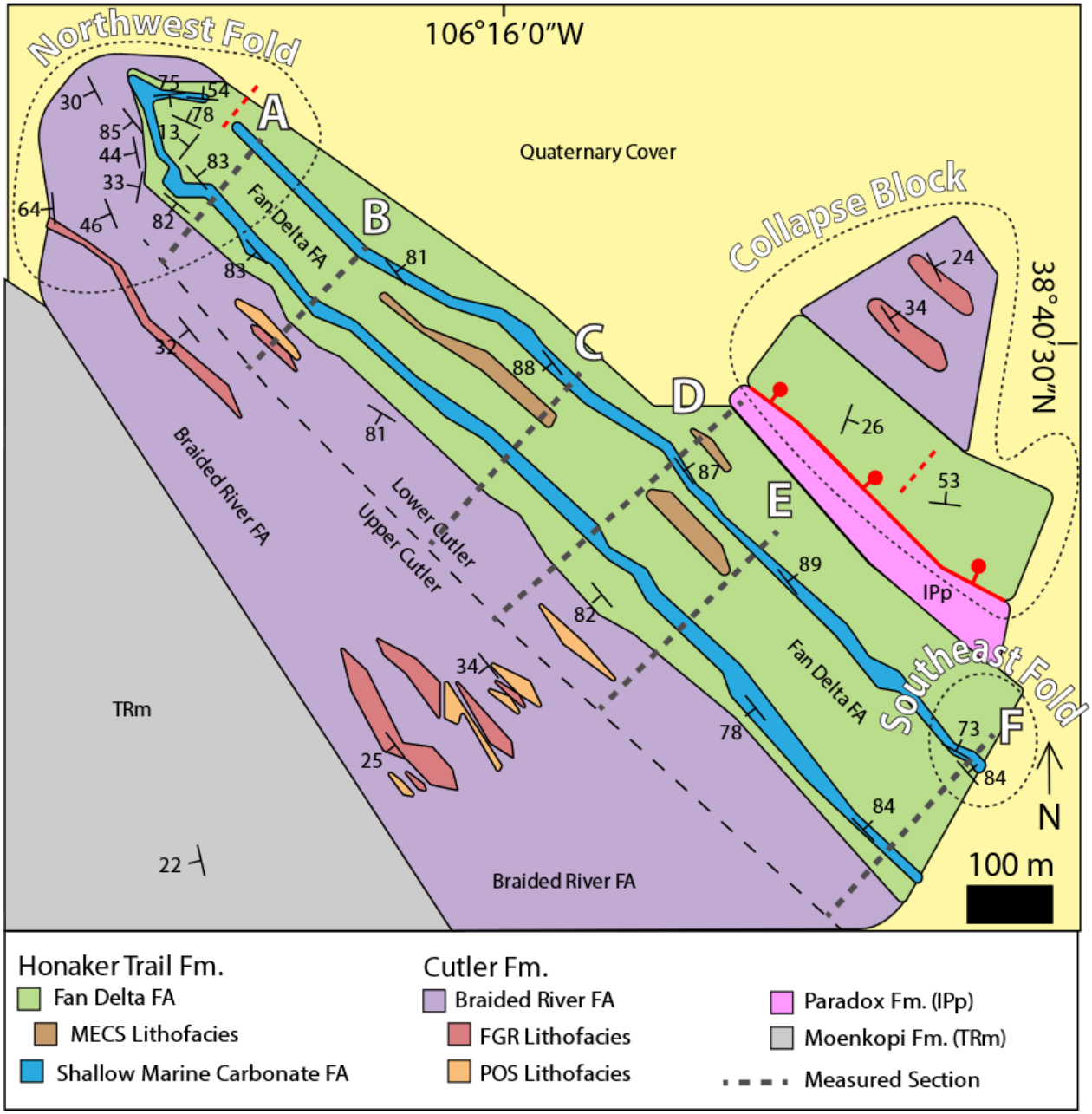

Figure 39: Depositional facies and structural map of the Fisher Valley megaflap. Northwest Fold, Southeast Fold and Collapse Block represent distinct structural domains recognized in the field area.

3.2.1 THE NORTHWEST FOLD

The Northwest Fold terminates the northwestern end of the Fisher Valley megaflap and is one of the most striking structural features of the megaflap. The fold involves Honaker Trail through Cutler strata; Quarternary alluvium cover over the northwestern plunge of the fold precludes observation of potentially deformed Moenkopi Formation. The fold is defined by Upper Shallow Marine Carbonate FA ledges that wrap tightly around to face the ledges of Basal Shallow Marine Carbonate FA. The fold tightness is accomodated by highly thinned Fan Delta FA 2 and the probable fault termination of Basal Shallow Marine Carbonate FA. The confidence in this fold—because some cover did exist in the area—was based on the walking out of the resistant ledges of the Fusulinid Packstone of the upper Shallow Marine Carbonate FA, a lithofacies which is not present in the basal carbonate. Figure 40 is an annotated drone image taken of the fold.

The Northwest Fold structural data was put into a stereonet analysis program (Rick Allmendinger's Stereonet 10), which calculated a trend and plunge of 305, 25º and axial plane of 142, 58º (Table 5, Figure 41, Figure 42). This northwest-southeast orientation is parallel to the trend of the Fisher Valley salt wall and is perpendicular to the principle stress direction inferred for ARM tectonism and the Laramide Orogeny (English and Johnston, 2004).

Figure 40: Annotated drone photo of the Northwest Fold structural domain at the NW termination of the megaflap. Red dashed line is the inferred fault.

Table 5: Structural data collected at the Northwest Fold structural domain with calculations from Rick Allmendinger's Stereonet 10 of the trend and plunge of the fold axis and axial plane.

strike	dip
171	44
126	82
130	74
314	83
222	13
296	78
158	30
84	75
276	54
142	85
195	33
175	64
159	46
Trend & plunge of fold axis:	305.4, 25.2
Strike & dip of axial plane:	142.3, 58.4 W

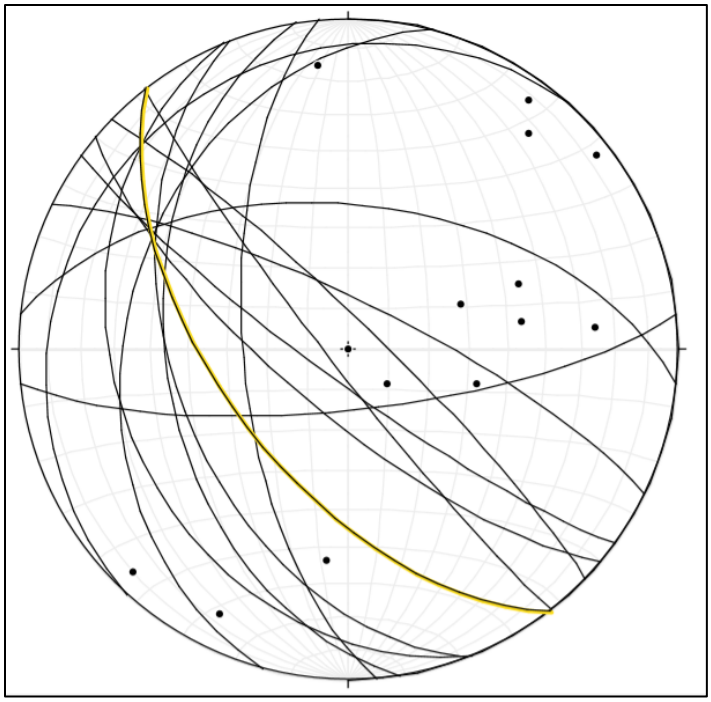

Figure 41: Planes and poles to planes of the northwest fold. Axial plane is highlighted in yellow. Graphic created with Rick Allmendinger's Stereonet 10.

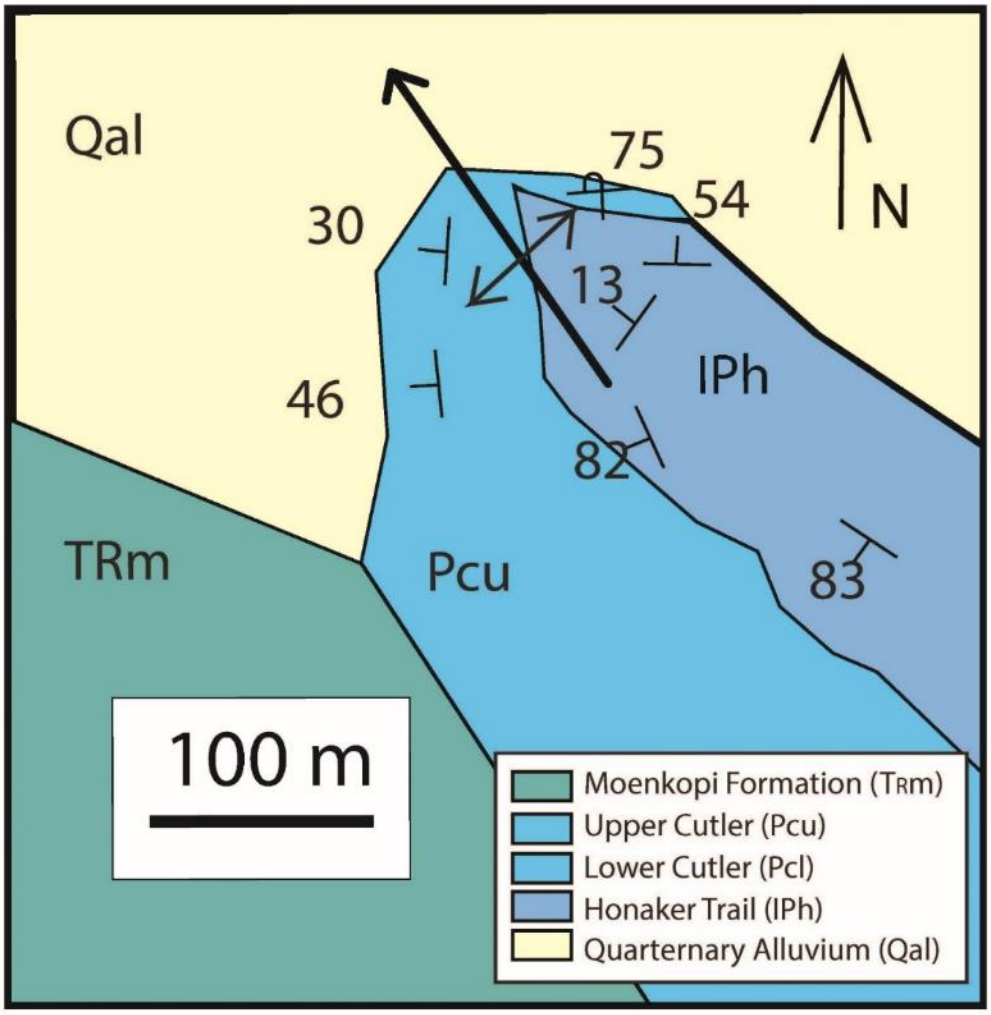

Figure 42: Geologic map of the Northwest Fold, the northwestern termination of the megaflap. The trend and plunge of the fold is 305, 25º , with axial plane strike and dip of 142, 58º.

3.2.2 THE SOUTHEAST FOLD

The Southeast Fold structural domain is present on the eastern end of the megaflap and is much less dramatic (~20-degree orientation change) than the Northwest Fold. Figure 41 shows what the fold looks like from the sky (drone photo) and on the ground. The fold is mostly confined to the Basal Shallow Marine Carbonate FA and it serves as the base for the thickest (most southeasternmost) measured section. The basal carbonate here is an atypical orangey-brown instead of the usual dull gray of the Shallow Marine Carbonate FA.

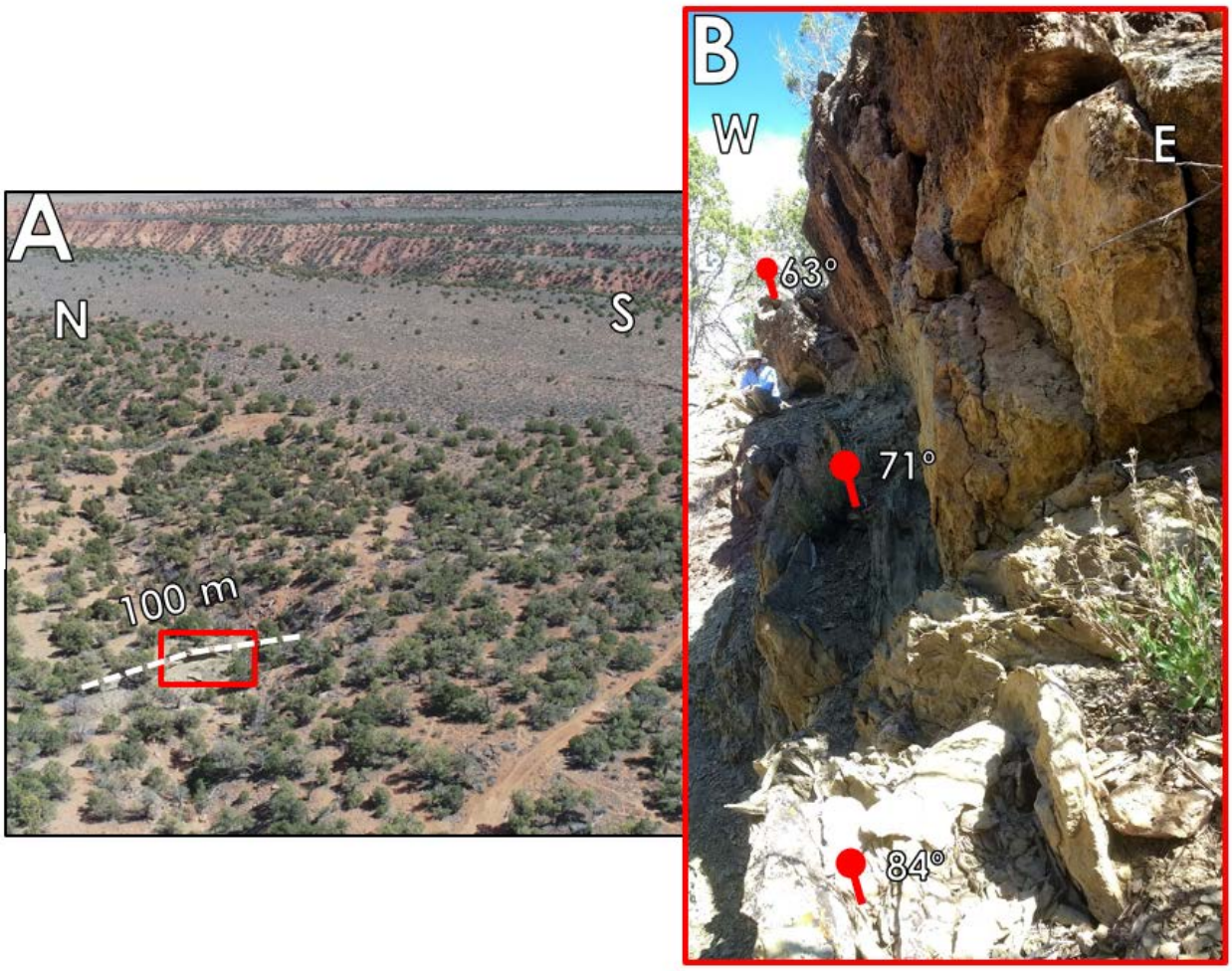

Figure 43: The southeastern termination of the megaflap. A is taken from the air and shows the location and orientation of the right image and the trend of the fold. Field assistant Ezequiel is in the background of the inset B for scale.

3.2.3 COLLAPSE BLOCK

Adjacent to the Fisher Valley megaflap is an outcrop of Paradox Formation gypsum that is bounded to the north by a collapse block of Honaker Trail and Cutler formations (Doelling, 2002). Figure 44 shows the relationships between the collapse features, the diapir, and the megaflap.

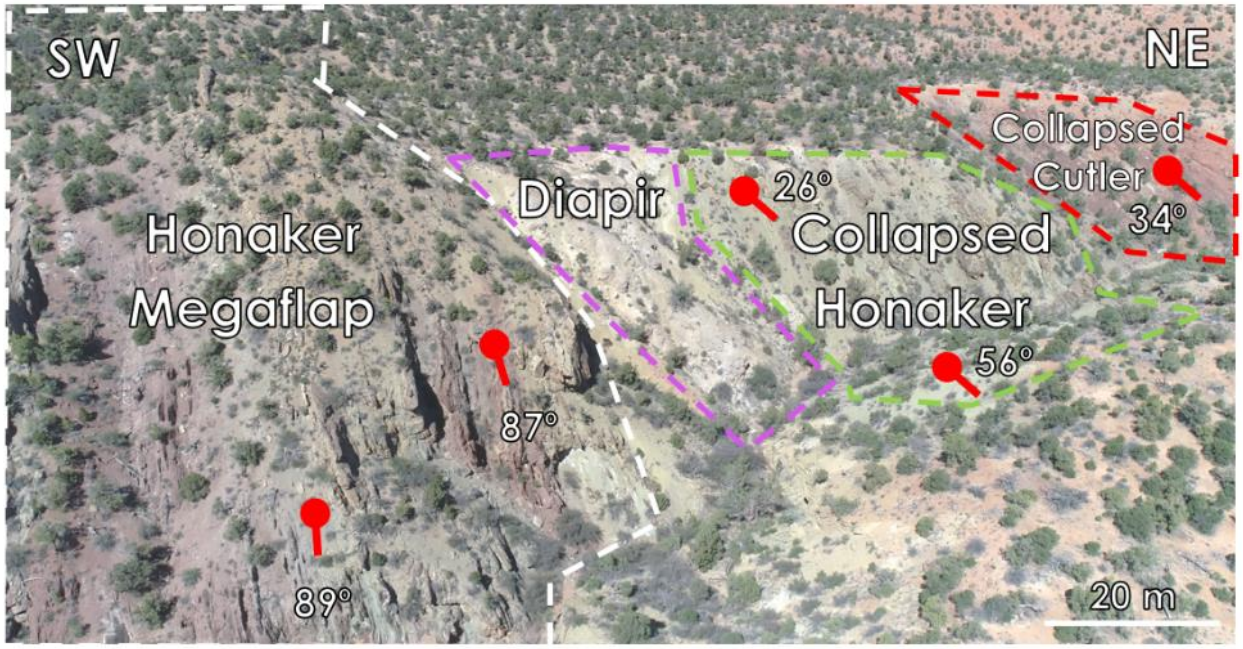

Figure 44: The relationship between the Fisher Valley megaflap, Paradox Fm. gypsum, and collapse block. Drone image looking north.

The outcrop of Paradox Formation to the northeast of the megaflap is more than a kilometer from the other exposures of Onion Creek diapir. Between these outcrops, it is covered by Quaternary fluvial and lacustrine strata (Doelling, 2002). Adjacent to the megaflap, it outcrops well in the upper deep gully walls as a mostly massive gypsum breccia unit (Figure 43).

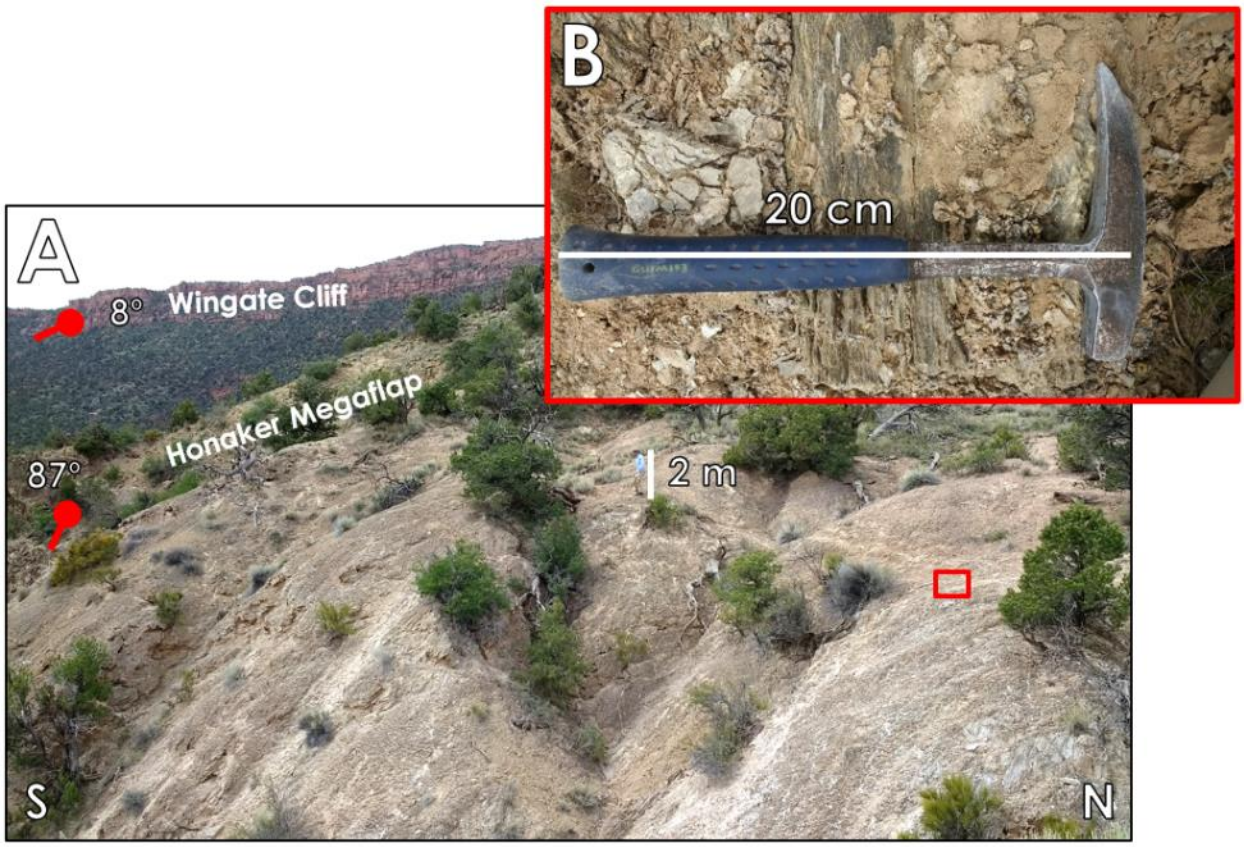

Figure 45: The Paradox Formation outcrop adjacent to the Fisher Valley megaflap, with field assistant Ezequeil for scale. Inset B shows recrystallized gypsum. Wingate Fm. measurement from Doelling (2002).

Directly north of the Paradox Formation gypsum outcrop is the collapse block of Honaker Trail and Cutler strata (Figures 44, 45, 46). The block outcrops into the gully, but not in the base of the gully or atop the hills. Within the gully, different strikes and dips were obtained for the two sides (about 200 m apart) suggesting there is a fault separating them (Figure 38). The

measurements taken in the Cutler were consistent, but the Cutler only outcrops on one side of the valley.

Additionally, the collapse block could potentially be a continuation of the Northwest Fold system. The changes in strike and dip between the Honaker Trail blocks and lack of the Shallow Marine FA or MECS is easier explained with a system of irregular collapse through some combination of salt wall dissolution and withdrawal. As for the diapir outcrop, I believe this portion of the Paradox Formation connects to the larger salt wall body, a connection we cannot see today due to this collapse block feature.

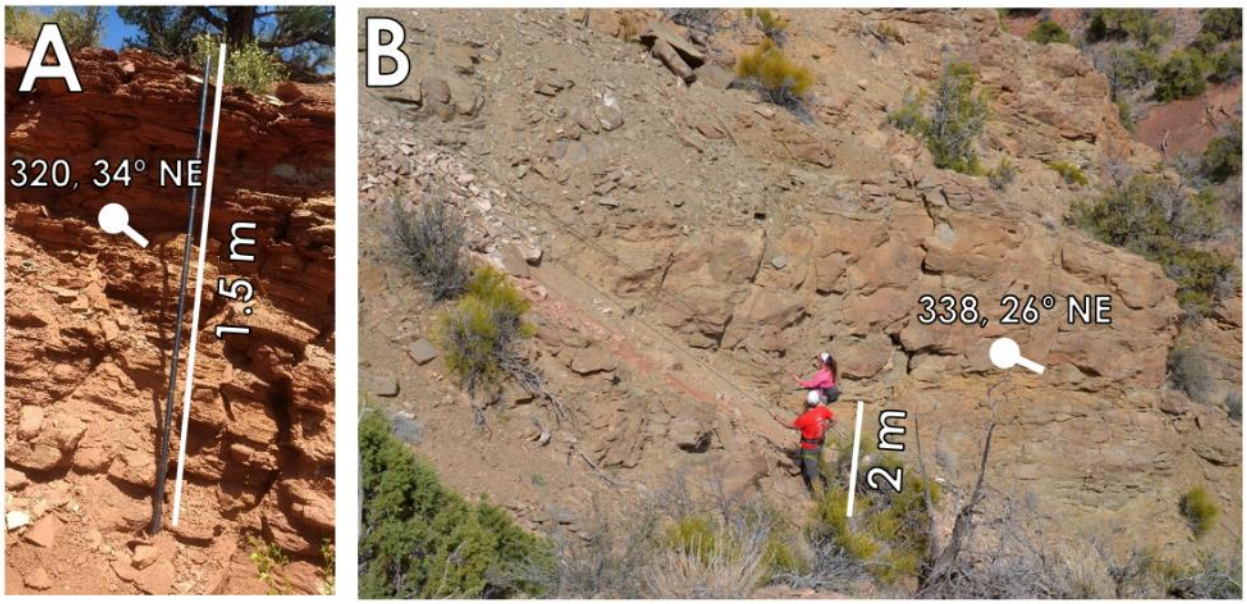

Figure 46: (A) Cutler collapse block strata, here the Braided River Overbank Interdune Facies Association. (B) Honaker Trail collapse block strata, here the Fan Delta FA.

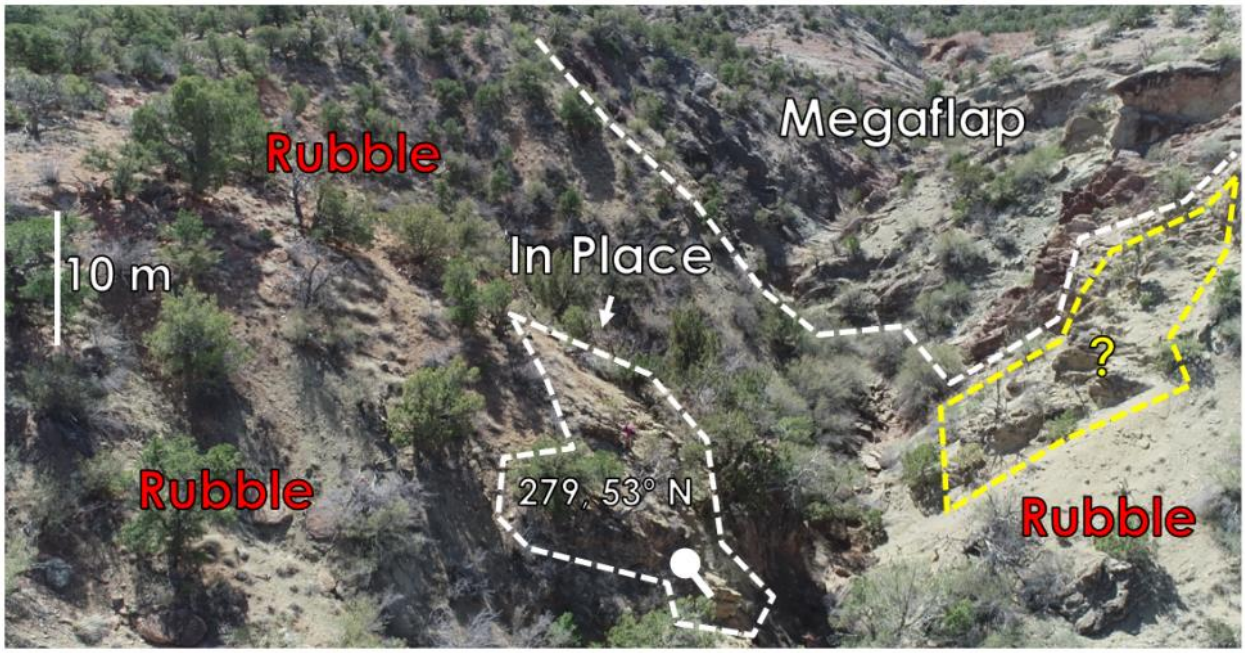

Figure 47: Drone image of collapse strata of the Honaker Fm.

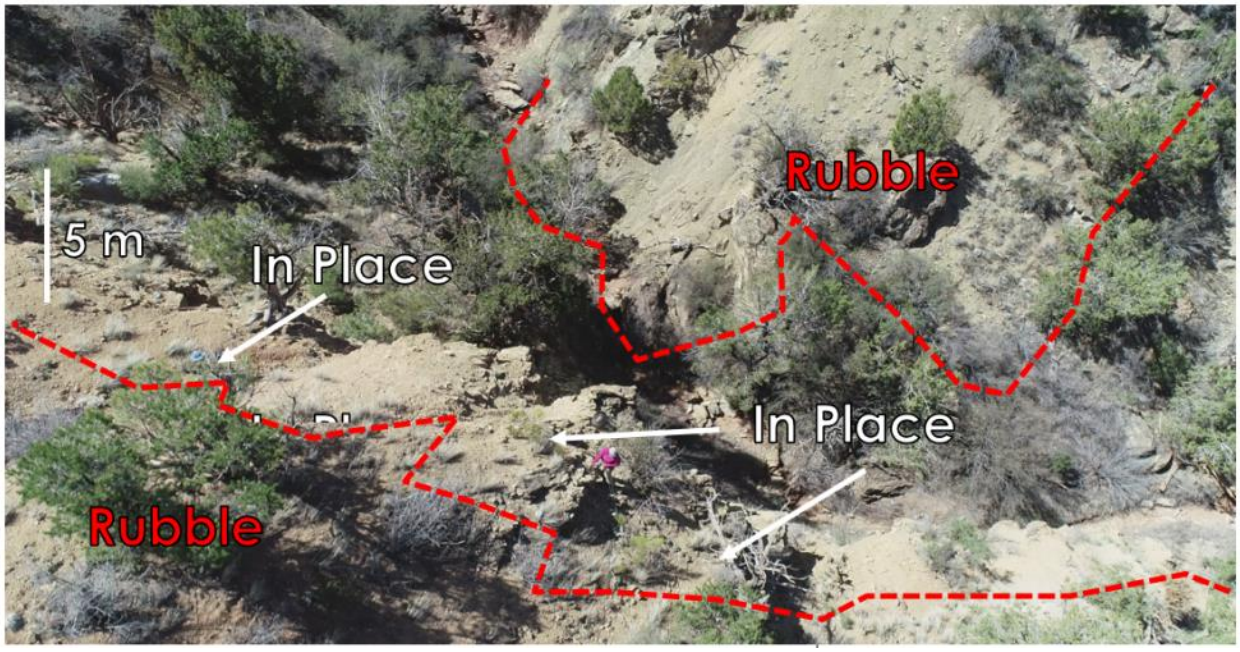

Figure 48: Same location as Figure 45, but from directly above.

4. DISCUSSION

4.1 ORIGIN OF FISHER VALLEY MEGAFLAP NORTHWEST FOLD

Several possibilities exist for the folding seen at the northwest end of the megaflap in the Northwest Fold structural domain. The folding could have been created through compressional tectonics, either in the Late Paleozoic ARM system or the Late Cretaceous to Paleocene Laramide Orogeny (Ge, 1996; English and Johnston, 2004). Non-compressional, halokinetically-driven folding produced during megaflap rotation is also possible (Thompson et al., 2018; Thompson-Jobe et al., *in prep*). ARM generated folding is difficult to explain with the lack of evidence of Late Paleozoic compressional tectonics in the Paradox Basin (Ge, 1996). However, the northeast-southwest trend of ARM compressional stress inferred from the northwest-southeast trend of the Uncompahgre reverse faults (Ye et al., 1996; Hoy and Ridgway, 2002; Barbeau, 2003; Leary et al., 2017) is consistent with the trend of the Northwest Fold. Researchers have also previously documented evidence of Laramide orogenic overprinting or reactivations of structures in the Paradox Basin, including the deformation of the salt walls (Baars and Stevenson, 1981; Mankowski et al., 2002; Kluth and DuChene, 2009; Trudgill and Paz, 2009). The principle direction of Laramide stress was northeast-southwest (English and Johnston, 2004), which is perpendicular to the axial plane of the Northwest Fold and thus possibly generated this structure.

Alternatively to the compressional explanations, Thompson et al. (2018) and Thompson-Jobe et al. (*in prep*) recently presented a hinge migration model for similar style folding in the Sinbad Valley megaflap. In their model, passive salt rise drives drape folding near the surface as it drives megaflap rotation (Figure 47). Drape folding can be accommodated either by hinge migration or limb rotation (Rowan et al., 2016). In hinge migration, the fold axis would be parallel with the salt wall, which is the case with the Northwest Fold. In the case of an eroded top salt

scenario, the fold hinge could be preserved in a down-plunge position (Figure 49), which is consistent with Northwest Fold plunge direction. In this case, we would also expect the pre-rotation strata to thin toward the fold hinge, as strata over the diapir are depositionally and erosionally thinned, as we do see in the Fisher Valley megaflap. Additionally, the Lower Cutler Formation is erosionally thinned beneath the angular unconformity with the overlying Upper Cutler Formation toward the Northwest Fold axis. While a tectonically-driven, compressional stress origin for the Northwest Fold cannot be ruled out, the hinge migration model is more compelling.

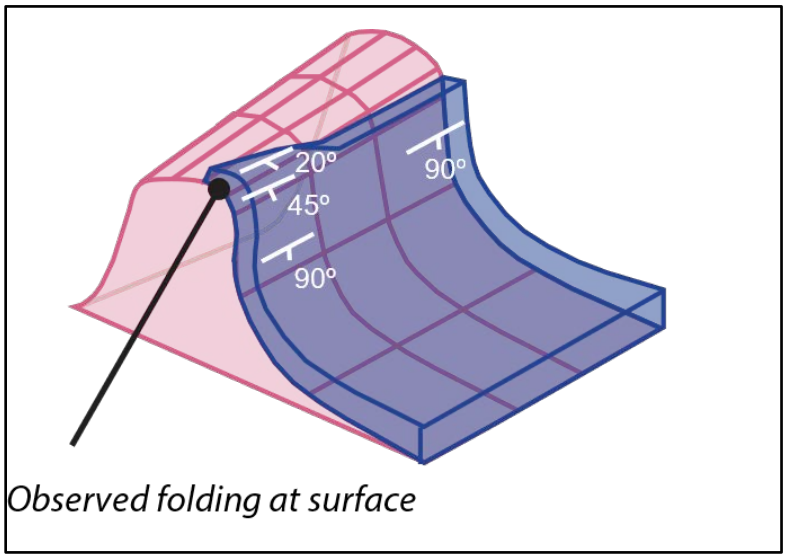

Figure 49: The hinge migration model of megaflap folding. Modified from Thompson et al. (2018) and Thompson-Jobe et al. (*in prep*).

4.2 FISHER VS. GYPSUM VALLEY MEGAFLAPS: TESTING THE DIFFERENTIAL SEDIMENT LOADING HYPOTHESIS

My hypothesis was that the halokinetic drape folding of Fisher and Gypsum Valley megaflaps was driven by differential sediment loading. I predicted that: 1) The proximal Fisher Valley megaflap started to rotate earlier than the distal Gypsum Valley megaflap, 2)The proximal

megaflap will be siliciclastic dominated and will have coarser-grained facies, 3) The proximal megaflap will be thicker, and 4) The proximal megaflap will have wider lateral extent.

4.2.1 TIMING OF MEGAFLAP ROTATION

Trudgill's (2011) cross section across Fisher Valley salt wall showed that more sediment was deposited on the northeast side of the salt wall than the southwest side, beginning with Honaker Trail deposition and continuing through the Cutler (Figure 7). Therefore, if greater sediment loading to the northeast of the salt wall was the driver of megaflap rotation, the angular unconformity indicating the start of megaflap drape fold rotation would occur early, during Honaker Trail time at Fisher Valley. At Gypsum Valley, the differential sediment load occurs during deposition of the Upper Cutler Formation and thus megaflap rotation began after the Mid-Cutler erosional unconformity (Rowan et al, 2016).

To test my first prediction, I looked at the position of the angular unconformity that defines the top of the megaflap at Fisher Valley, to see when megaflap rotation started. My field mapping showed that rotation of the megaflap panel began after the deposition of the Lower Cutler, where the dip changes from near vertical in the Lower Cutler to ~45 degrees in the Upper Cutler. Thus at both megaflaps, the angular unconformity occurs between the Lower and Upper Cutler formations, which means that megaflap rotation started at approximately the same time at both megaflaps, which doesn't support the regional differential loading hypothesis for initiation of drape fold rotation in the Paradox Basin. However, it is possible that the differential load from the northeast side to the southwest side of Fisher Valley was not great enough during Honaker Trail deposition to initiate drape-fold rotation but reached a critical point during deposition of the Upper Cutler Formation. Alternatively, a Cutler-age differential load may have been generated by differential erosional stripping off the top of the diapir to set up drape-fold rotation. The Mid-

Cutler unconformity is observed throughout the Paradox Basin as a regional erosional surface (Parker, 1968; DuChene et al., 2009) and may have created the differential load via differential erosion.

At Fisher Valley, shallowing of dips continues from the onset of Upper Cutler deposition, reaching 22 degrees in the lowest Moenkopi Formation strata. Doelling's (2002) closest measurement beyond this is on top of the Jurassic Wingate cliff in the Jurassic Kayenta, where dips range from 4-8 degrees. Based on this evidence, I believe Fisher Valley megaflap rotation concluded sometime during the Triassic, during latest Moenkopi or Chinle deposition.

4.2.2 MEGAFLAP FACIES

To test my second prediction, I compared the Fisher and Gypsum megaflap facies in terms of lithofacies type and dominance of siliciclastics versus carbonates. Figures 50, 51, and 52 show a transection between Fisher and Gypsum Valleys, location of Gypsum Valley measured sections, and a facies fence correlation diagram between megaflaps. The two major marine carbonate flooding events were used as a basis for tentative correlation between the two megaflaps, which areseparated by nearly 90 km. The Gypsum Valley megaflap includes strata from the Pennsylvanian Paradox Formation as well as the Honaker Trail and Cutler formations. The Paradox Formation in the Gypsum Valley megaflap comprises roughly 65 m of alternating marine black mudstone and laminated dolomite and limestone (Mast, 2016). Mast (2016) concluded that since the upper cycles of the Paradox Formation in the Gypsum Valley area do not contain salt layers, that mechanically these cycles would behave as salt overburden and deform with the rest of the megaflap strata. The overlying Honaker Trail and Lower Cutler formations were divided by Deatrick et al. (2015) into three facies associations. Two of these facies associations are marine

(Shelf FA and Lagoon FA) and the other is nonmarine (Fluvial FA). Table 5 lists the Gypsum Valley lithofacies within the three facies associations.

The Gypsum Valley megaflap has a variety of carbonates, from shelf to lagoonal, which have diverse fossil assemblages. Figure 53 shows photos of these carbonate outcrops, which can be broad, well exposed, and thick, and not broken up by cover or overshadowed by siliciclastics as in Fisher Valley's megaflap. Greater than fifty percent of the Gypsum Valley megaflap strata are marine carbonate facies, whereas Fisher Valley carbonate facies form less than ten percent of the megaflap strata. The reverse is true for siliciclatics. Gypsum Valley has less than 50 percent, with less variety of siliciclastic facies (mostly fine-grained fluvial floodplain) compared to Fisher Valley (Figure 52). Its most distinctive siliciclastic units (Deatrick et al., 2015) are the Lenticular Conglomeratic Sandstone Lithofacies and Red Silty Micaceous Mudstone Lithofacies (Figure 54). The Lenticular Conglomeratic Sandstone is best compared to Fisher Valley's Honaker Trail GCC conglomerate lithofacies, but is much finer-grained in comparison (Figure 54-A). The Red Silty Micaceous Mudstone Lithofacies is best compared to Fisher Valley's Honaker Trail Laminated Micaceous Sandstone Lithofacies, but has none of Fisher Valley's thick, dramatic outcrops as the LMS interbeds with other siliciclastic packages to form outcrops 10s of meters thick.

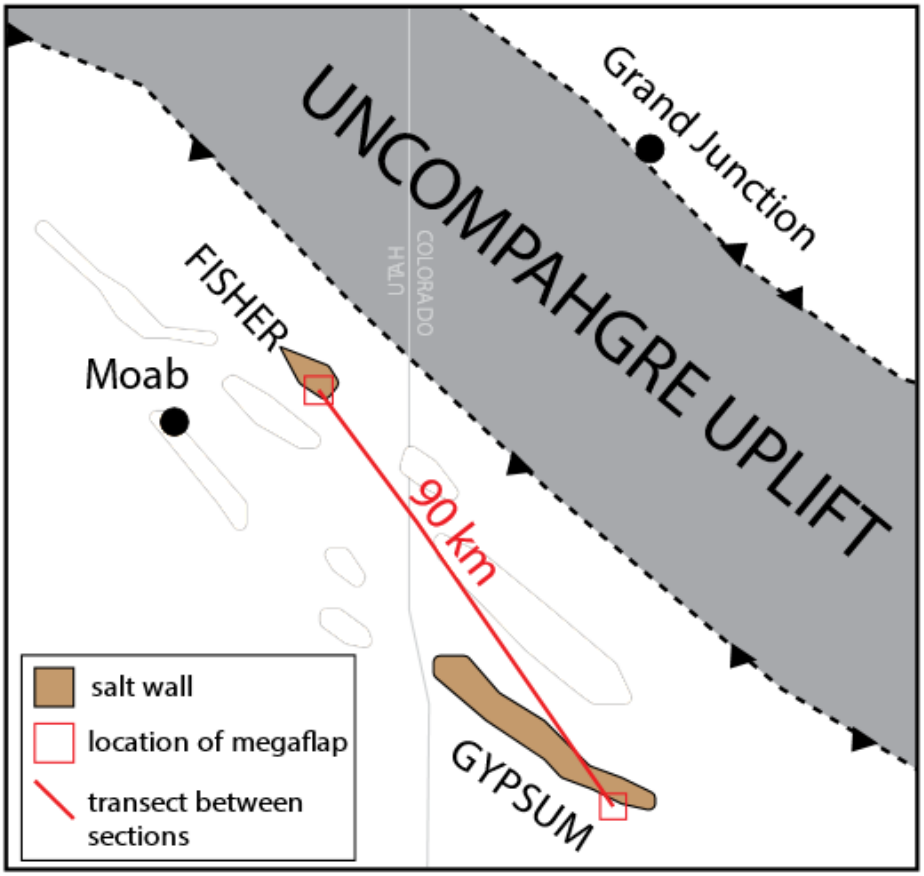

Figure 50: The fence diagram transect between Fisher Valley and Gypsum Valley. Modified from Barbeau (2003).

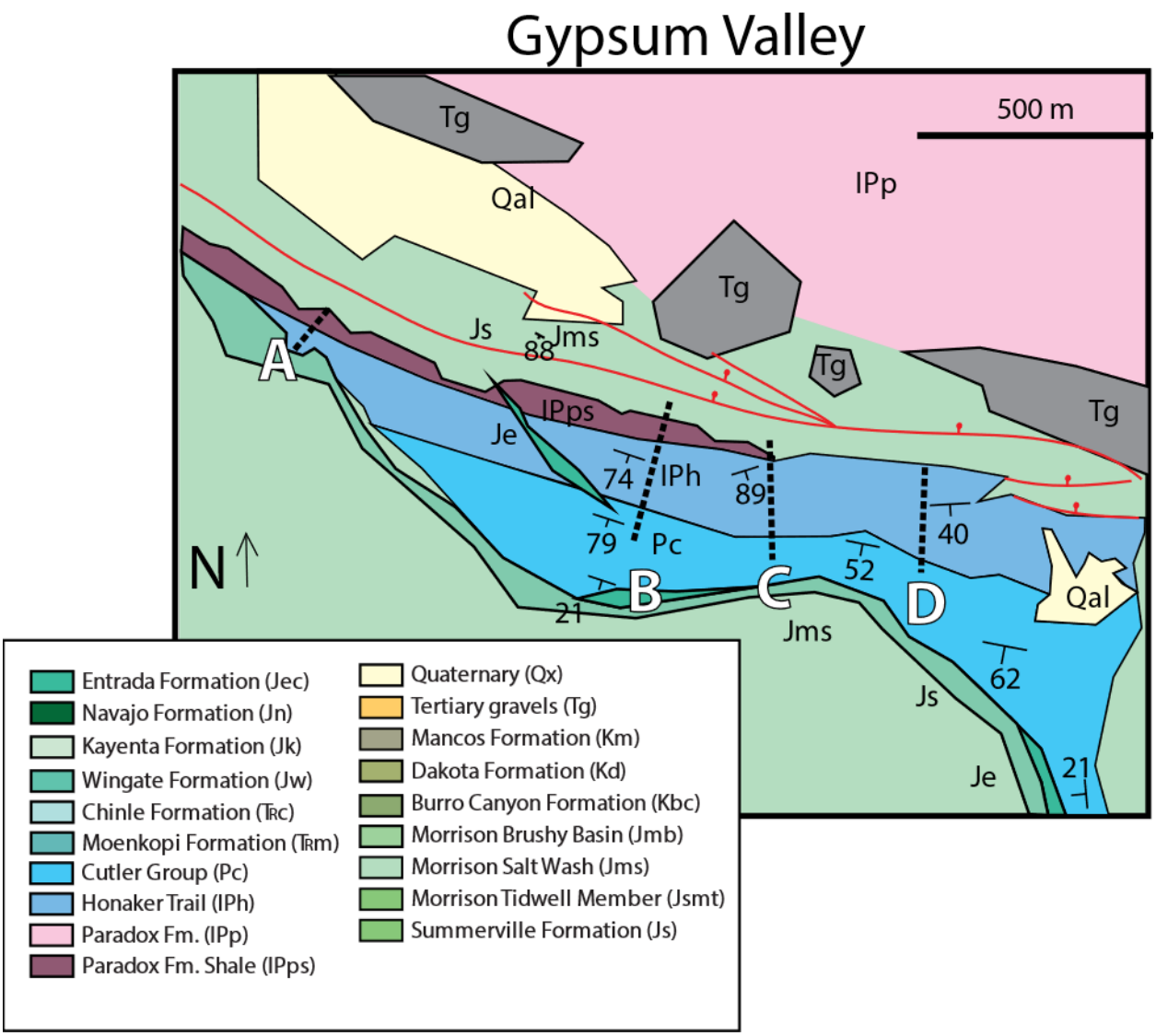

Figure 51: Locations of the Gypsum Valley measured sections.

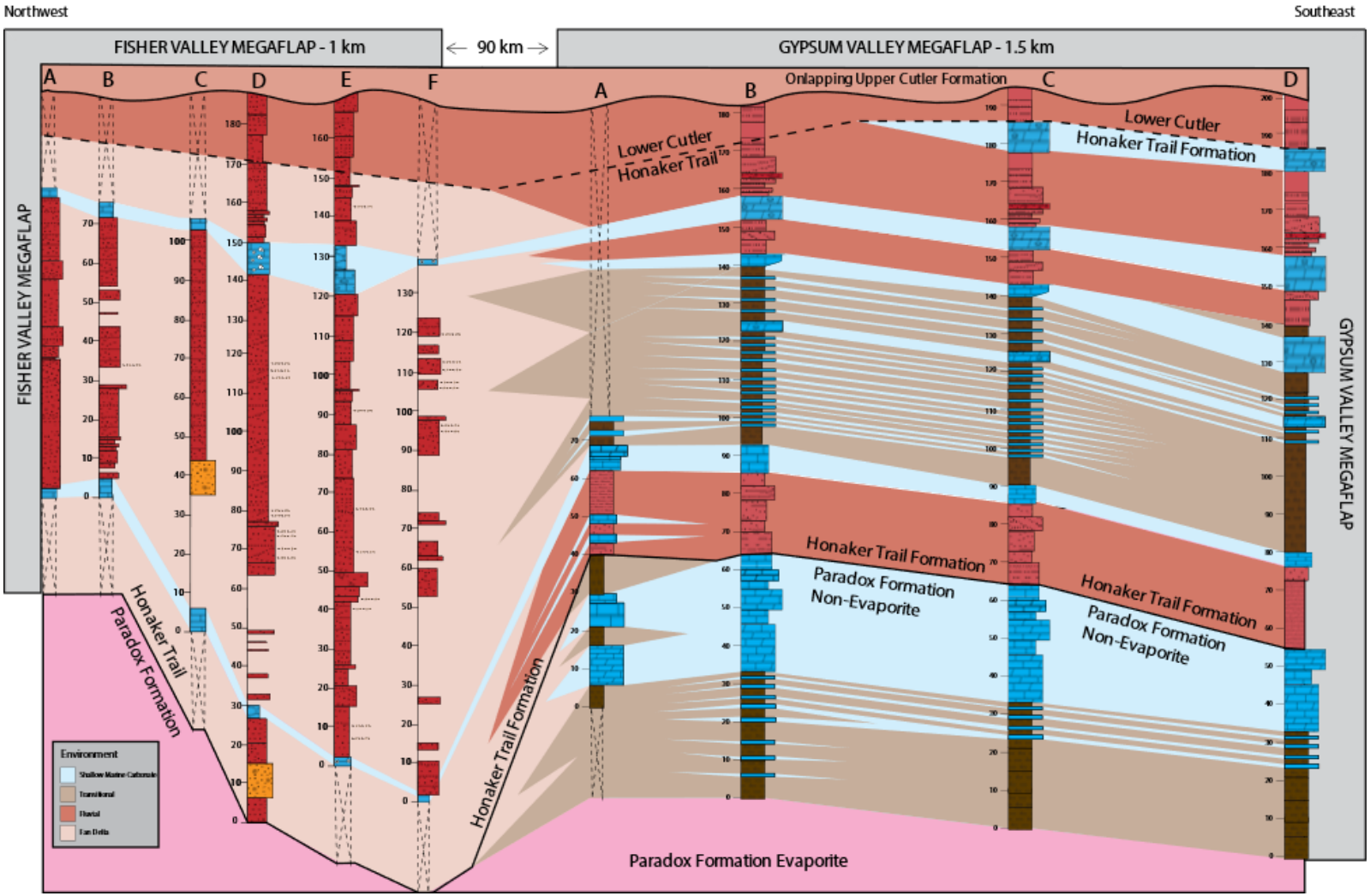

Figure 52: Fence diagram correlation between Fisher Valley and Gypsum Valley

Table 6: Facies associations and their respective lithofacies of the Gypsusm Valley megaflap.

Lithofacies of Shelf Facies Association
Laminated Carbonate
Phylloid Algae Wackestone-Baffelstone
Bryozoan/Productid Wackestone-Packstone
Skeletal Cap/Crinoid Grainstone
Ripple Cross-Laminated Calcareous Micaceous Sandstone
Lithofacies of the Lagoon Facies Association
Sponge Spicule Packstone-Grainstone
Gastropod/Brachiopod Mudstone-Packstone
Lithofacies of the Fluvial Facies Association
Lenticular Conglomeratic Sandstone
Red Silty Micaceous Mudstones/Thin Sandstone

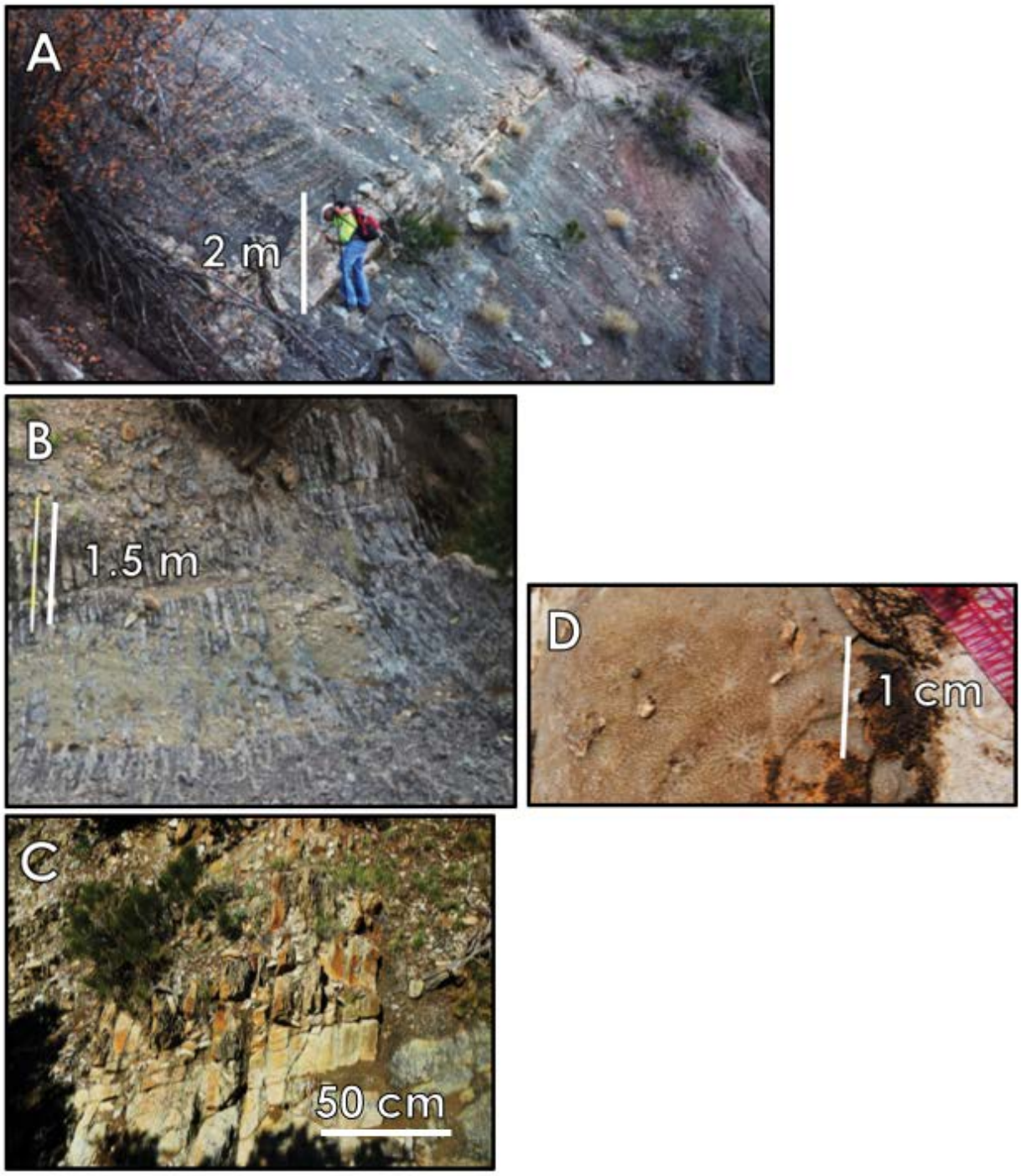

Figure 53: Outcrop photos of the Gypsum Valley megaflap's marine facies. (A) Phylloid Algae Wackestone-Baffelstone Lithofacies of the Shelf FA. (B) Gastropod/Brachiopod Mudstone-Packstone of the Lagoon FA. (C) Sponge Spicule Packstone-Grainstone of the Lagoon FA. (D) Bryozoan/Productid Wackestone-Packstone of the Shelf FA.

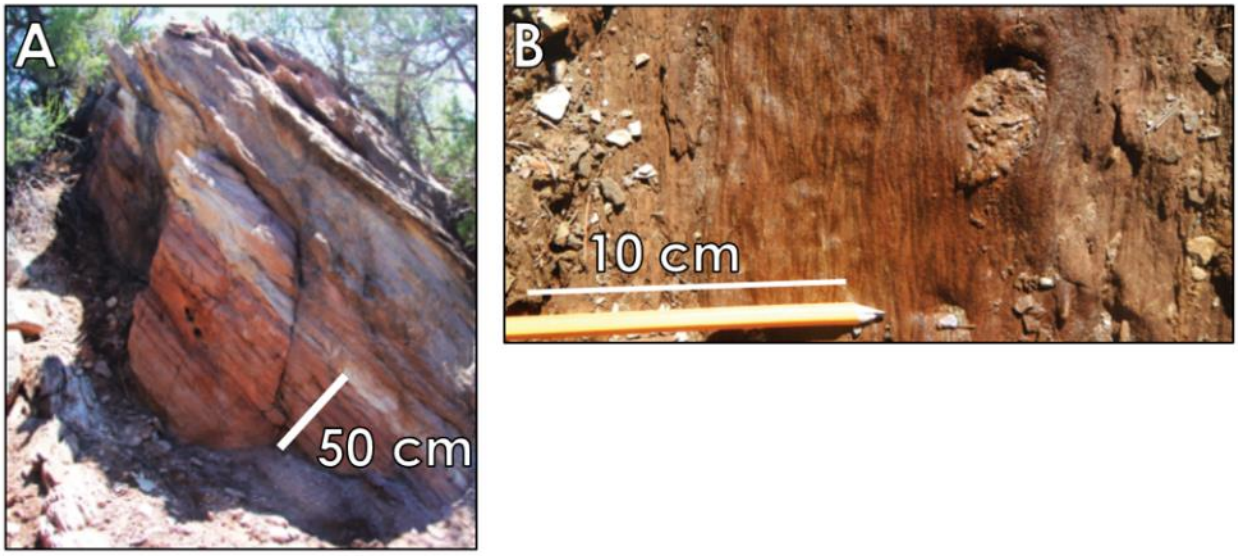

Figure 54: Outcrop photos of Gypsum Valley's terrestrial facies, the Fluvial FA. (A) Lenticular Conglomeratic Sandstone Lithofacies. (B) Red Silty Micaceous Mudstone/Thin Sandstone Lithofacies.

Table 7: Comparison of Gypsum Valley and Fisher Valley facies associations by average grain size, percentage of carbonates, and percentage of the megaflap each FA makes up.

Locality	Facies Association	Average Grain Size	% Carbonates	% Megaflap
Gypsum Valley	Shelf	Wackestone	100	55
	Lagoon	Packstone	100	5
	Fluvial	Fine-Grained	0	40
Fisher Valley	Shelf	Wackestone	100	10
	Fan Delta	Medium-Grained	0	60
	Braided River	Medium-Grained	0	30

Table 8: Comparison of the Gypsum Valley and Fisher Valley formation thicknesses, megaflap thickness, lateral extent, and their major features.

Locality	Honaker Trail Thickness[1]	Cutler Thickness[1]	Megaflap Thickness[1]	Lateral Extent[2]	Major Features
Gypsum Valley	140 m	15 m	200 m	2 km	Laterally continuous stratigraphy + stratigraphic thickness, radial faults, collapse block
Fisher Valley	170 m	15 m	190 m	1 km	Laterally discontinuous stratigraphic + pronounced thinning, major and minor folding, collapse block

1- Maxium Thickness
2- Of exposure

Table 9: Gypsum Valley vs. Fisher Valley facies association environments and their respective lithofacies.

Gypsum Valley		Fisher Valley	
Shelf	Phylloid Algae Wackestone-Baffelstone	**Shelf**	Irregularly Bedded Dolomitic Wackestone
	Laminated Carbonate		Crinoid Wackestone-Packstone
	Bryozoan/Productid Wackestone-Packstone		Fusulinid Packstone
	Skeletal Cap/Crinoid Grainstone		
	Ripple Cross-Laminated Calcareous Micaceous Sandstone		
Lagoon	Sponge Spicule Packstone-Grainstone	**Fan Delta**	Cross-Bedded-Cross-Laminated Micaceous Sandstone
	Gastropod/Brachiopod Mudstone-Packstone		Soft-Sediment Deformed Micaceous Sandstone
			Laminated Micaceous Sandstone
			Burrowed Micaceous Sandstone
			Conglomerate
Fluvial	Lenticular Conglomeratic Sandstone		Massive Extensive Conglomeratic Sandstone
	Red Silty Micaceous Mudstones/Thin Sandstone		
		Braided River	Cross-Bedded Sandstone
			Laminated Sandstone
			Massive Sandstone
			Bedded to Cross-Bedded Micaceous Sandstone
			Burrowed Fine-Grained Sandstone
			Pinstriped Orange Sandstone

4.2.3 INTERPRETATION OF FACIES TRENDS

Gypsum Valley's megaflap strata might be of the same formations as in the Fisher Valley megaflap, but they comprise very different lithofacies that record different depositional processes and depositional systems. Table 6 details the different environments that the two megaflaps record. Due to proximity to the source area, the Uncompahgre-derived siliciclastics of the Fisher Valley megaflap are substantially coarser –grained and are dominated by alluvial fan delta depositional processes. Whereas Gypsum Valley's rivers were much further from the source and so the carried a finer-grained sediment load on a gentler gradient, in less erosive, closer to meandering than braided streams.

One of the big questions surrounding the two megaflaps facies is why there are only two marine carbonate units at Fisher Valley, but at least five thick carbonate units and more than a dozen thin carbonates at Gypsum Valley. Tracing Honaker Trail carbonates across the basin is problematic and some have been shown to grade out across exposures (Atchley and Loope, 1993; Condon, 1997). However, if each of these carbonate units represent a marine transgression, how can Fisher Valley only have two? There are two possibilities: 1) Only the greatest magnitude transgressions reached Fisher Valley. Since transgressions progressed from west to east across the Paradox Basin, Gypsum Valley may record many small transgressions that did not reach Fisher Valley (Gianniny and Simo, 1996). 2) The Honaker Trail Formation may have progressively onlapped the Fisher Valley salt dome so that the exposed megaflap strata represents only a small portion of the total Honaker Trail deposition. Figure 7 shows that the Honaker Trail Formation on the southwestern side of Fisher Valley salt wall significantly thickens at depth into the southern minibasin. How did this thinning occur? It could have occurred depositionally, with thinner strata deposited on top of the rising salt; non-depositionally, if the salt created a topographic high, a sort

of depositional island; or by differential erosion of the Honaker Trail over the diapiric high. The second scenario involving onlap would require progressive onlapping from south to north of Honaker Trail alluvial fans, which is counter-intuitive when their clearly defined source area is directly to the north.

Another big question for the megaflap facies trends is why does Fisher Valley lithofacies thin to the northwest along strike while Gypsum Valley lithofacies are roughly isopachous along strike? Additionally, why is it that Fisher Valley thinning is accommodated entirely within Fan Delta FA 2, between the two marine carbonate flooding events? That the thinning is confined just to the Fan Delta FA 2 suggests that this Fan Delta FA interval was distinct from Fan Delta FA 1 or 3. Some of this thinning could be attributed to the lobate nature of a proximal fan delta system; the thinning is too pronounced to be wholly produced by this system (Patranabis-Deb, 2007; Deptuck et al., 2008). Alternatively, the Gypsum Valley system is on the shelf and more stable deposition allows for more laterally consistent facies and thicknesses across the megaflap.

Gianniny and Simo (1996) studied accommodation trends of the Honaker Trail of the southwestern Paradox Basin and found that incomplete preservation of transgressive-regressive cycles was due to a lack of accommodation space—or an overwhelming sediment supply, while complete transgressive-regressive cycles demonstrated plentiful accommodation space and/or a lack of sediment supply. In the case of Gypsum Valley and Fisher Valley, Gypsum Valley would have been sediment-starved and/or with overwhelming subsidence, while Fisher Valley would have had overwhelming sediment supply and/or a lack of subsidence.

4.2.4 MEGAFLAP THICKNESS

To test my third prediction, I looked at the thickness of the megaflaps (the strata between the basal contact with the diapir and the significant angular unconformity). Fisher Valley and

Gypsum Valley megaflaps are approximately the same thickness (FV = 190 m thick, GV = 200 m thick), though the Fisher Valley megaflap thickness varied along strike, while the Gypsum Valley didn't. Why wasn't the Fisher Valley megaflap in fact thicker, being closer to the source? There are a few possibilities 1) The depositional systems were too different if sediment type and processes to be comparable, 2) Transgressions that reached Gypsum Valley and deposited carbonates may not have reached Fisher Valley, 3) Transgressions that reached Gypsum Valley and deposited thick carbonates may only have deposited thin carbonates at Fisher Valley, and 4) Fisher Valley was in fact thicker, but its strata was eroded at the top megaflap angular unconformity.

4.2.5 MEGAFLAP LATERAL EXTENT

To test my fourth and last prediction, I mapped the Fisher Valley megaflap as Deatrick et al. (2015) had mapped Gypsum Valley. To the northwest, Fisher Valley is clearly terminated in a fold, but to the southeast, it may continue to extend beneath the Quaternary cover. Gypsum Valley is terminated to the southeast by a radial fault and plunges into the subsurface on the northwest end, so we also don't know its true extent, but what is exposed is ~2 km long and Fisher's megaflap is ~1 km long, which is the opposite of my prediction. Because of the limitations of the outcrop exposure, the lateral extent of the megaflaps cannot be accurately evaluated.

4.2.6 TESTING THE DIFFERENTIAL LOAD HYPOTHESIS

Three out of the four predictions of my differential load hypothesis appear to be false. The Gypsum Valley megaflap began rotation at the same time as the Fisher Valley megaflap, is about the same thickness, and appears more laterally extensive than Fisher Valley. Fisher Valley does, however, have more and coarser-grained siliciclastics as predicted. Since I cannot prove Fisher and Gypsum's full lateral extents, I will focus on the first two predictions, which I have shown are

false: rotational timing and thickness, which are comparable between the megaflaps. It appears that despite their distances from the Uncompahgre Uplift—and despite Gypsum Valley not getting as much sediment or as coarse -grained sediment—the megaflaps began formation at the same time. Why could this have happened? There are two possible reasons: 1) Rotation was not caused by differential loading and was instead driven by differential erosion, or 2) The majority of differential loading did not occur in Honaker Trail time, but in Upper Cutler time. The second idea seems less likely because the cross section of Fisher Valley (Figure 7) shows an extremely thick Honer Trail section on the northeast side as compared to the southwest side and the Cutler Formation thickness is just as dramatic. Rowan et al. (2016) found that the major differential sediment load in Gypsum Valley occurs during the deposition of the Upper Cutler Formation and megaflap rotation began after the Lower Cutler-Upper Cutler regional erosional unconformity. The Mid-Cutler regional erosional unconformity may have also significantly stripped down the thickness of the Fisher Valley megaflap strata, which created a substantial differential load on the northeast minibasin leading to initiation of megaflap rotation.

5. CONCLUSIONS

5.1 THE FISHER VALLEY MEGAFLAP

5.1.1 THE FISHER VALLEY MEGAFLAP FACIES

The Fisher Valley megaflap comprises mostly siliciclastic sediments and minor carbonates of the Pennsylvanian Honaker Trail Formation and siliciclastics of the Permian Lower Cutler Formation. The megaflap strata contain three depositional facies associations (FA): Fan Delta FA, Shallow Marine Carbonate FA and Braided Fluvial FA, each of which has several lithofacies. In the Honaker Trail Formation, the Fan Delta FA comprises most of the strata, with its lithofacies of Laminated Micaceous Sandstone, Cross-Bedded to Cross-Laminated Micaceous Sandstone, Massive Extensive Conglomeratic Sandstone, Granule-Cobble Conglomerate, Soft-Sediment Deformed Micaceous Sandstone, and finally Burrowed Micaceous Sandstone. Together these record a fan delta environment of shelf sandstone (LMS, SSD, BMS), debris flows (MECS), fan delta bottomsets and topsets (GCC), and shoreface sands (XBXL). The Honaker Trail Formation also records transgression of carbonate shelf environments, ranging from low to moderate energy with good circulation (CWP, FP) to dysaerobia (IBDW). The Cutler Formation records a single facies association, Braided River FA, which has the following lithofacies: Laminated Micaceous Sandstone, Cross-Bedded Sandstone, Massive Sandstone, Fine-Grained Red Sandstone, Burrowed Micaceous Sandstone, and Pinestriped Orange Sandstone. These lithofacies record sheetflood (LMS, BMS, FGR), braided river channel (XBS), debris flow (MS), and eolian deposition (POS).

The stratigraphic cyclicity typically seen in the Honaker Trail and Lower Cutler formations in other parts of the Paradox Basin is not observed in the Fisher Valley megaflap. However, there are distinct depositional episodes defined by two marine flooding events of the Shallow Marine Carbonate FA that delineate three major phases of fan delta development in the Fan Delta FA

before nonmarine Braided River FA progradation occurs. The megaflap contains 4 depositional sequences. Sequences 1, 2 and 3 contain Lowstand Systems Tracts comprising Fan Delta FA. Sequence 1 and 2 contain Transgressive Systems Tracts comprising Shallow Marine FA. Sequence 4 contains only a Lowstand System Tract of Braided River FA. Depositional Sequences 1 through 4 display overall progradation whereby the shallow marine carbonates and marginal marine fan delta complexes of the Honaker Trail give rise to the braided fluvial succession of the overlying Cutler Formation. This stratigraphic architecture is consistent with Trudgill's (2011) seismic and well log interpretation of basinward progradation of Uncompahgre-derived siliciclastics towards the distal part of the Paradox Basin during this time period.

5.1.2 THE FISHER VALLEY MEGAFLAP STRUCTURE

The Fisher Valley megaflap is a vertical to overturned stratal panel adjacent to the Fisher Valley salt wall. To the northeast, closest to the salt wall, it is overturned; moving southwest, it rotates back to vertical, then steeply inclined to about 80 degrees before an angular unconformity with the Lower Cutler Formation. At the northwest end of the megaflap, the megaflap is sharply folded such that top Honaker faces basal Honaker. This folding most likely began during the Late Paleozoic due to hinge migration, but may have been overprinted during the Laramide Orogeny.

Thicker packages of sediment were deposited on the northeastern side of the Fisher Valley salt wall than the southwestern side, beginning with Honaker Trail deposition and continuing through the Cutler, Formation showing that differential loading began during Honaker Trail time. At Gypsum Valley, the differential sediment load occurs during deposition of the Upper Cutler Formation and thus megaflap rotation began after the Mid-Cutler erosional unconformity (Rowan et al, 2016). Fisher Valley megaflap's angular unconformity also occurs at the Mid-Cutler Unconformity, which means that megaflap rotation started at approximately the same time at both

megaflaps, but this doesn't support the regional differential sediment load hypothesis for initiation of megaflap drape folding when Fisher Valley differential loading began in Honaker time. Perhaps, the Fisher Valley differential load was not great enough during Honaker Trail time to initiate drape-fold rotation, but reached a critical point during deposition of the Upper Cutler Formation. Alternatively, a Upper Cutler-age erosional differential load may have been generated as the top of the diapir was stripped off at the Mid-Cutler Unconformity. Fisher Valley megaflap rotation concluded in the Triassic during the late Moenkopi or Chinle, based on the continuing shallowing of dips.

5.2 FISHER VS. GYPSUM VALLEY MEGAFLAPS

5.2.1 FISHER VS. GYPSUM VALLEY MEGAFLAP FACIES

Fisher Valley and Gypsum Valley differ in several regards to facies: proportion of siliciclastics to carbonates, coarse-ness of clastics, and lateral facies changes. Carbonates at Fisher Valley occur only twice during megaflap deposition, while carbonates at Gypsum Valley occur consistently throughout deposition. Siliciclastics at Fisher Valley include a large proportion of conglomerates and conglomeratic sandstones, while coarse-grained siliciclastics and clastics as a whole are not common in Gypsum Valley. Lastly, while most Fisher Valley lithofacies are discontinuous laterally, at Gypsum Valley a lithofacies may be easily traced.

5.2.2 MEGAFLAP VARIABILITY

The megaflaps of Fisher Valley and Gypsum Valley should have been relatively similar with their shared basin history and formations; both were deposited in the Paradox Basin during the Late Paleozoic and are composed dominantly of Honaker Trail and Cutler strata. However, this study has shown they have significant differences in stratigraphy and sedimentology. If we can have so much variability within a salt system, we could have so much more between other

megaflaps. What these outcrop analogues have shown us is that a single difference—proximity to sediment source—can have a large impact on megaflap formation, sedimentology, stratigraphy, and structure. While improving the predictably of the subsurface megaflaps was the goal of this study, what I have found is that what can be predicted about megaflaps is that they are unpredictable. Future work should include more studies of outcrop analogue megaflaps that appear comparable at first glance to determine if the variability seen between Fisher and Gypsum Valley megaflaps is in fact the rule.

REFERENCES

Ashley, G.M., Southard, J.B. and Boothroyd, J.C., 1982, Deposition of climbing-ripple beds: a flume simulation: Sedimentology, vol. 29, no. 1, p. 67-79.

Atchley, S.C., and Loope, D.B., 1993, Low-stand aeolian influence on stratigraphic completeness; upper member of the Hermosa Formation (latest Carboniferous), southeast Utah, USA; *in* Pye, K., and Lancaster, N., eds., Aeolian Sediments, Ancient and Modern: Special Publication 16 of the International Association of Sedimentologists, p. 127–149.

Aydin, A., and Nur, A., 1982, Evolution of pull-apart basins and their scale independence: Tectonics, vol. 1, p. 91–105.

Baars, D.L., and Stevenson, G.M., 1981, Tectonic evolution of western Colorado and eastern Utah: *in* Epis, R.C., and Callender, J.R., eds., Western Slope Colorado: Albuquerque, New Mexico Geological Society Guidebook, 32nd Field Conference, p. 105-112.

Baars, D. L., and Stevenson, G. M., 1982, Subtle stratigraphic traps in Paleozoic rocks of Paradox Basin; *in* The Deliberate Search for the Subtle Trap, M. T. Halbouty, ed.: American Association of Petroleum Geologists, Memoir 32, p. 131-158

Baars, D.L., 1966, Pre-Pennsylvanian Paleotectonics--Key to Basin Evolution and Petroleum Occurrences in Paradox Basin, Utah and Colorado: AAPG Bulletin, vol. 50, no. 10, p. 2082-2111.

Baldschuhn, R., F. Binot, S. Fleig, and F. Kockel, 2001, Geotektonischer atlas von Nordwest-Deutschland und dem deutschen Nordsee-sektor—Strukturen, struckurenwicklung, pal¨aogeographie: Geologisches Jahrbuch, vol. A 153, p. 1–88 (in German).

Barbeau, D.L., 2003, A flexural model for the Paradox Basin: implications for the tectonics of the Ancestral Rocky Mountains: Basin Research, vol. 15, p. 97–115.

Blakey, R.C., 1973, Stratigraphy and origin of the Moenkopi Formation (Triassic) of southeastern Utah: The Mountain Geologist, vol. 10, no. 1, p. 1-17.

Byers, C.W., 1977, Biofacies Patterns in Euxinic Basins a General Model: SEPM Special Publications, no. 25, p. 5-7.

Catuneanu, O., Galloway, W.E., Kendall, C.G.S.C., Miall, A.D., Posamentier, H.W., Strasser, A. and Tucker, M.E., 2011, Sequence stratigraphy: methodology and nomenclature. Newsletters on stratigraphy, vol. 44, no. 3, p. 173-245.

Curtis, B.F., 1958, Pennsylvanian Paleotetonics of Colorado and Adjacent Areas: Symposium on Pennsylvanian Rocks of Colorado and Adjacent Areas, Rocky Mountain Association of Geologists, p. 9-12.

Coe, A. L. (ed.) 2002, The Sedimentary Record of Sea Level Change: Cambridge University Press.

Colburn, I.P. and West, E.R., 1981, Conglomerates of the Chatsworth Formation: a discussion of petrology and provenance: *in* Link, M. H., Squires. R. L., and Colburn. I. P.. eds., Stmt Mils Cretaceous Turbidites, Southern California, Pacific Section, Society Economic Paleontologists and Mineralogists, Fall Field Trip Guidebook, pg. 75-88

Condon, S. M., 1997, Geology of the Pennsylvanian and Permian Cutler Group and Permian Kaibab Limestone in the Paradox Basin, Southeastern Utah and southwestern Colorado: U. S. Geological Survey, Professional Paper, 2000-P.

Dasgupta, P., 1998, Recumbent flame structures in the Lower Gondwana rocks of the Jharia Basin, India—a plausible origin: Sedimentary Geology, vol. 119 no. 3-4, p. 253-261.

Deatrick, K., Giles, K., Langford, R., Rowan, M., and Hearon, T., 2015, Depositional Facies and Geometry of an Exposed Megaflap: Pennsylvanian Honaker Trail Formation, Gypsum

Valley Salt Wall, Paradox Basin, Colorado(abs): Gulf Coast Association of Geological Societies and Gulf Coast Section of SEPM 65th Annual Convention, September 20-22, 2015, Houston, Texas.

Deptuck, M.E., Piper, D.J., Savoye, B. and Gervais, A., 2008, Dimensions and architecture of late Pleistocene submarine lobes off the northern margin of East Corsica: Sedimentology, vol. 55, no. 4, p. 869-898.

Dickerson, P.W., 2003, Intraplate mountain building in response to continent–continent collision—the Ancestral Rocky Mountains (North America) and inferences drawn from the Tien Shan (Central Asia): Tectonophysics, vol. 365, p. 129–142.

Dickinson, W.R., Soreghan, G.S. and Giles, K.A., 1996, Glacio-eustatic origin of Permo-Carboniferous stratigraphic cycles: Evidence from the southern Cordilleran foreland region: *in* Tectonic and Eustatic Controls on Sedimentary Cycles, SEPM Concepts in Sedimentology and Paleontology #4, p. 25-34.

Dickinson, W.R., and Lawton, T.F., 2003, Sequential intercontinental suturing as the ultimate control for Pennsylvanian Ancestral Rocky Mountains deformation: Geology, vol. 31, p. 609–612.

Doelling, H.H., Oviatt, C.G. and Huntoon, P.W., 1988, Salt deformation in the Paradox region: Utah Geological Survey Bulletin, vol. 122.

Doelling, H.H., 2002, Geologic Map of the Fishers Towers 7.5'Quadrangle, Grand County, Utah: Utah Geological Survey, Map 183, p. 22.

Doelling, H.H. and Morgan, C.D., 2000, Geologic Map of the Merrimac Butte Quadrangle, Grand County, Utah. Utah Geological Survey, Map 178, p 22.

Driese, S.G. and Dott Jr, R.H., 1984, Model for Sandstone-Carbonate: AAPG Bulletin, vol. 68, no. 5, p. 574-597.

DuChene, H.R., Cole III, S.L. and Greenberg, N., 2009. Geology of the Double Eagle Unit, Andy's Mesa Field, San Miguel County, Colorado: The Paradox Basin Revisted, New Developments in Petroleum Systems and Basin Analysis, Rocky Mountain Association of Geologists Special Publication, p. 519-533.

Elston, D.P., Shoemaker, E.M. and Landis, E.R., 1962, Uncompahgre front and salt anticline region of Paradox Basin, Colorado and Utah: AAPG Bulletin, vol. 46, no. 10, p.1857-1878.

English, J.M. and Johnston, S.T., 2004, The Laramide orogeny: What were the driving forces?: International Geology Review, vol. 46, no. 9, p. 833-838.

Ferrer, O., N. Carrera, E. Roca, J. A. Muñoz, M. G. Rowan, and K. A. Giles, 2016, Experimental approach to megaflap development during passive salt diapirism: Controlling factors and kinematics (abs.): AAPG/Society of Exploration Geophysicists International Conference and Exhibition, Barcelona, Spain, April 3–6, 2016, p. 285.

Fielding, C.R., 2006, Upper flow regime sheets, lenses and scour fills: extending the range of architectural elements for fluvial sediment bodies: Sedimentary Geology, vol. 190, no 1-4, p. 227-240.

Fryberger, S.G., 1980, Eolian-Fluviatile (Continental) Origin of Ancient Stratigraphic Trap for Petroleum in Weber Formation, Rangely Oil Field, Colorado: AAPG Bulletin, vol. 64, no. 5, p. 709-710.

Fryberger, S.G., 1984, The Permian Upper Minnelusa Formation, Wyoming: Ancient example of an offshore-prograding eolian sand sea with geomorphic facies, and system-boundary traps for petroleum: *in* The Permian and Pennsylvanian Geology of Wyoming, 35th Annual Field Conference Guidebook, p. 241-27.

Frahme, C.W., and Vaughn, E.B., 1983, Paleozoic Geology and Seismic Stratigraphy of the Northen Uncompahgre Front, Grand County, Utah: Rocky Mountain Foreland Basins and Uplifts, Rocky Mountain Association of Geologists, p. 201-212.

Franczyk, K. F., and G. Clark, 1994, Mixed clastic and carbonate Pennsylvanian lithofacies distributions, southeastern Paradox basin, Colorado: Implications for eustatic and local tectonic controls(abs.): GSA Abstracts with Programs, Rocky Mountain Section Annual Meeting, Durango, CO, May 1994, vol. 25, no. 6, p. 13.

Gannaway, C. E., K. Giles, M. G. Rowan, T. E. Hearon, and J. C. Fiduk, 2015, Stratigraphic and structural characteristics of a megaflap flanking Witchelina Diapir, Willouran Ranges, South Australia (abs.): AAPG Annual Convention and Exhibition, Denver, Colorado, May 31–June 3, 2015.

Ge, H., 1996, Kinematics and dynamics of salt tectonics in the Paradox Basin, Utah and Colorado: Field observations and scaled modeling; PhD Thesis, The University of Texas at Austin.

Gianniny, G.L. and Simo, J.T., 1996, Implications of unfilled accommodation space for sequence stratigraphy on mixed carbonate-siliciclastic platforms: an example from the lower Desmoinesian (middle Pennsylvanian), southwestern Paradox basin, Utah: Rocky Mountain Section (SEPM), Paleozoic Systems of the Rocky Mountain Region, p. 213-234.

Gianniny, G.L. and Miskell-Gerhardt, K.J., 2009, Progradational mixed siliciclastic/carbonate sequence sets on the tectonically active eastern margin of the Pennsylvanian Paradox Basin, southwestern Colorado: Rocky Mountain Association of Geologists Special Publication, the Paradox Basin Revisted, New Developments in Petroleum Systems and Basin Analysis, p. 310-380.

Giles, K. A., and T. F. Lawton, 2002, Halokinetic sequence stratigraphy adjacent to the El Papalote diapir, northeastern Mexico: AAPG Bulletin, vol. 86, no. 5, p. 823–840.

Giles, K. A., and M. G. Rowan, 2012, Concepts in halokineticsequence deformation and stratigraphy: *in* G. I. Alsop, S. G. Archer, A. J. Hartley, N. T. Grant, and R. Hodgkinson, eds., Salt tectonics, sediments and prospectivity: Geological Society, London, Special Publications 2012, vol. 363, p. 7–31.

Giles KA, Hearon TE, Rowan MG, and Langford R, 2017, The Paradox Salt Basin, Utah and Colorado: Recognition of New Types of Salt Features and Their Impact on Salt-Related Traps (abs): AAPG Annual Convention and Exhibition, Houston, Texas, April 2-5, 2017.

Grammer, G.M., Eberli, G.P., Van Buchem, F.S., Stevenson, G.M. and Homewood, P., 1996. Application of high-resolution sequence stratigraphy to evaluate lateral variability in outcrop and subsurface—Desert Creek and Ismay intervals, Paradox Basin: Rocky Mountain Section (SEPM), Paleozoic Systems of the Rocky Mountain Region, p. 235-266.

Gobo, K., Ghinassi, M. and Nemec, W., 2015, Gilbert-type deltas recording short-term base-level changes: Delta-brink morphodynamics and related foreset facies: Sedimentology, vol. 62, no. 7, p.1923-1949.

Goldhammer, R.K., Oswald, E.J. and Dunn, P.A., 1991, Hierarchy of stratigraphic forcing: Example from Middle Pennsylvanian shelf carbonates of the Paradox Basin; *in* Sedimentary Modeling: Computer Simulations and Methods for Improved Parameter Definition, Kansas Geological Survey Bulletin, vol. 233, p. 361-413.

Hazel, J.E., 1994, Sedimentary response to intrabasinal salt tectonism in the Upper Triassic Chinle Formation, Paradox basin, Utah: U.S. Geological Survey Bulletin, vol. 2000-F.

Hearon, T. E. IV, M. G. Rowan, T. F. Lawton, P. T. Hannah, and K. A. Giles, 2015, Geology and tectonics of Neoproterozoic salt diapirs and salt sheets in the eastern Willouran Ranges, South Australia: Basin Research, vol. 27, p. 183–207.

Herman, G. and Sharps, S.L., 1956, Pennsylvanian and Permian stratigraphy of the Paradox salt embayment: *in* Geology and Economic Deposits of East Central Utah, Seventh Annual Field Conference, Utah Geological Association, p. 77-84.

Hite, R.J., Anders, D.E., and Ging, T.G., 1984, Organic-rich source rocks of Pennsylvanian age in the Paradox Basin of Utah and Colorado: *in* Hydrocarbon Source Rocks of the Greater Rocky Mountain Region, Rocky Mountain Association of Geologists, p. 255-271.

Hoy, R.G. and Ridgway, K.D., 2002, Syndepositional thrust-related deformation and sedimentation in an Ancestral Rocky Mountains basin, Central Colorado trough, Colorado, USA: Geological Society of America Bulletin, vol. 114 no. 7, p. 804-828.

Huffman Jr, A.C. and Taylor, D.J., 1994, Pennsylvanian thrust faulting along the northeastern margin of the Paradox basin (abs): Geological Society of America Abstracts with Programs, vol. 26, no. 6, p.19.

Jordan, O.D. and Mountney, N.P., 2012, Sequence stratigraphic evolution and cyclicity of an ancient coastal desert system: the Pennsylvanian–Permian Lower Cutler Beds, Paradox Basin, Utah, USA: Journal of Sedimentary Research, vol. 82, no. 10, p. 755-780.

Kluth, C.F., and Coney, P.J., 1981, Plate tectonics of the ancestral Rocky Mountains: Geology, vol. 9, p. 10–15.

Kluth, C.F., and DuChene, H.R., 2009, Late Pennsylvanian and early Permian structural geology and tectonic history of the Paradox Basin and Uncompahgre Uplift, Colorado and Utah: *in* the Paradox Basin Revisited – New Developments in Petroleum Systems and Basin Analysis, Rocky Mountain Association of Geologists Special Publication, p. 178-197.

Kluth, C.F., Ye, H., Royden, L., Burchfiel, C., and Schuepbach, M., 1998, Late Paleozoic Deformation of Interior North America: The Greater Ancestral Rocky Mountains: Discussion & Reply: AAPG Bulletin, vol. 82, p. 2272–2276.

Kneller, B.C. and Branney, M.J., 1995, Sustained high-density turbidity currents and the deposition of thick massive sands: Sedimentology, vol. 42, no. 4, p. 607-616.

Lawton, T.F., Pollock, S.L. and Robinson, R.A.J., 2003, Integrating sandstone petrology and nonmarine sequence stratigraphy: application to the Late Cretaceous fluvial systems of southwestern Utah, USA: Journal of Sedimentary Research, vol. 73, no. 3, p. 389-406.

Leary, R.J., Umhoefer, P., Smith, M.E., and Riggs, N., 2017, A three-sided orogen: A new tectonic model for Ancestral Rocky Mountain uplift and basin development: Geology, vol. 45, no. 8, p. 735-738.

Loope, D.B., 1984, Eolian origin of upper Paleozoic sandstones, southeastern Utah: Journal of Sedimentary Research, vol. 54, no. 2, p. 563-580.

Mercier, E., Rafini, S. and Ahmadi, R., 2007, Folds kinematics in “Fold-and-Thrust Belts” the “Hinge Migration” question, a review: *In* Thrust Belts and Foreland Basins, p. 135-147.

Mack, G.H., and Rasmussen, K.A., 1984, Alluvial-fan sedimentation of the Cutler Formation (Permo-Pennsylvanian) near Gateway, Colorado: Geological Society of America Bulletin, vol. 95, p. 109–116.

Mankowski, L.C., Campbell, T.L., Huntoon, J.E., Gregg, W.J. and Linari, D.J., 2002, Late Paleozoic Tectonics and Hydrocarbon Systems of Western North America–The Greater Ancestral Rocky Mountains: AAPG Hedberg Conference, Vail, Colorado, July 21-26.

Mast, A.M., 2016, The origin of anomalous carbonate units outcropping at the salt sediment interface of the southern end of Gypsum Valley Salt Wall, Paradox Basin, southwest Colorado: M.S. Thesis, The University of Texas at El Paso.

Maughan, E.K., 1990, Summary of the Ancestral Rocky Mountains epeirogeny in Wyoming and adjacent areas: US Geological Survey, vol. 90, no. 477.

McKenzie, D., 1978, Some remarks on the development of sedimentary basins: Earth and Planetary science letters, vol. 40, p. 25–32.

Nuccio, V.F., and Condon, S.M., 1996, Burial and Thermal History of the Paradox Basin, Utah and Colorado, and Petroleum Potential of the Middle Pennsylvanian Paradox Formation: U.S. Geological Survey Bulletin 2000-O, p. 57-76.

Owen, G., Moretti, M. and Alfaro, P., 2011, Recognising triggers for soft-sediment deformation: current understanding and future directions: Sedimentary Geology, vol. 235, no. 3-4, p. 133-140.

Owen, G. and Moretti, M., 2011, Identifying triggers for liquefaction-induced soft-sediment deformation in sands: Sedimentary Geology, vol. 235, no. 3-4, p. 141-147.

Parker, J.M., 1968, Lisbon field area, San Juan County, Utah: Rocky Mountain Association Of Geologists Field Conference, p. 89-100

Patranabis-Deb, S. and Chaudhuri, A.K., 2007, A retreating fan-delta system in the Neoproterozoic Chattisgarh rift basin, central India: Major controls on its evolution: AAPG Bulletin, vol. 91, no. 6, p. 785-808.

Peterson, J.A. and Hite, R.J., 1969, Pennsylvanian evaporite-carbonate cycles and their relation to petroleum occurrence, southern Rocky Mountains: AAPG Bulletin, vol. 53, no. 4, p. 884-908.

Peterson, J. A., and Ohlen, 1963, Pennsylvanian shelf carbonates, Paradox Basin: *in* Shelf Carbonates of the Paradox Basin, Four Corners Geological Society 4th Field Conference Guidebook, p. 65–79.

Pitman III, W.C., and Andrews, J.A., 1985, Subsidence and thermal history of small pull apart basins: *in* the Society of Economic Paleontologists and Mineralogists (SEPM) Special Publication Strike-Slip Deformation, Basin Formation, and Sedimentation (SP37), p. 49-45.

Pray, L.C. and Wray, J.L., 1963, Porous algal facies (Pennsylvanian) Honaker Trail, San Juan Canyon, Utah: Four Corners Geological Society Special Publication Shelf Carbonates of the Paradox Basin, Fourth Field Conference, p. 204-234.

Prochnow, S.J., Atchley, S.C., Boucher, T.E., Nordt, L.C. and Hudec, M.R., 2006, The influence of salt withdrawal subsidence on palaeosol maturity and cyclic fluvial deposition in the Upper Triassic Chinle Formation: Castle Valley, Utah: Sedimentology, vol. 53, no. 6, p. 1319-1345.

Rees, C., Palmer, J. and Palmer, A., 2018, Gilbert-style Pleistocene fan delta reveals tectonic development of North Island axial ranges, New Zealand: New Zealand Journal of Geology and Geophysics, vol. 61, no. 1, p. 64-78.

Rowan, M. G., K. A. Giles, T. E. Hearon IV, C. E. Gannaway, and J. C. Fiduk, 2014, Megaflaps along the edges of steep diapirs and beneath salt sheets: Models and examples (abs.): AAPG International Conference and Exhibition, Istanbul, Turkey, September 14–17, 2014.

Rowan, M.G., Giles, K.A., Hearon IV, T.E. and Fiduk, J.C., 2016, Megaflaps adjacent to salt diapirs: AAPG Bulletin, vol. 100, no. 11, p.1723-1747.

Shen, S.Z., Crowley, J.L., Wang, Y., Bowring, S.A., Erwin, D.H., Sadler, P.M., Cao, C.Q., Rothman, D.H., Henderson, C.M., Ramezani, J. and Zhang, H., 2011, Calibrating the end-Permian mass extinction: Science, vol. 334, no. 6061, p. 1367-1372.

Shinn, E.A., 1973, Sedimentary accretion along the leeward, SE coast of Qatar Peninsula, Persian Gulf: *in* The Persian Gulf, p. 199-209.

Soreghan, G.S. and Dickinson, W.R., 1994, Generic types of stratigraphic cycles controlled by eustasy: Geology, vol. 22, no. 8, p. 759-761.

Soreghan, G.S., Soreghan, M.J., Sweet, D.E. and Moore, K.D., 2009, Hot fan or cold outwash? Hypothesized proglacial deposition in the upper Paleozoic Cutler Formation, western tropical Pangea: Journal of Sedimentary Research, vol. 79, no. 7, p. 495-522.

Soreghan, G.S., Keller, G.R., Gilbert, M.C., Chase, C.G., and Sweet, D.E., 2012, Load-induced subsidence of the Ancestral Rocky Mountains recorded by preservation of Permian landscapes: Geosphere, vol. 8, p. 654–668.

Spearing, D.R., 1974, Alluvial fan deposits: Geological Society of America Special Publication, Summary sheets of sedimentary deposits, Sheet 1.

Sweet, D.E., 2017, Fine-Grained Debris Flows In Coarse-Grained Alluvial Systems: Paleoenvironmental Implications For the Late Paleozoic Fountain and Cutler Formations, Colorado, USA: Journal of Sedimentary Research, vol. 87, no. 8, p. 763-779.

Taylor, A.M. and Goldring, R., 1993, Description and analysis of bioturbation and ichnofabric: Journal of the Geological Society, vol. 150, no. 1, p. 141-148.

Thompson, J.A., Giles, K., Hearon, T.E., Trudgill, B., Gannaway, C.E., Jobe, Z. and Rowan, M.G., 2018, Structural and Stratigraphic Evolution of the Sinbad Valley Salt Wall, NE Paradox Basin, SW Colorado(abs): ACE 2018 Annual Convention & Exhibition.

Thompson-Jobe, J. A., K. A. Giles, T. E. Hearon IV, M. G. Rowan, B. Trudgill, C. E. Gannaway Dalton, & Z. R. Jobe (in prep): Structural and Stratigraphic Evolution of the Sinbad Valley Salt Wall, NE Paradox Basin, SW Colorado.

Trudgill, B.D., Banbury, N., Underhill, J., and Post, P.J., 2004, Salt evolution as a control on structural and stratigraphic systems: Northern Paradox foreland basin, southeast Utah, USA, in Salt-Sediment Interactions and Hydrocarbon Prospectivity: Proceedings, Gulf Coast Section SEPM Foundation, Annual Bob F. Perkins Research Conference, SEPM, vol. 24, p. 669–700.

Trudgill, B.D. and Paz, M., 2009. Restoration of mountain front and salt structures in the northern Paradox Basin, SE Utah: *in* The Paradox Basin Revisited – New Developments in Petroleum Systems and Basin Analysis, p. 132-177.

Trudgill, B.D., 2011, Evolution of salt structures in the northern Paradox Basin: Controls on evaporite deposition, salt wall growth and supra-salt stratigraphic architecture, Basin Research, vol. 23, no. 2, p.208-238.

Wengerd, S.A. and Matheny, M.L., 1958. Pennsylvanian system of Four Corners region. AAPG Bulletin, vol. 42, no. 9, p. 2048-2106.

White, M.A., and Jacobson, M.I., 1983, Structures associated with the southwest margin of the ancestral Uncompahgre Uplift: *in* Northern Paradox Basin - Uncompahgre Uplift, Grand Junction Geological Society, p. 33-39.

Williams, G.E., 1971, Flood deposits of the sandbed ephemeral streams of central Australia: Sedimentology, v. 17, p. 1-40.

Ye, H., Royden, L., Burchfiel, C., and Schuepbach, M., 1996, Late Paleozoic deformation of interior North America: the greater Ancestral Rocky Mountains: AAPG Bulletin, vol. 80, p. 1397–1432.

APPENDIX

Appendix: Full-Size Stratigraphic Columns (Oversized)

VITA

Kate Crawford Grisi was born and raised in northern New York State. She obtained a B.S. in geology from the State University of New York (SUNY) at Potsdam in Potsdam, NY and went to field camp at Indiana University's Geologic Field School (IUGFS) in Cardwell, Montana. At SUNY Potsdam, she was a student researcher and presented at the Geological Society of America conference in 2015, winning the Sigma Gamma Epsilon National Counsel Best Poster Award. After her student year at IUGFS in 2014, she was an associate instructor in 2015 and 2016. In graduate school, Kate has received a University of Texas at El Paso Dodson Research Grant, an American Association of Petroleum Geologists (AAPG) Grant-in-Aid, and a Geological Society of America (GSA) Graduate Student Research Grant, as well as a West Texas Geology Foundation Hal Dean Memorial Scholarship and AAPG Southwest Section Scholarship. In the summers of 2017 and 2018, she interned for the Department of Defense in Washington, DC, where she has now accepted a full-time job.

Permanent email address: kategrisi@gmail.com

This thesis was typed by Kate C. Grisi

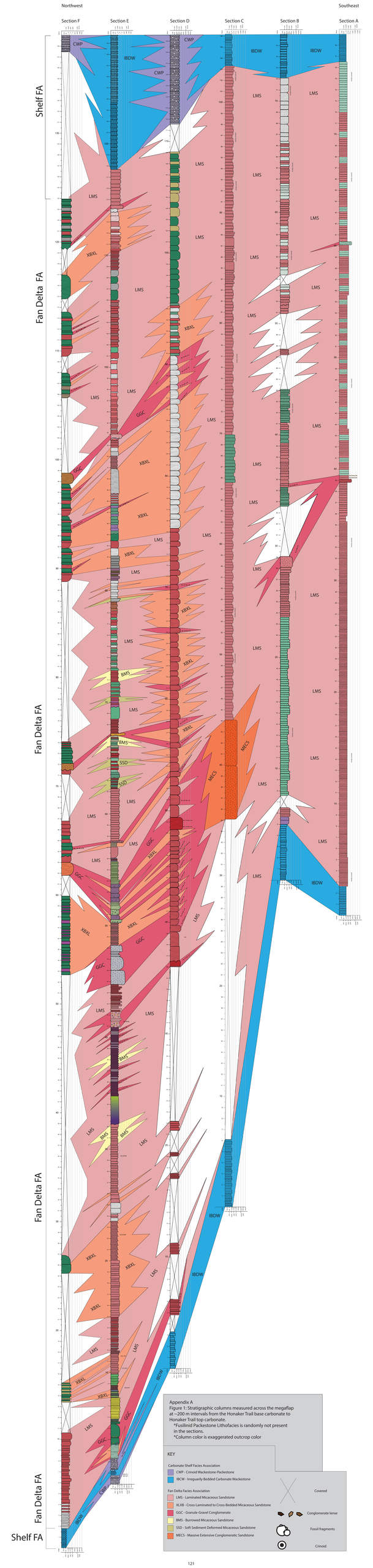

Appendix A
Figure 1: Stratigraphic columns measured across the megaflap at ~200 m intervals from the Honaker Trail base carbonate to Honaker Trail top carbonate.
*Fusilinid Packestone Lithofacies is randomly not present in the sections.
*Column color is exaggerated outcrop color